RhoGTPases and their relevance for the afterload-dependent myocardial fibrosis

Doctoral Thesis
In partial fulfillment of the requirements for the degree
“Doctor rerum naturalium (Dr. rer. nat.)”
in the Molecular Medicine Study Program
at the Georg-August University Göttingen

submitted by
Anita Ongherth

born in
Fogarasch

Göttingen, 2016

Members of the Thesis Committee

Supervisor

Prof. Susanne Lutz
Institute of Pharmacology and Toxicology
University Medical Center Göttingen
Georg-August-University Göttingen

Second member of the thesis committee

Prof. Hubertus Jarry
Prof. for Endocrinology
Animal Protection Commission
University Medical Center Göttingen
Georg-August-University Göttingen

Third member of the thesis committee

Prof. Peter Schu
Department of Cellular Biochemistry,
University Medical Center Göttingen
Georg-August-University Göttingen

Date of Disputation:…….

AFFIDAVIT

Here I declare that my doctoral thesis entitled "**RhoGTPases and their relevance for the afterload-dependent myocardiac fibrosis**" has been written independently with no other sources and aids than quoted.

Anita Ongherth
Göttingen, September 2016

Acknowledgement

At this point, I would like to thank a lot of people, who accompanied me on this journey for the last 4 years.

First of all, I would like to thank very much my thesis committee members Prof. Hubertus Jarry and Prof. Peter Schu for constructive comments, interesting questions and valuable suggestions during our progress report meetings.

Many thanks go also to Prof. Ralf Dressel, Dr. Laura Zelarayan and Dr. Katrin Streckfuß-Bömeke for accepting to participate in the examination committee.

Thank you, Prof. Zimmermann, for giving me the opportunity to work in the institute of pharmacology and toxicology. I really appreciated the international environment and multicultural atmosphere.

Most of all I would like to thank my supervisor Prof. Susanne Lutz for the chance to do my PhD in your group. Thank you for your immense scientific advice, continuous support and enormous patience during this time. I learned so many things from you - from scientific presentation and writing to data analysis and interpretation. Without your guidance and help this thesis would have never been realized.

A huge thank you goes to the whole institute of pharmacology. I enjoyed the time working with and next to everyone in the lab. In particular, I would like to thank Shu, Farah, Eriona, PL, Satish, Elif, and Norman – I will miss the chats with you in and outside the lab.

Of course, I would like to thank the Lutz Lab with all the old and new members: Christina, Kerstin, Aline, Naim, Wiebke, Simran, Laura, my namesake Nenja and especially Sebastian, Svenja and Feli for your scientific help and advice, the “perfect” soundtrack, encouraging and cheering words and for creating a very nice working atmosphere in our lab.
Very warm thanks belong to Beate Ramba for her constant help and support.

My dearest thanks go to my family for their continuous support, help, understanding and believing in me, not only for the last 4 years, but also for all the years of my education.

Konrad, thank you so much for your love, support, encouragement and patience throughout my PhD time and especially during the last months.

I Table of Contents

II List of Abbrevations

2D	Two-dimensional
3D	Three-dimensional
AMCF	Adult mouse cardiac fibroblast
α-MHC	α-Myosin heavy chain
Ang II	Angiotensin II
ANP	Atrial natriuretic peptide
APS	Ammonium persulfate
AT1R	Angiotensin II-type 1 receptor
β-MHC	β-Myosin heavy chain
BNP	Brain natriuretic peptide
BSA	Bovine serum albumin
BW	Body weight
cDNA	Complementary DNA
CEE	Chicken embryo extract
CO_2	Carbon dioxide
CSA	Cross sectional area
CTGF	Connective tissue growth factor
CBFHH	Calcium and bicarbonate-free Hanks´ solution with HEPES
DAPI	4´,6-diamidino-2-phenylindole
DH	Dbl-homolgy
DMEM	Dulbecco´s modified eagle medium
DMSO	Dimethyl sulfoxide
DNA	Deoxyribonucleic acid
dNTP	Deoxyribonucleoside triphophate
ECM	Extracellular matrix
ECT	Engineered connective tissue
EDTA	Ethylenediaminetetraacetic acid
EF	Ejection fraction
EGFP	Enhanced green fluorescent protein
EHM	Engineered heart muscle tissue
EMT	Epithelial-mesenchymal transition
EndEMT	Endothelial-mesenchymal transition
FAS	Fractional area shortening
FCS	Fetal calf serum
FOC	Force of contraction
FITC	Fluorescein isothiocyanate
FSP-1	Fibroblast specific protein-1
GAP	GTPase-activating protein
GDI	Guanine nucleotide dissociation inhibitor

GDP	Guanosine diphosphate
GEF	Guanine nucleotide exchange factor
GFP	Guanosine triphosphate
GPCR	G-protein-coupled receptor
GTP	Guanine triphosphate
HBSS	Hanks´ balanced salt solution
HEK293A	Human embryonic kidney 293A cells
HEPES	4-(2-hydroxyethyl)-1-piperazineethanesulfonic acid
HET	Heterozygous
HRP	Horseradish peroxidase
IB	Immunoblot
IF	Immunofluorescence
i.p.	Intraperitoneal
KO	Knockout
LVID d	Left ventricular inner diameter diastole
LVID s	Left ventricular inner diameter systole
LVW	Left ventricular weight
MI	Myocardial infarction
MMP	Matrix metalloproteinase
MOPS	3-N-morpholino-propanesulfonic-acid
MRTF	Myocardin-related transcription factor
NEAA	Non-essential amino acids
NKM	Non-cardiomyocyte medium
NRCF	Neonatal rat cardiac fibroblast
o/n	Over night
PBGD	Porphobilinogen deaminase
PBS	Phosphate-buffered saline
PCR	Polymerase chain reaction
Pen/Strep	Penicillin/streptomycin
PFA	Paraformaldehyde
qRT-PCR	quantitative real time polymerase chain reaction
RhoA	Ras homolog (gene) family member A
RNA	Ribonucleic acid
RT	Room temperature
ROCK	Rho-associated kinase
S1PR	Sphingosine-1-phosphate receptor
s.c.	Subcutaneous
SDS	Sodium dodecyl sulfate
SEM	Standard error of the mean
SMC	Smooth muscle cells
SRF	Serum response factor

TAC	Transverse aortic constriction
TBS	Tris-buffered saline
TBST	Tris-buffered saline with tween 20
TEMED	Tetramethylethylendiamine
Tris	Tris (hydroymethyl) aminomethane
TGF-β	Transforming growth factor-β
TRITC	Tetramethylrhodamine
UV	Ultra violet
Vol d	Volume diastole
Vol s	Volume systole
WGA	Wheat germ agglutinin
WT	Wildtype

Symbols and units

α	Alpha
β	Beta
°C	Degree Celsius
Da	Dalton
g	Gram
h	Hour
Hz	Hertz
k	Kilo (10^3)
kb	Kilo basepair
L	Liter
µ	Micro (10^{-6})
m	Milli (10^{-3})
min	Minute
M	Molar concentration
n	Nano (10^{-9})
rpm	Rounds per minute
sec	Second
%	Percent
U	Unit
V	Volt

III List of Figures

IV List of Tables

1 Summary

The guanine exchange factor p63RhoGEF was identified as a specific activator of the RhoGTPase RhoA and its transcript was found to be abundant in brain and heart tissue. Amongst cardiac cells, the highest expression of p63RhoGEF was detected in smooth muscle cells and cardiac fibroblasts. Within this thesis the relevance of p63RhoGEF in the healthy myocardium and under pathological conditions was under investigation with a special focus on its function in cardiac fibroblasts in the context of auto- and paracrine signaling.

In a model of cardiac fibrosis, in which wild type mice were subjected to transverse aortic constriction (TAC), p63RhoGEF expression was found to be up-regulated in the myocardium. Furthermore, its expression correlated positively with the fibrosis marker CTGF (connective tissue growth factor) as well as with the level of hypertrophy, and negatively with the contractility of the heart. Due to the lack of specific mouse models targeting cardiac fibroblasts, the role of p63RhoGEF was first assessed with the help of 2D and 3D cultures of neonatal rat cardiac fibroblasts (NRCF). In 2D culture it was demonstrated that p63RhoGEF regulates the expression and secretion of CTGF involving the activation of the serum response factor (SRF) and its actin-dependent co-factor myocardin-related transcription factor (MRTF). Moreover, confocal microscopy studies revealed a partial co-localization of p63RhoGEF and CTGF at the trans-Golgi network. In 3D engineered connective tissue cultures (ECT), p63RhoGEF was demonstrated to regulate viscoelastic properties. While overexpression of p63RhoGEF increased the stiffness, the dominant negative truncated p63ΔN decreased the rigidity of the tissue. An influence of p63RhoGEF on CTGF expression in ECT could be detected. CTGF itself was however not sufficient to regulate viscoelastic properties of ECT. Next the heterogeneous engineered heart muscle model (EHM) was used to demonstrate that p63RhoGEF overexpression in cardiac fibroblasts enhanced resting and twitch tension, whereas p63ΔN reduced both. In contrast, overexpression of p63RhoGEF in cardiomyocytes (CM) failed to improve the contractile function validating the importance of p63RhoGEF in cardiac fibroblasts for cell-cell communication via paracrine signaling.

In the following, a global p63RhoGEF knockout mouse line was used to study the effect of a complete (KO) and partial (HET) deletion of p63RhoGEF. In HET mice already under basal condition an impaired cardiac phenotype was present, while the KO mice showed no major difference compared to the WT phenotype. Mice subjected to TAC developed all heart failure within 5 weeks after intervention. While the HET mice showed the most detrimental cardiac dysfunction accompanied by a faster dilation of the left ventricle, the KO animals resembled the WT phenotype. Interestingly, mortality was increased in KO male mice leading to a survival rate of less than 60% within the first 2 weeks after TAC. So far, excessive hypertrophy and fibrosis as a cause could be excluded. In the surviving animals the degree of hypertrophy was identical after 5 weeks independent of the genotype. However, in the HET mice a decrease in fibrosis could be detected.

To further study the role p63RhoGEF in adult mouse cardiac fibroblasts (AMCF), cells were isolated from the generated mouse line and displayed a prominent myofibroblast character in culture regardless of the genotype. The genetic deletion of p63RhoGEF in these cells exhibited a paradox signaling. While the total RhoA and cytoskeletal protein expression was unchanged, the genetic deletion resulted in a higher phosphorylation of direct ROCK targets cofilin and ERM proteins, increased CTGF secretion and up-regulation of fibrosis-associated factors TGF-β and collagen in a dose-dependent manner showing the most pronounced response detected in the KO AMCF. Moreover, the knockout of p63RhoGEF led to activation of cell survival and growth pathways and improved proliferation as well as prevented cell death.

1.1 Zusammenfassung

Der Nukleotid-Austauschfaktor p63RhoGEF wurde als spezifischer Aktivator der RhoGTPase RhoA identifiziert und sein Transkript konnte vermehrt in Hirn-und Herzgewebe detektiert werden. Innerhalb der kardialen Zellen konnte die höchste Expression von p63RhoGEF in glatten Muskelzellen der Aorta sowie kardialen Fibroblasten nachgewiesen werden. Im Rahmen dieser Arbeit wurde die Bedeutung von p63RhoGEF im gesunden Herzen und unter pathologischen Bedingungen untersucht, wobei ein Fokus auf seine Funktion in kardialen Fibroblasten im Zusammenhang mit autokrinen und parakrinen Signalwegen gelegt wurde.
Anhand eine Tiermodells der kardialen Fibrose, in denen Wildtyp Mäuse einer transversalen Aortenkonstriktion (TAC) unterzogen wurden, konnte eine erhöhte Expression von p63RhoGEF im Herzgewebe nachgewiesen werden. Zudem konnte eine positive Korrelation der Expression von p63RhoGEF mit dem Fibrose-Marker CTGF („connective tissue growth factor“) und dem Ausmaß der Hypertrophie, sowie ein negativer Zusammenhang mit der Kontraktilität des Herzen gezeigt werden. Aus Mangel an fehlenden Fibroblasten-spezifischen Mausmodellen, wurde die Rolle von p63RhoGEF zunächst in 2D und 3D Zellkulturen neonataler kardialer Fibroblasten der Ratte (NRCF) analysiert. Mit Hilfe von 2D Zellkulturen konnte belegt werden, dass p63RhoGEF sowohl die Expression als auch Sekretion von CTGF reguliert und dies durch die Aktivierung des Serum-Response-Faktor (SRF) und des Aktin-abhängigen Co-Faktor Myocardin-related Transkriptionsfaktor (MRTF) vermittlelt wird. Konfokal mikroskopische Aufnahmen konnten zudem eine partielle Kolokalisation von p63RhoGEF mit CTGF am trans-Golgi Netzwerk belegen. Im 3D Gewebemodell des “engineered connective tissue“ (ECT) konnte gezeigt werden, dass p63RhoGEF die Viskoelastizität reguliert, indem eine Überexpression von p63RhoGEF zu einer erhöhten Steifigkeit des Gewebes führt, während Gewebe mit der Expression des dominant negativen Konstrukts p63ΔN eine verminderte Steifigkeit aufweist. In diesem Zusammenhang konnte der Einfluss von p63RhoGEF auf die Expression von CTGF auch in den Geweben gezeigt werden, wobei eine vermehrte Expression von CTGF allein nicht ausreichte

die Eigenschaften des Gewebes zu beeinflussen. In einem heterogenen 3D Herzgewebe, dem „engineered heart muscle“ (EHM) führte eine erhöhte Expression von p63RhoGEF ausschließlich in kardialen Fibroblasten zu einer verbesserten Calcium-abhängigen Kontraktilität und gleichzeitig gesteigerten Gewebespannung, während Gewebe mit der Expression des blockierenden p63ΔN Konstruktes beide Eigenschaften negativ regulierte. Im Gegensatz dazu, konnte eine Überexpression von p63RhoGEF ausschließlich in Kardiomyozyten keine Verbesserung der Kontraktilität erzielen, was auf eine entscheidende Rolle von p63RhoGEF in kardialen Fibroblasten für die parakrin-vermittelte Zell-Zell-Kommunikation hinweist.

Des Weiteren wurde eine Mauslinie mit einem globalen p63RhoGEF Knockout generiert, um den Effekt eines kompletten (KO) und eines partiellen (HET) Verlustes von p63RhoGEF zu untersuchen. Bei den HET Mäusen zeigte sich bereits unter basalen Bedingungen ein Beeinträchtigung des kardialen Phänotyps, während die KO Mäuse keinen sichtbaren Unterschied im Vergleich mit zu dem WT Phänotyp aufwiesen. Alle Mäuse, die einer TAC-OP unterzogen wurden, entwickelten innerhalb von 5 Wochen nach dem Eingriff ein progressives Herzversagen. Die HET Mäuse zeigten hierbei die größte kontraktile Verschlechterung einhergehend mit einer schnelleren Dilation des linken Ventrikels, während die KO Mäuse hingegen das Erscheinungsbild des WT Phänotyp widerspiegelten. Dennoch war die Mortalität der KO Mäuse mit einer Überlebensrate von unter 60% innerhalb der ersten 2 Wochen nach der OP stark erhöht. Eine massive Zunahme der Hypertrophie und Fibrose konnten als mögliche Gründe ausgeschlossen werden und bei den überlebenden KO Tieren war das Ausmaß der Hypertrophie ziemlich identisch. Interessanterweise wurde in den HET Mäusen eine Reduzierung von fibrotischem Gewebe verzeichnet.

Um die Funktion von p63RhoGEF in adulten kardialen Fibroblasten der Maus (AMCF) näher zu charakterisieren, wurden diese Zellen aus den transgenen Mäusen isoliert. In Kultur entwickelten die Zellen unabhängig vom Genotyp einen sehr ausgeprägten Myofibroblasten-Charakter. Die Reduzierung bzw. der totale Verlust von p63RhoGEF äußerte sich durch eine paradoxe Regulation. Während keine Veränderung hinsichtlich der Expression von total RhoA sowie diverser Zytoskelettproteinen zu verzeichnen war, führte die Deletion von p63RhoGEF zu einer erhöhten Phosphorylierung der direkten ROCK Zielproteine Cofilin und ERM, zu einem Anstieg an sezerniertem CTGF und zu einer Zunahme von Fibrose-Markern wie TGF-β und Kollagen auf mRNA Ebene. Dabei zeigte sich die größte Zellantwort in den KO AMCF. Zusätzlich konnte in den KO Zellen eine Aktivierung von Signalwegen, die für das Überleben und Wachstum eine entscheidende Rolle spielen, beobachtet werden, wodurch die Zellen einerseits eine erhöhte Proliferation und gleichzeitig einen besseren Schutz vor Apoptose aufweisen konnten.

2 Introduction

2.1 Heart failure

Cardiovascular diseases are one of the most common death causes worldwide. According to the World Health Organization (WHO) 17.5 million people died from cardiovascular diseases in 2012, representing 31% of all global death. Despite improved drug treatments and therapies over the last decades this trend is further increasing. For this reason, further investigations about the underlying mechanisms leading to the development of heart failure are needed to define new therapeutic targets.

2.1.1 Cardiac remodeling

Cardiac remodeling occurs when myocardial injury or hemodynamic overload initiates a series of structural changes throughout the myocardium that eventually leads to a global deterioration of cardiac function [1]. The most prominent structural changes include compensatory cardiomyocyte hypertrophy and myocardial fibrosis.
Myocardial hypertrophy is an essential adaptive process through which the heart responds to various mechanical, metabolic or genetic stresses. For instance, physiological hypertrophy, which is in most cases reversible, occurs during pregnancy or chronic exercise in an athlete´s heart improving the cardiac output to fulfill the body´s demand for nutrients and oxygen [2].

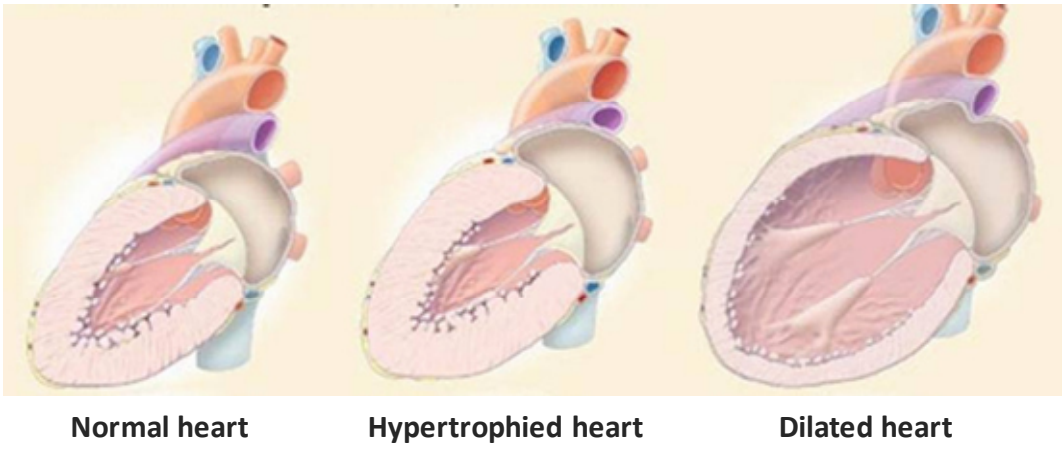

Figure 2.1: Transition from normal healthy heart to heart failure by cardiac remodeling
The scheme shows the different structural changes during cardiac remodeling. Figure was adapted from Jessup & Brozena, 2003 [3].

However, hypertrophy due to persistent overload ultimately leads to contractile dysfunction and dilation of the left ventricle (Figure 2.1) [4]. Pathological remodeling, as a consequence of hypertension, valve malfunction, virus infection or genetic predisposition, is often irreversible and results in severe heart failure [5]. In addition to growth of individual cardiomyocytes, the hypertrophied myocardium undergoes further complex structural remodeling involving rearrangement of the muscle fibers and interstitial as well as perivascular fibrosis [6-8].
Like cardiomyocyte hypertrophy, the remodeling of the extracellular matrix (ECM) may initially represent an adaptive response to cardiac stress, but ultimately impairs cardiac structure and function [9], thereby contributing to the high morbidity and mortality of cardiac diseases [8].

2.1.2 Myocardial fibrosis

Cardiac fibrosis is an important contributor to the development of cardiac dysfunction in diverse pathological conditions, such as ischaemic and hypertensive cardiac disease. It can be defined as an inappropriate accumulation of connective tissue in the myocardium [7, 10-12], resulting from excessive deposition and/or decreased degradation of extracellular matrix (ECM) components, including mainly collagen type 1 [13].
Cardiac fibrosis leads to an increased myocardial stiffness, impairment of electrical connections between cardiomyocytes and hence to a higher risk of arrhythmias [14]. Additionally, the increased diffusion distance for nutrients and oxygen from the blood vessels to the cardiomyocytes can negatively influence the myocardial balance between energy demand and supply [7, 11].
Cardiac fibrosis is generally categorized in two types: reparative and reactive fibrosis. Reparative fibrosis occurs immediately after a myocardial infarction (MI). During the acute ischemic event cardiomyocytes are lost due to necrosis and apoptosis. This leads to hyperplasia of non-myocytes, including fibroblasts. As a consequence more collagen fibers are deposited and scar tissue is formed to ensure structural integrity. In contrast, reactive fibrosis generally occurs in the absence of cell loss as a result of changes in local mechanical and biochemical factors in the process of cardiac remodelling, as can be seen e.g. in hypertensive conditions. While reparative fibrosis usually affects interstitial ECM, reactive fibrosis with excessive collagen deposition can be observed in the interstitial as well as perivascular area [10, 11, 15].

2.2 Cardiac fibroblasts

The normal heart is comprised of four major cell types: cardiomyocytes, endothelial cells, smooth muscle cells and fibroblasts. While cardiomyocytes make up most of the volume, fibroblasts are considered to be numerously the most abundant cell type in the heart, which can make up to 70% of the total cell population depending on the species [16]. Recently, a study revisited the cellular composition of the heart, demonstrating that fibroblasts comprise with less than 20% a relatively minor population [17]. Cardiac fibroblasts depict a spindle shaped cell body, a prominent Golgi apparatus and endoplasmatic reticulum indicative of high cellular activity [18]. Like all fibroblasts, cardiac fibroblasts do not have a basement membrane [19].
As cardiac fibroblasts are of mesenchymal origin they do not possess definite cell marker and share most of the available marker with other cell types. Amongst the more robust marker for detection of fibroblasts are the Discoidin Domain Receptor 2 (DDR2) [20], Transcription factor 21 (TCF21) [21] and the Platelet-derived growth factor receptor-alpha (PDGFRα) [22]. Subsets, but not all fibroblasts also express the classical myofibroblast marker α-smooth muscle actin (αSMA) [15]. In the tissue, cardiac fibroblasts are located in the interstitial matrix surrounding the cardiomyocytes [23] and contribute to the structural, mechanical and electric properties of the healthy myocardium. As the predominant matrix-producing cells [24], fibroblasts play a key role in regulating the structural integrity of the heart through controlled proliferation and ECM turnover [11, 16]. To maintain ECM homeostasis cardiac fibroblasts secrete ECM proteins, mostly collagen type 1 and 3 and fibronectin, to create a scaffold [25]. Simultaneously, they express and secrete matrix degrading proteins, e.g. matrix metalloproteases (MMPs) to maintain the balance between ECM synthesis and degradation [11, 26]. Beside the control of ECM homeostasis, cardiac fibroblasts support the distribution of contractile force and mechanical stress through the heart [25], as they are connected to cardiomyocytes via gap junctions and to the ECM via integrins [19, 27]. Moreover, cardiac fibroblasts can serve as conductors propagating electrical signals, as they possess a high membrane resistance and are not electrically excitable. In that way, they could also act as insulators [28].

2.2.1 Myofibroblasts – the activated fibroblast

Within a healthy tissue cardiac fibroblasts remain rather quiescent with a low potential for migration, proliferation and secretion [16, 29]. In response to neurohumoral or biomechanical stress, cardiac fibroblasts become activated and undergo a phenotypic transition to profibrogenic myofibroblasts, which are characterized by the expression of αSMA and pronounced stress fiber formation [11, 16], significantly increasing their contractile activity. Myofibroblasts display a more mobile phenotype and migrate through the tissue to sites of injury [18] and highly produce and secrete collagen-rich ECM and a number of profibrotic and inflammatory cytokines including the transforming growth

factor-β (TGF-β) and IL-1β [30]. Like fibroblasts, myofibroblasts are non-excitable cells and are not directly involved in conduction of the heart. Instead, they are more likely to produce conduction barriers by increasing the distance between adjacent cardiomyocytes and thus decreasing cardiomyocyte to cardiomyocyte coupling via gap junctions [31].
Over time, excessive formation of fibrous connective tissue and ECM leads to cardiac fibrosis. This impairs electrical coupling between cardiomyocytes and increases myocardial stiffness, leading to arrhythmias and severe diastolic dysfunctions [32].
Myofibroblasts are involved in both reparative and fibrotic processes and increased myofibroblast accumulation in the cardiac interstitium was found not only in myocardial infarction [33], but also in the pressure and volume overloaded myocardium [34, 35] and in the aging heart [36].

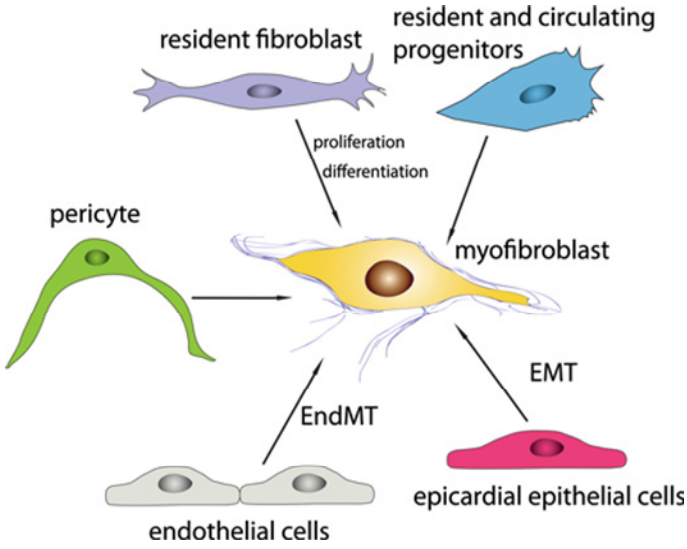

Figure 2.2: Sources of myofibroblasts
Shown are possible sources of cells that could contribute to a myofibroblast phenotype. Figure was adapted from Kong et al., 2014[37].

The origin of myofibroblasts constituting the fibrotic lesions of failing hearts is still not clear. Some reports have shown that myofibroblasts are derived solely from resident fibroblasts [15, 38], whereas others have suggested that other cell types transdifferentiate into fibroblasts (Figure 2.2). Other sources of myofibroblasts include epithelial cells undergoing epithelial-to-mesenchymal transition (EMT), bone marrow derived progenitor cell like fibrocytes, endothelial cells undergoing endothelial-to-mesenchymal transition (EndMT), pericytes or smooth muscle cells [37]. After scar formation most of the myofibroblasts undergo apoptosis, while some still reside in the scar tissue [39].

2.3 Connective tissue growth factor

The connective tissue growth factor (CTGF), also referred to as CCN2, is a cysteine-rich 36-38 kDa secreted protein and a member of the CCN (Cyr61, CTGF and Nov) family of multifunctional matricellular proteins [40-42]. Matricellular proteins do not fulfill a significant structural role, but bind to cell surface receptors, ECM proteins, growth factors and proteases. In this way they modulate the biological activity of other growth factors, cell-matrix interaction and cell function. CTGF is a typical example of such a matricellular protein, involved in modulating the activity of a variety of local factors in ECM homeostasis, and strongly implicated in fibrogenic processes in several tissues, including the heart [15].

2.3.1 Protein structure of CTGF

Like other members of the CCN family, CTGF has a similar genomic organization and modular protein structure. The CTGF gene contains five exons. Exon 1 encodes a signal peptide (SP) for secretion, while exons 2–5 encode for 4 different modules, which can bind to various growth factors, ECM components and cell membrane proteins (Figure 2.3). Module 1 is the insulin-like growth factor binding protein (IGFBP) domain, which interacts with IGF-I and IGF-II [43]. These two growth factors are involved in physiological cell growth [44], but at high level contribute to the development of cardiac fibrosis [45]. In this context, it was shown that IGF-I induces proliferation of cardiac fibroblasts and promotes collagen production [46, 47]. Module 2, the von Willebrand factor type C (VWC) domain, was shown to bind to bone morphogenetic protein 4 (BMP4) and TGF-β1. Interaction of CTGF with BMP4 inhibits BMP signaling, whereas binding of CTGF to TGF-β1 increased TGF-β signaling [48]. CTGF also interacts with BMP7 by antagonizing BMP7 signaling, thereby contributing to the development of fibrosis as demonstrated in various fibrotic kidney diseases [49, 50]. The third module, named the thrombospondin type 1 (TSP1) domain, serves as a binding domain for the vascular endothelial growth factor (VEGF) inhibiting angiogenesis induced by VEGF [51]. Finally, module 4 encodes for the C-terminal (CT) Cysteine knot module, which binds to proteoglycans allowing the interaction with ECM proteins [52].

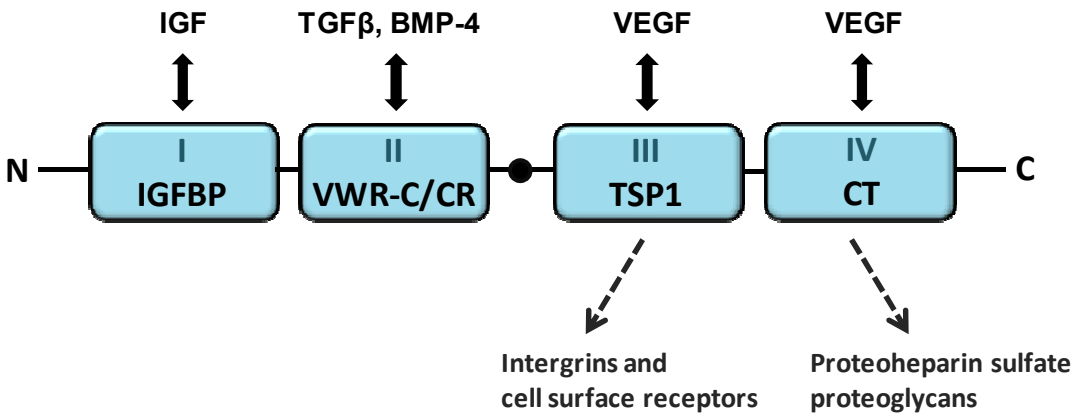

Figure 2.3: Protein structure of CTGF
Scheme of the 4 modules of CTGF and its interaction partners including growth factors, cell surface and ECM proteins. The scheme was adapted with modifications from Gressner and Gressner, 2008[53].

In addition, the region between module 2 and 3, rich in cysteine residues, is prone to proteolytic cleavage. CTGF can be cleaved by several elastases, MMPs, e.g. MMP2 and plasmin [54, 55], which, in turn, influences the activity and function of CTGF and its fragments. For instance, cleavage of CTGF can reactivate the angiogenic activity of VEGF, by relieving the competitive binding of VEGF with the TSP-1 domain [54, 55]. Based on the structure and its numerous binding partners, CTGF is suggested to be involved in a variety of cellular processes including adhesion, migration, proliferation, differentiation, angiogenesis and apoptosis [56, 57], all common features of cardiac remodeling. Under pathological condition CTGF mediates tissue repair and fibrosis of several organs through the regulation of several factors in ECM homeostasis [52, 58, 59].

2.3.2 Function and regulation of CTGF in the heart

CTGF is expressed in multiple tissues and cell types [58, 60, 61]. With respect to the heart, CTGF expression was found in the fetal mouse myocardium [62] and becomes restricted to the atria and large blood vessels in the adult heart [62, 63]. Mice deficient in CTGF did not show any cardiac abnormalities or signs of cardiac dysfunction at birth [64]. The expression of CTGF is regulated by a variety of stimuli [52, 65]. TGF-β is a potent fibrogenic factor and a major inducer of CTGF expression in many cell types including cardiomyocytes and fibroblasts [61, 66, 67].
Besides angiotensin II (Ang II), other G protein coupled receptor (GPCR) agonists such as endothelin-1 and phenylephrine were demonstrated to enhance CTGF expression in neonatal cardiomyocytes [68-71]. In a human fibroblast cell line it was shown that induction of CTGF by Ang II involved the Ang II-type 1 receptor (AT_1R) and activation of mitogen-activated protein kinases ERK1/2 (p42/44 MAPK). In line with this, a role of RhoA and SRF controlling CTGF expression in cardiomyocytes was postulated [72, 73].

Many *in vitro* studies have shown that CTGF stimulates the proliferation of fibroblasts, their differentiation towards myofibroblasts and enhances ECM production [74-77]. As CTGF expression correlates with the level of fibrosis, CTGF seems to play an important role in tissue response to injury and fibrosis [78-80].

2.3.3 Role of CTGF in myocardial fibrosis

With respect to cardiac diseases, increased levels of CTGF were found in patients with heart failure, MI, ischemia, hypertension and coronary artery disease [61, 81-83] as well as in injury-induced animal models of cardiac hypertrophy and fibrosis [69, 83-86].
As an example, pressure-overload cardiac hypertrophy in aorta-banded rats showed increased CTGF expression accompanied with elevated levels of TGF-β, collagen I and brain natriuretic peptide (BNP) [83], supporting CTGF as a profibrotic factor. In this context, it was shown that CTGF alone is not sufficient to initiate fibrosis, but the presence of both CTGF and TGF-β resulted in persistent fibrosis [74, 87].
In contrast, some studies also reported a decrease in fibrosis after inhibition of CTGF [88]. However, recent studies using transgenic mice overexpressing CTGF with similar amount of fibrosis as in the control mice pointed towards a cardio-protective effect of CTGF and thereby a beneficial effect of CTGF expression for cardiomyocyte survival [89]. Other reports demonstrated that neither a cardiac specific CTGF deletion in mice [90] nor a conditional knockout of CTGF had any influence on the development of fibrosis [86]. To date, no direct proof for a causal role of CTGF in the development of cardiac fibrosis has been reported.

2.4. RhoGTPases

2.4.1 Structure and function of RhoGTPases

RhoGTPases are monomeric GDP/GTP binding proteins (G proteins) belonging to the Ras-superfamily of small (~21 kDa) G proteins [91]. There are 22 RhoGTPases identified in humans, which can be classified into eight subgroups [92, 93]. RhoGTPases act as molecular switches that mediate a wide variety of cellular processes, such as actin cytoskeletal organization, cell migration, cell cycle progression, and transcriptional control [94-96]. Moreover, they have been implicated in phagocytosis, cytokinesis, neurite extension and retraction, cellular morphogenesis and polarization, growth and cell survival [97-99].
The best characterized members are RhoA, Rac1 and Cdc42, which can induce different cytoskeletal structures. RhoA activation leads to the formation of stress fibers associated with focal adhesions, Rac1 induces the formation of lamellipodia or membrane ruffles and

Cdc42 produces filopodia [91, 100, 101]. They also stimulate gene transcription through several transcription factors, such as the serum response factor (SRF) or NFκB [102, 103]. All RhoGTPases share a similar GTP binding site and most of them are posttranslationally modified at the C-terminus by an isoprenoid lipid, which serves as a plasma membrane anchor [104].
In the cardiovascular field, RhoGTPases play a key role in several signaling pathways activated by GPCR agonists such as endothelin-1 [105, 106], Ang II [107], phenylephrine (PE) [108] and lysophosphatidic acid (LPA) [109]. It has been demonstrated that RhoA is involved in the α1-adrenergic receptor-mediated hypertrophy in cardiomyocytes along with an increased gene expression of atrial natriuretic peptide (ANP), myosin light chain 2 (MLC-2), β-myosin heavy chain (β-MHC) and skeletal α-actin [108].

2.4.2 Activation of RhoGTPases

As mentioned above, RhoGTPases act as bi-molecular switches cycling between an inactive (GDP-bound) and an active (GTP-bound) conformation. This cycling is regulated by three types of accessory proteins (Figure 2.4). Guanine nucleotide exchange factors (GEFs) catalyze the exchange of GDP for GTP, thereby activating the GTPase [110], whereas GTPase-activating proteins (GAPs) increase the relatively slow intrinsic GTP hydrolysis rate of the GTPase, which inactivates the RhoGTPase. Guanine nucleotide dissociation inhibitors (GDIs) sequester the GDP-bound form of some GTPases in the cytosol, stabilize the inactive GDP-bound state and prevent them from localizing at membranes or being activated by GEFs [110].

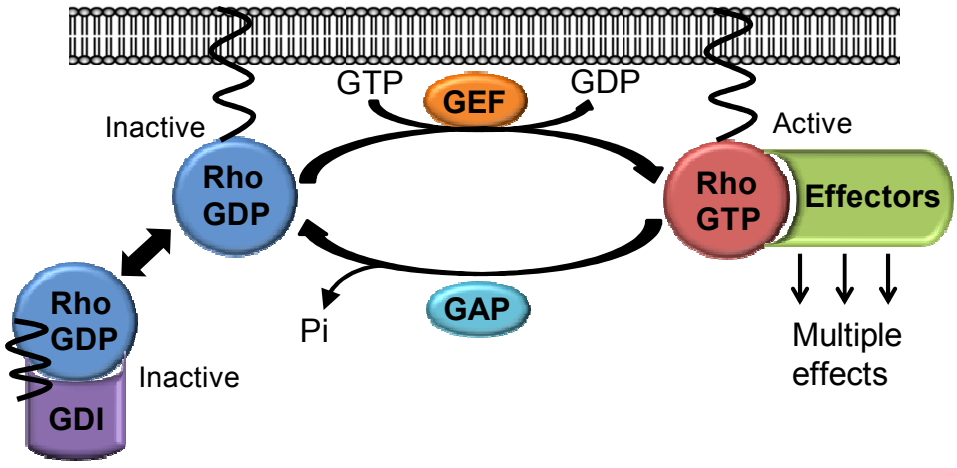

Figure 2.4: Activation cycle of RhoGTPases
Schematic overview of the activation of RhoGTPases by guanine nucleotide exchange factor (GEF), the inactivation by GTPase-activating protein (GAP) and stabilization of the inactive GDP-bound RhoGTPase by guanine nucleotide dissociation inhibitors (GDI). Scheme was adapted with modifications from Aktories, 2005.

The activation of Rho family proteins is often mediated through various cell-surface receptors, including the cytokine, tyrosine kinase and adhesion receptors, as well as GPCRs [111, 112]. Upon activation, RhoGTPases actively transduce signals by interacting with downstream effectors [113, 114] including kinases, actin regulators and adaptor proteins, leading to changes in cell behavior. A single RhoGTPase can activate a range of cellular responses, depending on the stimulus and cell type [115].

2.4.3 The RhoGTPase RhoA

RhoA is a monomeric GTPase of 21kDa in size and belongs to the Rho subfamily of GTP-binding proteins [116] . It is expressed in all type of cells, where it controls many cellular functions mainly by regulation of the actin cytoskeleton [117]. In this way, RhoA promotes the formation of stress fibers and focal adhesions important for cell shape, attachment and motility of cells [91, 118, 119]. In addition, RhoA is also involved in transcriptional regulation. In common with all monomeric GTPases, RhoA acts as a molecular switch, which is activated and inactivated by GDP/GTP exchange and GTP hydrolysis, respectively. The exchange of guanine nucleotide is mediated by the two switch regions, switch I and II, of the N-terminal sequence of RhoA, which undergo massive conformational changes. In addition, both switch regions interact with the Dbl-homology domain of GEFs and mediate the formation of the RhoA/RhoGEF complex [110]. The C-terminus of RhoA is modified via prenylation by a geranylgeranyl-residue, enabling the translocation and anchoring of RhoA to the cell membrane as part of the activation [120].

RhoA can be activated by multiple upstream signals including GPCRs, integrins and growth factor receptors [121]. Amongst the wide spectrum of GPCRs, the sphingosine-1-phosphate receptor (S1PR) in cardiomyocytes [122], the AT_1R in smooth muscle cells [123] and the muscarinic M1 acetylcholine receptor (M_1R) in embryonic neural crest cells [117] were identified and were shown to be involved in RhoA signaling.

Once activated, GPCRs signal via associated heterotrimeric G proteins, which consists of an α- and β/γ-subunit and can be divided into four sub-classes: $G\alpha_s$, $G\alpha_{i/o}$, $G\alpha_{q/11}$ and $G\alpha_{12/13}$. By the exchange of GDP for GTP, the G-protein dissociates into the α-subunit with the bound GTP and the β/γ-dimer and further transduces the intracellular signal [124] by interacting with various downstream effectors including RhoGEFs.

For RhoA, the subfamilies of the $G\alpha_{q/11}$ and $G\alpha_{12/13}$ proteins have been shown to mediate RhoA activation. While $G\alpha_{12/13}$ proteins can activate RhoA by binding to the three RhoGEFs p115RhoGEF, PDZ-RhoGEF and the leukemia-associated RhoGEF (LARG) via their regulator of G protein signaling (RGS) domains [125], activation via the $G\alpha_{q/11}$ proteins is mediated e.g. by p63RhoGEF.

2.4.4 RhoA signaling in the heart and in cardiac disease

A variety of *in vitro* and *in vivo* studies were performed, to elucidate the role of RhoA in the heart. In cardiomyocytes, RhoA has been associated to morphological changes and induction of gene expression as part of the hypertrophic response mediated by factors such as phenylephrine, endothelin-1 or Ang II [107, 126]. Conversely, inhibition of RhoA and its effectors the Rho-associated protein kinases prevented morphological and cytoskeleton changes as well as reduced expression of hypertrophy-associated proteins like ANP and α-myosin heavy chain (α-MHC) [127-129]. One important downstream mediator of the RhoA/ROCK-dependent hypertrophic response, represents the myocardin-related transcription factor A (MRTF-A) and serum response factor (SRF), which initiate the transcriptional activation of the hypertrophic-dependent fetal gene program [130].
In vivo, several studies support the involvement of the RhoA/ROCK signaling during cardiac remodeling. It was demonstrated that RhoA was strongly activated upon pressure overload induced by transverse aortic constriction (TAC) [131] and its expression was also increased in a model of diabetic cardiomyopathy [132]. Likewise, ROCKs were found to be rapidly induced in the adult rat myocardium after TAC intervention [133] suggesting that activation of the RhoA/ROCK pathway promotes adverse effects. In accordance, pharmacological inhibition of RhoA [134] and ROCK [135-138] using selective inhibitors preserved the cardiac function and reduced cardiac remodeling.
Genetic models provided further insights regarding the impact of RhoA/ROCK signaling (Figure 2.5) for the underlying processes of cardiac remodeling. Mice with a cardiomyocyte-specific overexpression of RhoA did not develop cardiac hypertrophy as expected based on the *in vitro* data from cardiomyocytes. In contrast, these mice displayed a strong deterioration of the left ventricle with chamber dilation, interstitial fibrosis and reduced contractility and hence premature death [129]. Moreover, these animals exhibited conductive dysfunction observed by atrioventricular blocks accompanied by bradycardia [129].
Accordingly, the overexpression of the upstream G protein $G\alpha_q$ [139] and expression of a constitutive active form of $G\alpha_q$ [140] had showed a similar detrimental phenotype regarding contractility and survival with development of cardiac hypertrophy. For the downstream effectors of Rho kinases (ROCKs), a constitutive active expression of ROCK1 resulted in fibrotic cardiomyopathy and diastolic dysfunction due to increased TGF-β expression [141]. Conversely, animal studies with a ROCK1 knockout (KO) resulted in an opposite outcome regarding fibrosis. In a model of global haploinsufficient $ROCK1^{+/-}$ mice, perivascular fibrosis and associated factors as TGF-β, CTGF and collagen type III were less increased in an Ang II infusion model and TAC model, while hypertrophy was established to the same extent [142]. Furthermore, mice with a global ROCK1 deletion showed a similar phenotype with a decrease in perivascular and interstitial fibrosis accompanied by reduced expression and secretion of fibrotic factors such as TGF-β and CTGF as well as ECM proteins. No effect on the development of hypertrophy was observed [143]. This was further supported, as mice with a cardiomyocyte-specific overexpression of $G\alpha_q$ and homozygous KO of ROCK1 led to a

similar outcome regarding cardiac fibrosis and hypertrophy [143]. Recently, a mouse study with a cardiomyocyte-specific knockout of RhoA was described. These mice exhibited an impaired contractile function associated with a faster dilation, but less fibrosis and reduced expression of fibrotic genes, e.g. TGF-β [144]. Again, the development of hypertrophy was not affected suggesting a relevant role for the RhoA/ROCK pathway in the development of cardiac fibrosis thereby influencing the contractile function in the context of cardiac diseases. However, ROCK2 was proposed as the Rho kinase playing a role in cardiac hypertrophy as the cardiomyocyte-specific deletion led to a reduced hypertrophic response in an Ang II infusion model [145].

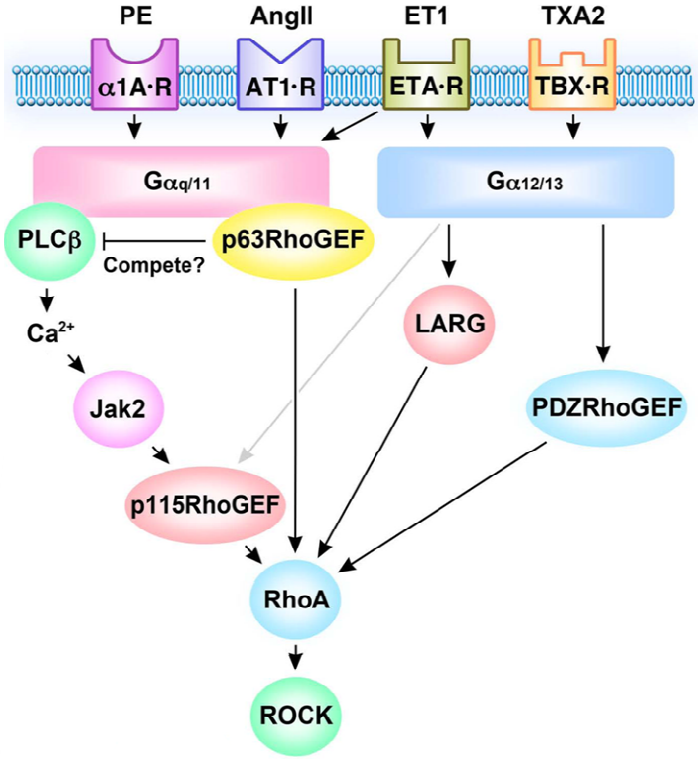

Figure 2.5: RhoA signaling in cardiovascular cells
The Scheme illustrates signaling pathways for p63RhoGEF, p115RhoGEF, LARG and PDZRhoGEF leading to RhoA activation. GPCRs for phenylephrine (PE), angiotensin (AngII), endothelin (ET-1) and thromboxane (TXA2) couple through $G\alpha_{q/11}$ and or $G\alpha_{12/13}$ to activate various RhoGEFs. Activated RhoGEFs differently or synergistically catalyze GTP loading and activation of RhoA and downstream effector Rho kinase (ROCK). Figure was adapted with modifications from Momotami and Somlyo, 2012[146].

Interestingly, inhibition of the $G\alpha_{12/13}$-pathway by cardiomyocyte-specific deletion of LARG, which regulates RhoA via $G\alpha_{12/13}$-activation, exhibited a beneficial outcome, as these mice developed no hypertrophy, less fibrosis and were protected from cardiac decompensation [131]. On the other side, it was shown that expression of RhoA can have a cardioprotective effect on cardiomyocytes in a model of ischemia/reperfusion (I/R), as the infarct area was decreased by 70% compared to control [147].

2.5 RhoGEFs

2.5.1 Structure and function of RhoGEFs

RhoGTPases are activated by Rho guanine nucleotide exchange factors (RhoGEFs), which accelerate the GDP/GTP exchange. To date, about 69 GEFs for Rho family members are described. Several GEFs for RhoGTPases are expressed preferentially in specific cells and tissues, suggesting cell- and tissue-specific effects of these GEFs.
Based on the sequence homology with the central part of the Dbl oncogene from diffuse B-cell-lymphoma cells, the first identified mammalian RhoGEF was designated Dbl [148, 149]. Proteins of the Dbl family of RhoGEF share a typical tandem motif consisting of a Dbl homology (DH) and a pleckstrin homology (PH) domain [150]. The DH domain interacts directly with the RhoGTPase and is responsible for the catalytic activity that accelerates the exchange of GDP for GTP on the RhoGTPase [110]. In tandem with the DH domain is found a pleckstrin homology (PH) domain of 140 amino acids, which modulates nucleotide exchange by the DH domain [151, 152]. By binding to phosphoinositides, PH domains have been proposed to localize Dbl proteins to plasma membranes and to regulate their GEF activity through allosteric mechanisms [110]. The RhoGEF PH domain can promote the GEF activity, when it is directly in contact to the bound GTPase or *vice versa*. It can even inhibit the GEF activity by masking the binding site of the DH domain [153]. In some RhoGEFs, the PH domain appears to autoinhibit the intrinsic GEF activity of the DH domain [154-156]. Besides this tandem motif, RhoGEFs often contain one or more additional signal transduction domains and additional PH domains [150, 157] that might play a role for the localization or control of the GEF activity [158].
Most of the Rho GEFs isolated so far display activity on RhoGTPases, at least *in vitro*. Some RhoGEFs appear to exhibit *in vivo* selectivity for a specific GTPase (e.g. Lbc for Rho,Tiam1 for Rac, and FGD1 for Cdc42), whereas others seem to act on several GTPases (e.g. Vav, Dbl and Trio) [150, 158]. Apart from receptor tyrosine kinases, a large variety of G-protein-coupled receptors (GPCRs) are upstream regulators of Rho proteins [112, 159], particularly those coupling to the $G_{12/13}$ and $G_{q/11}$ types of heterotrimeric G proteins [160]. With respect to the RhoGTPase RhoA, RhoA-specific GEFs, including p115RhoGEF, PDZRhoGEF and leukemia-associated RhoGEF (LARG) have been identified [161], which all possess a RGS homology domain for direct interaction with and activation by $G_{12/13}$ proteins.
In contrast to RhoGTPases, many RhoGEFs are low-abundance proteins with restricted expression patterns and therefore designated to be the limiting factors in the respective signaling cascades. In 2002, a novel member of the Dbl-family of GEFs that specifically activates RhoA was found: the nucleotide exchange factor p63RhoGEF

2.5.2 p63RhoGEF

The nucleotide exchange factor p63RhoGEF, encoded by the gene ARHGEF25, was originally identified by Souchet in 2002. The authors detected the human transcript in oligodendrocytes and astrocytes of the brain and in cardiomyocytes in the heart. Immunofluorescence analysis revealed that it is localized in the sarcomeric I-band of cardiomyocytes. Based on its homologues sequence (Figure 2.6), it could be classified as a member of the Dbl family of RhoGEFs [162]. p63RhoGEF is a protein of 580 amino acids and thus has a protein weight of approximately 63 kDa. It was further reported that p63RhoGEF specifically catalyzes the GDP/GTP exchange for RhoA, but is not involved in the activation of Rac1 or Cdc42 [162].
The crystal structure of the $G\alpha_q$-p63RhoGEF-RhoA complex revealed that p63RhoGEF directly binds to the activated $G\alpha_{q/11}$, but not $G\alpha_{12/13}$ subunits of heterotrimeric G proteins linking $G\alpha_{q/11}$-signaling to RhoA activation. Hence, it was postulated that p63RhoGEF is regulated by G-protein-coupled receptors (GPCRs). Further biochemical studies revealed that p63RhoGEF is activated by relieving the autoinhibition of the catalytic DH domain by the PH domain [160, 163, 164]. Moreover, p63RhoGEF is competing with PLC-β for the binding to $G\alpha_{q/11}$, as it was shown that overexpression of p63RhoGEF reduced the activation of PLC-β and hence IP_3 production [160].

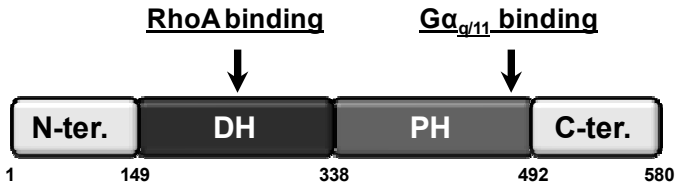

Figure 2.6: Structure of p63RhoGEF
The scheme shows the structure of p63RhoGEF and respective binding domains for interaction. N-ter. = N-terminal part, DH = Dbl homology domain, PH = pleckstrin homology domain, C-ter. = C-terminal part. The numbers refer to the sequence in amino acids.

Apart from p63RhoGEF, Trio and Duet, a splice variant of the GEF Kalirin, were identified as two other guanine nucleotide exchange factor, which contain a p63RhoGEF homologues sequence including the RhoA specific DH/PH domain. Like p63RhoGEF, these GEFs showed an interaction with $G\alpha_{q/11}$ and are thereby involved in RhoA-dependent SRF activation. In addition, an N-terminally truncated variant of p63RhoGEF, termed GEFT, was identified as a splice variant derived from the same gene and lacking the first 106 amino acids [165]. It was reported that this splice variant specifically activates Rac1 and Cdc42 [166], but later studies showed only activation of RhoA [160, 163, 164].
Moreover, Goedhart et al. demonstrated that p63RhoGEF located at the plasma membrane due to palmitoylation [152] interacts efficiently with $G\alpha_q$, while the cytoplasmatic GEFT does

not, as it lacks the N-terminal lipidation motif [167]. This was further supported by van Unen, showing that restriction to the plasma membrane is sufficient for p63RhoGEF activity to mediate RhoA-dependent actin polymerization [168]. With respect to cardiac cells, for the first time it was shown in smooth muscle cells of the rat aorta that p63RhoGEF is specifically mediating the Ang II activation from activated AT_1R to $G\alpha_q$ to RhoA/ROCK activation [169] via binding of the α subunit of $G\alpha_q$ [153, 170].

Recently, evidence for the relevance of p63RhoGEF within RhoA/ROCK signaling in cardiac disease of hypertensive patients was reported [171]. The authors compared the level of p63RhoGEF and the phosphorylation status of the direct ROCK downstream target myosin phosphatase target protein 1 (MYPT-1) and found that both were up-regulated in hypertensive patients. In contrast, in patients with the Bartter´s and Gitelman syndrome, a human model opposite to hypertension, level of p63RhoGEF and MYPT-1 were decreased [171]. The results of this clinical study together with the *in vitro* data support the importance of p63RhoGEF in Ang II-mediated RhoA signaling in the context of cardiovascular remodeling.

3 Previous results and aims of the project

As described the first time by Souchet et al. in 2002, the nucleotide exchange factor p63RhoGEF was found to be expressed in heart and brain tissue [162]. Initial experiments performed in our group aimed to determine its distribution amongst the different cells within the cardiac tissue. Immunohistochemistry stainings of neonatal and adults rat hearts using a specific antibody revealed that p63RhoGEF is predominantly expressed in cells located in and around blood vessels and cells residing in the interstitium (Figure 3.1). Amongst the different heart cells it was found that p63RhoGEF is highly expressed in smooth muscle cells followed by cardiac fibroblasts and to a lesser extent in cardiomyocytes (Wuertz, C., Dissertation "Die Rolle des Guaninnukleotid-Austauschfaktors p63RhoGEF in Physiologie und Pathophysiologie glatter Gefäßmuskelzellen", 2011).

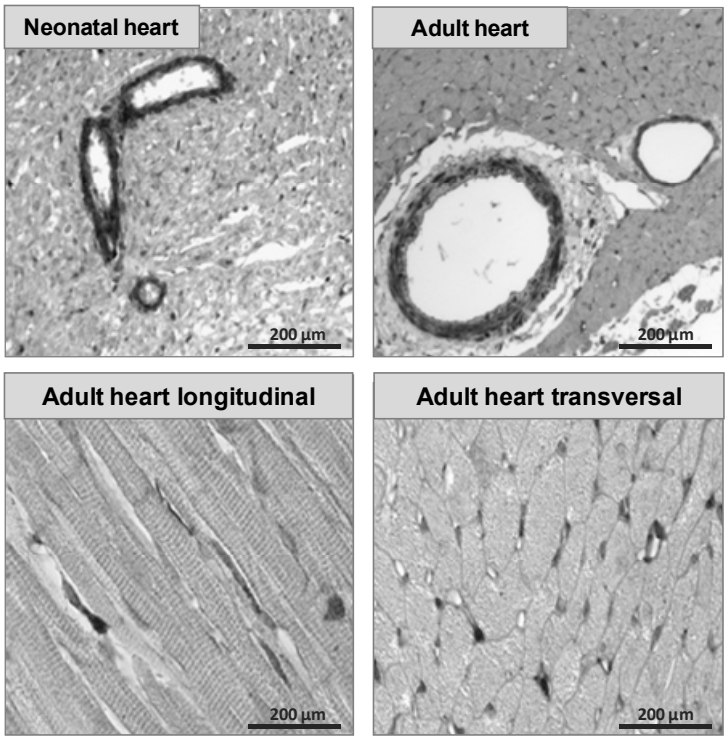

Figure 3.1: Expression of p63RhoGEF in the heart
Paraffine sections of neonatal and adult rat hearts were stained with a specific p63RhoGEF antibody. Scale bar 200 µm. *(Wuertz, C., Dissertation "Die Rolle des Guaninnukleotid-Austauschfaktors p63RhoGEF in Physiologie und Pathophysiologie glatter Gefäßmuskelzellen", 2011)*

In further experiments the endogenous function of p63RhoGEF was investigated in rat smooth muscle cells of the aorta showing that p63RhoGEF mediates the Ang II-dependent RhoA activation and is involved in the regulation of contractility. Moreover, it was

demonstrated that p63RhoGEF is a specific factor of the Ang II-induced proliferation in these cells [169].

Preliminary data in NRCM also demonstrated that overexpression of p63RhoGEF led to endothelin I (ET-1)-associated RhoA activation resulting in an enhanced CTGF secretion. Consequently, the role of p63RhoGEF in cardiac fibroblasts should be closer investigated. First experiments in neonatal rat cardiac fibroblasts illustrated that upon treatment with well-known cardiovascular GPCR agonists, Ang II was the only efficient activator for RhoA in NRCF, while ET-1 and phenylephrine (PE) did not increase the RhoA-GTP level (Figure 3.2 A).

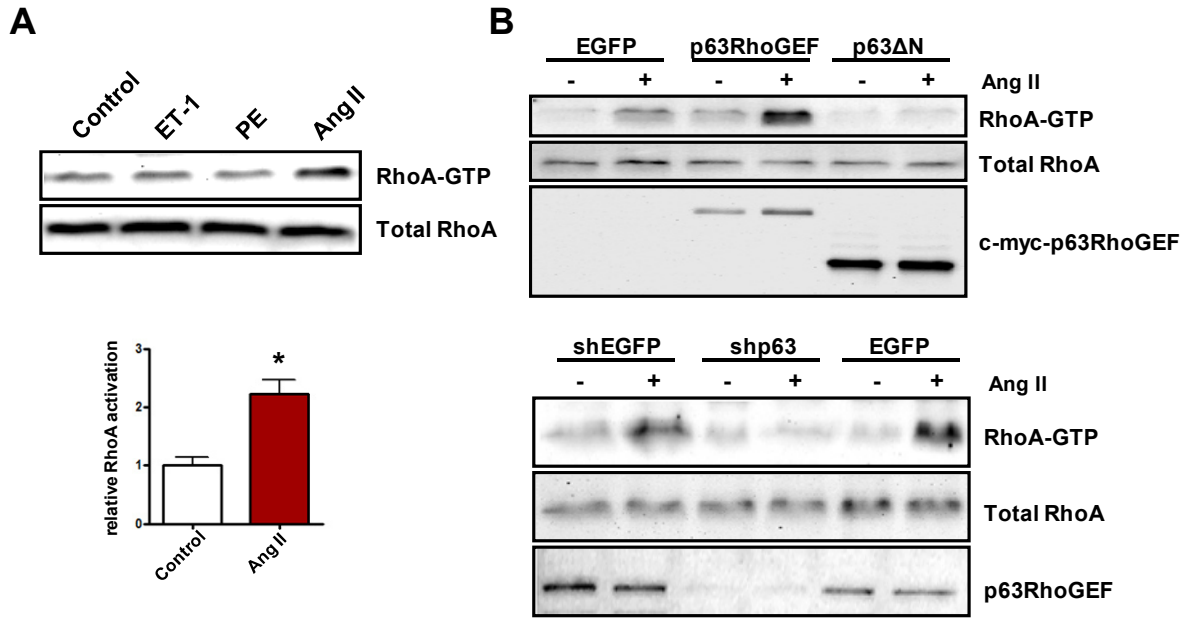

Figure 3.2: Impact of p63RhoGEF expression on the Ang II-dependent RhoA activation

(A) Serum-starved NRCF were treated with 100 nM ET-1, 10 µM PE or 100 nM Ang II for 30 sec and RhoA activation was determined by pulldown assay and subsequent immunoblot analysis. Ang II-induced RhoA activation is given relative to unstimulated control as means ± SEM, n=15, *p < 0.05 vs. control. (B) NRCFs were transduced with Ad-EGFP, Ad-p63RhoGEF or Ad-p63ΔN as well as Ad-shEGFP, Adsh-p63 and Ad-EGFP for 24 h and 100 nM Ang II was added for 30 sec. By pulldown assay and immunoblot RhoA activation was evaluated. p63RhoGEF expression was analyzed via a c-myc antibody. Representative immunoblots are shown, n = 2-3.

Experiments were performed by Christiane Vettel, Medical Faculty Mannheim, Institute for Experimental and Clinical Pharmacology and Toxicology Mannheim) (Vettel, C. Dissertation "Charakterisierung des Guaninnukleotid-Austauschfaktors p63RhoGEF als neuen Mediator der $G\alpha_{q/11}$-induzierten RhoA-Aktivierung", 2009)

Moreover, the impact of p63RhoGEF expression on the Ang II-dependent RhoA activation was examined by adenoviral infection with constructs resulting either in an overexpression of p63RhoGEF, a downregulation by shp63 or blocking of the $G\alpha_{q/11}$-pathway by the use of the p63ΔN construct. Pulldown assays of RhoA-GTP with stimulation of Ang II revealed an increase in RhoA activation when p63RhoGEF was overexpressed. In contrast,

downregulation of p63RhoGEF expression and blocking with the p63ΔN resulted in a decrease of RhoA-GTP level, clearly underlining the p63RhoGEF-dependent regulation of the GTPase RhoA in cardiac fibroblasts (Figure 3.2 B).

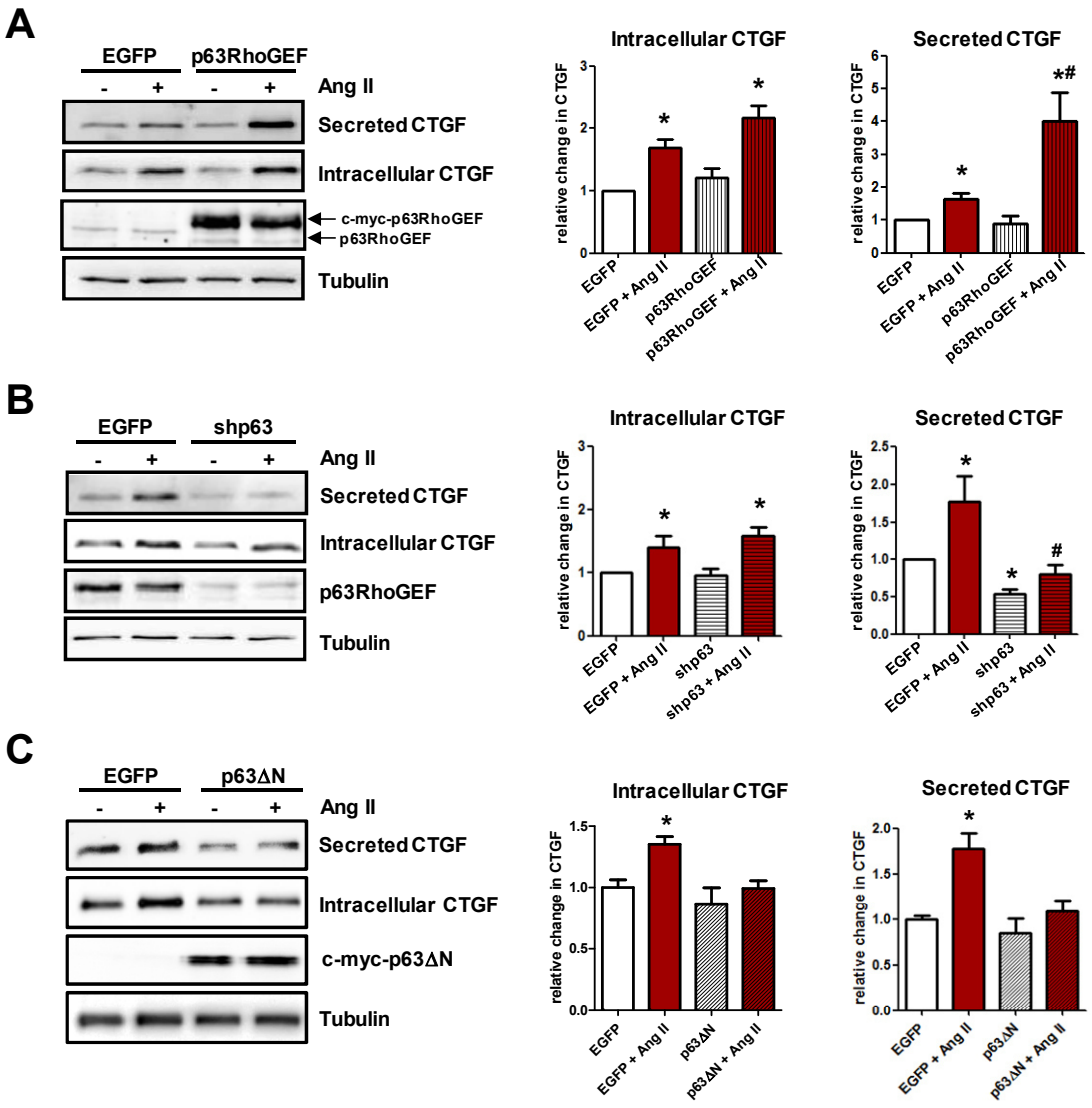

Figure 3.3: p63RhoGEF is involved in the regulation of CTGF

NRCF were transduced with Ad-EGFP (A), Ad-p63RhoGEF (B) and Ad-p63ΔN (C) for 24 h and stimulated with 100 nM Ang II for another 24 h. Cell lysates and conditioned medium were collected and the amounts of intracellular and secreted CTGF were determined by immunoblot. In addition the expression of p63RhoGEF was analyzed. Representative immunoblots are shown. Values are given as means ± SEM, normalized to tubulin and relative to EGFP as control, *$p < 0.05$ vs. EGFP, #$p < 0.05$ vs. EGFP + Ang II, n = 5-12.

Experiments were performed by Cleo Weis, Medical Faculty Mannheim, Institute for Experimental and Clinical Pharmacology and Toxicology Mannheim. (Weis, C., Dissertation "Charakterisierung und zelluläre Lokalisation des Guaninnukleotid-Austauschfaktors p63RhoGEF als Mediator der Ang II-induzierten Sekretion des profibrotischen Faktors CTGF in neonatalen kardialen Fibroblasten", 2013)

To elucidate the effect of p63RhoGEF expression downstream of the GPCR-dependent RhoA activation, expression of the connective tissue growth factor (CTGF) was investigated. The overexpression of p63RhoGEF increased the secretion of CTGF with a 4-fold change upon Ang II stimulation, while the intracellular CTGF amount was only slightly affected (Figure 3.3 A).
According to this, downregulation of p63RhoGEF led to a 70% decrease in secreted CTGF compared to the stimulated control. No significant change in the amount of intracellular CTGF was observed (Figure 3.3 B). Similar results were obtained with the blocking p63ΔN construct regarding the secretion of CTGF. In this case, also a decrease of intracellular CTGF upon Ang II stimulation was detected (Figure 3.3 C), suggesting that the expression and secretion of CTGF is p63RhoGEF-dependent, but its expression also involves other downstream factors of the $G\alpha_{q/11}$-signaling.
In addition, qPCR studies confirmed the observed effects also on mRNA level (data not shown), demonstrating that p63RhoGEF is regulating the Ang II-induced CTGF expression.
In summary, p63RhoGEF expression regulates the Ang II-dependent activation of RhoA as well as CTGF expression on mRNA level and shows a more pronounced influence on the secretion of this factor.

Based on these previous data and given the fact that RhoA and CTGF are involved in pathomechanisms of cardiac diseases, following aims of this thesis were formulated:

- Further establishment of the influence of p63RhoGEF expression within the $G\alpha_{q/11}$-p63RhoGEF-RhoA signaling cascade in a context of auto- and paracrine signaling in cardiac fibroblasts with a focus on the secretion factor CTGF in 2D cell culture and 3D models

- Investigation of the relevance of p63RhoGEF expression and its genetic deletion in the heart under healthy and load-induced disease conditions

- Determination of the role of p63RhoGEF expression and its genetic deletion in adult cardiac fibroblast

4 Material and Methods

4.1 Material

4.1.1 Consumables

Table 4.1: Consumables

Article	Specification/Type	Company
Cell culture flasks	T25, T75, T175	Sarstedt
Cell culture dishes	6, 10, 15 cm	Sarstedt/ Greiner Bio One
Cell scrapers	1.7 cm blade	Sarstedt
Cover slips	18 mm Ø, Menzel	Thermo Scientific
Cover slides	24 x 50 mm, Menzel	Thermo Scientific
Cryotubes	1.8 mL	Nunc
Rat EHM/ECT molds	Inner diameter 8 mm, outer diameter 16 mm, depth 5 mm, 2 molds per 50 mm glass dish	Internal production of the Institute
Embedding molds mega cassette	40 x 28 x 12 mm	Bio optica
Embedding molds Peel-a-way	22 x 22 x 20 mm	Polysciences
Filter syringes	Non-pyrogenic, 0.2 µM	Sarstedt
Filtration sets	250, 500, 1000 mL, 0.22 µM	Corning
Flexitip pipette tips	0.5-200 µl	Peqlab
gentleMACS	C tubes	Miltenyi Biotec
gentleMACS	Dissociator	Miltenyi Biotec
Micro-Amp optical adhesive films	PCR compatible	Applied Biosystems
Micro-Amp optical reaction plates	384-well	Applied Biosystems
Microsope slide	25 x 75 x 1 mm, Menzel Superfrost Plus	Thermo Scientific
Multi-well cell culture plates	6, 12, 24, 96-well	Greiner Bio One
Nitrocellulose membrane, Protran	Pore size 0.2 µM	Whatman, GE Healthcare
PCR reaction tubes	0.2 mL	Sarstedt
Pipette tips	10, 100, 200,1000 µl	Sarstedt
Pipette tips with filters	10, 100, 200, 1000 µl	4titude, Starlab

Reaction and centrifuge tubes	15, 50 mL	Greiner Bio One
Reaction tubes	0.5, 1.5, 2 mL	Sarstedt
Serological pipettes	1, 2, 5, 10, 25 mL	Sarstedt
Wide opening, serological pipettes	10 mL	Falcon

4.1.2 Chemicals and reagents

Table 4.2: Chemicals and reagents

Chemicals and reagents	**Company**
Acetic acid	Carl Roth
Acrylamide rotiphorese gel 30 solution (30% acrylamide/0.8% bisacrylamide, mixing ratio 37.5:1)	Carl Roth
Agarose	AppliChem
Ammonium persulfate (APS)	AppliChem
Angiotensin II, human (Ang II)	Sigma-Aldrich
Aqua B. Braun	Braun
Ascorbic acid	AppliChem
Atipamezole (Revertor)	CP-Pharma
Bromophenol blue	Sigma-Aldrich
BSA, Fraction V	Sigma-Aldrich
Buprenorphine (Temgesic)	RB Pharmaceuticals
Calcium chloride ($CaCl_2$)	AppliChem
CCG-1423	Santa Cruz
Chicken embryo extract (CEE)	Self-made
Collagen Type 1 (rat tail)	Corning
cOmplete Protease Inhibitor Cocktail Tablets	Roche Applied Science
Dimethylsulfoxide (DMSO)	Sigma-Aldrich
DMEM (1g/L glucose, 3.7 g/L $NaHCO_3$) Cat-No. F 04150	Biochrom
DMEM/F12 Glutamax, high glucose Cat-No. 31331-028	Life Technologies
DMEM Glutamax, 1 g/L glucose, pyruvate Cat-No. 21068-028	Life Technologies
DMEM Glutamax, 4.5 g/L glucose Cat-No. 42430-025	Life Technologies
DMEM (powder) Cat-No. 52100-039	Life Technologies
Dulbecco´s Phosphate-buffered saline (DPBS) without Ca^{2+}, Mg^{2+} Cat-No. 14190-094	Life Technologies
DNase I, type V	Merck
Ethanol, absolute	J.T. Baker
Ethidium bromide	Sigma-Aldrich
Fetal calf serum (FCS)	Life Technologies
Fentanyl	Rotexmedica
Flumazenil	Inresa
Fluoromount	Sigma-Aldrich
Formaldehyde (37%) (FA)	Merck
Formamide	Sigma-Aldrich

GeneRuler 100 bp DNA ladder	Thermo-Scientific
Glucose	AppliChem
Glycerol	AppliChem
Glycine	AppliChem
4-(2-hydroxyethyl)-1-piperazineethanesulfonic acid (HEPES)	Carl Roth
HEPES-buffered saline solution	Lonza
Horse serum	Life Technologies
Igepal CA-630	Sigma-Aldrich
Isoflurane	Abbvie
Isopropanol	Carl Roth
Liberase DH	Roche Applied System
Lipofectamine	Invitrogen
Magnesium sulphate monohydrate ($MgSO_4.H_2O$)	AppliChem
Matrigel basement membrane matrix	BD Biosciences
Medetomidine (Cepetor)	CP-Pharma
Metamizole (Novaminsulfon)	Ratiopharm
Methanol	Carl Roth
Mini-Protean TGX 4-15% precast protein gels	Bio-Rad
β-mercaptoethanol	AppliChem
Midazolam	Rotexmedica
MOPS	AppliChem
Non-essential amino acids (NEAA) (100x)	Life Technologies
O.C.T. Compound Tissue Tek	Sakura
Paraformaldehyde (PFA)	Self made
Paraplast	Leica
Penicillin/streptomycin (P/S) (100x)	Life Technologies
PhosSTOP Phosphatase Inhibitor Cocktail Tablets	Roche Applied Science
Ponceau S	Sigma-Aldrich
Potassium chloride (KCl)	AppliChem
Potassium dihydrogen phosphate (KH_2PO_4)	AppliChem
Precision plus protein Kaleidoscope, prestained protein standard	Bio-Rad
RNaseZap, RNase decontamination solution	Ambion
Roti-block (10x)	Carl Roth
Roti-immunoblock (10x)	Carl Roth
Roti-mark standard, protein molecular weight marker	Carl Roth
Sodium chloride (NaCl)	AppliChem
Sodium dodecyl sulfate (SDS)	AppliChem
Sodium hydrogen phosphate dihydrate ($Na_2HPO_4*2H_2O$)	AppliChem
Sodium hydroxide (NaOH)	AppliChem
Super signal west femto	Thermo Scientific
Taurin	Roth
Tetramethylethylenediamine (TEMED)	Merck
peqGold TriFast	peqlab
Tris ultrapure (Tris base)	AppliChem

Triton X-100	Carl Roth
Trypan blue	Fluka
Tween 20	Carl Roth

4.1.3 Buffers and solutions

Table 4.3: Buffers and solutions

Immunoblotting	
Lysis buffer (GST-fish buffer)	6 g Tris 8.8 g NaCl 0.4g $MgCl_2$ 100 mL glycerol (v/v) 10 mL Igepal CA-630 (v/v) ad 1 L with distilled water
10x PhosSTOP Phosphatase Inhibitor Cocktail	1 tablet solved in 1 mL distilled water
7x cOmplete Protease Inhibitor Cocktail	1 tablet solved in 1.5 mL distilled water
4x SDS loading buffer (Laemmli buffer) without glycerol	10 mL β-mercaptoethanol 5.7 g SDS 3.6 g Tris 0.2 g bromophenol blue ad 100 mL with distilled water
4x SDS loading buffer (Laemmli buffer) with glycerol	50 mL glycerol 10 mL β-mercaptoethanol 5.7 g SDS 3.6 g Tris 0.2 g bromophenol blue ad 100 mL with distilled water
5x SDS-PAGE electrophoresis buffer	15.1 g Tris 94 g glycine 5 g SDS ad 1 L with distilled water pH 8.3 HCL
12% SDS-polyacrylamide gel (50 mL)	16.5 mL distilled water 20 mL acrylamide rotiphorese gel 30 solution 12.5 mL 1.5 M Tris (pH 8.8 with HCl) 0.5 mL 10% SDS 0.5 mL 10% APS 0.02 mL TEMED
15% SDS-polyacrylamide gel (50 mL)	11.5 mL distilled water 25 mL acrylamide rotiphorese gel 30 solution 12.5 mL 1.5 M Tris (pH 8.8 with HCl) 0.5 mL 10% SDS

	0.5 mL 10% APS 0.02 mL TEMED
5% SDS-polyacrylamide gel (20 mL)	13.6 mL distilled water 3.4 mL acrylamide rotiphorese gel 30 solution 2.5 mL 1 M Tris (pH 6.8 with HCl) 0.2 mL 10% SDS 0.2 mL 10% APS 0.02 mL TEMED
10% SDS	10 g SDS ad 100 mL with distilled water
10% APS	1 g APS ad 10 mL with distilled water
Immunoblot buffer	3.02 g Tris 14.4 g glycine 200 mL methanol ad 1 L with distilled water
10x Tris-buffered saline buffer (10x TBS)	12.12 g Tris 87.65 g NaCl ad 1000 mL with distilled water pH 7.4 with HCl
Tris-buffered saline buffer with tween 20 (TBS-T)	100 mL 10x TBS 1 mL tween 20 ad 1 L with distilled water
Ponceau S	3 mL acetic acid 0.2 g Ponceau S powder ad 100 mL with distilled water
1x Roti-block	5 mL 10x Roti-block ad 50 mL with distilled water
Immunofluorescence (IF)	
4% paraformaldehyde (PFA)	40 g paraformaldehyde 200 µl 10 N NaOH 100 mL 10x PBS up to 1 L distilled water sterile filtered pH adjusted to 7.4 with HCl
0.2% Triton	1 mL 10x Triton ad 50 mL with PBS
1x Roti-immunoblock	5 mL 10x Roti-immunoblock ad 50 mL with distilled water
Genotyping	
Lysis buffer	0,05 g NaOH 0.003 g EDTA ad 50 mL with distilled water pH 12.0
Neutralization buffer	0.32 g Tris/HCl

	ad 50 mL with distilled water pH 5.0
Formaldehyde (FA) agarose gel electrophoresis	
1.2% FA gel	1.2 g agarose 10 mL 10x FA gel buffer ad 100 mL RNase-free water 1.8 mL 37% FA 3 µl ethidium bromide (10 mg/mL)
10x FA gel buffer	41.46 g MOPS 6.8 g sodium acetate 2.9 g EDTA ad 1 L distilled water pH 7.0 with NaOH
1x FA gel running buffer	100 mL 10x FA gel buffer 20 mL 37% FA ad 1 L RNase-free water
5x RNA loading buffer	16 µl saturated aqueous bromophenol blue solution 80 µl 500 mM EDTA (pH 8.0 NaOH) 720 µl 37% FA 2 mL glycerol anhydrous 3.084 mL formamide 4 mL FA gel buffer ad 10 mL RNase-free water
DNA agarose gel electrophoresis	
1% DNA agarose gel	0.5 g agarose powder 50 mL 1x TAE buffer 2 µl ethidium bromide (10 mg/mL)
50x TAE buffer	242.28 g Tris 57.1 mL acetic acid 200 mL 0.25 M EDTA (pH 8.0 with NaOH) ad 1 L with distilled water
1x TAE buffer	200 mL 50x TAE buffer ad 10 L with distilled water
Cell isolation	
Basal buffer (for isolation of AMCF)	0.2 mL DNase I (2000 U/mg) 8 g NaCl 0.37 g KCl 0.1 g Na_2HPO_4 6 g HEPES 2 g glucose ad 1 L with distilled water pH 7.3 sterile filtered

Digestion buffer (for isolation of AMCF)	0.5 g BSA 80 mg Collagenase I (245 U) 120 µL Dispase (5000 U/mg) 240 µL 2.5% Trypsin 376 µL 0.1 M $CaCl_2$ ad 50 mL basal buffer
10x Perfusion buffer (for isolation of AMCF by Langendorff)	65.922 g NaCl 3.506 g KCl 816.6 mg KH_2PO_4 1.0679 g Na_2HPO_4 * 2 H_2O 2.958 g $MgSO_4$ * 7 H_2O 10.08 g $NaHCO_3$ 10.01 g $KHCO_3$ 23.831 g HEPES ad 1 L with distilled water sterile filtered pH 7.4 with 5 N NaOH
1x Perfusion buffer (for isolation of AMCF by Langendorff)	50 mL 10x perfusion buffer 0.5 g BDM 0.5 g glucose 1.8 g Taurin 0.5 g $NaHCO_3$ ad 0.5 L
Digestion buffer (for isolation of AMCF by Langendorff)	29.6 mL 1x perfusion buffer 3,75 µL $CaCl_2$ (100mM) 300 µL 2.5% trypsin 300-450 µL liberase
Stop buffer 1	2.5 mL 1x perfusion buffer 0.025 g BSA 1.25 µL $CaCl_2$
Stop buffer 2	4,75 mL 1x perfusion buffer 0.05 g BSA 1.9 µL $CaCl_2$
Calcium- and bicarbonate- free Hanks with HEPES (CBFHH)	40 mL NaCl stock (3.42 M) 10 mL KCl stock (0.54 M) 10 mL $MgSO_4$ stock (0.081 M) 10 mL KH_2PO_4 stock (0.044 M) 10 mL Na_2HPO_4*2 H_2O stock (0.034 M) 10 mL glucose stock (0.56 M) 100 mL HEPES stock ad 1 L with distilled water sterile filtered pH 7.4 with NaOH
HEPES	47.66 g HEPES ad 1 L with distilled H_2O pH 7.4 with NaOH sterile filtered

DNase I stock solution	100 mg DNase I type V ad 100 mL distilled water
0.4% Trypan blue	0.4 mg trypan blue ad 100 mL distilled water
Contraction experiments	
Calcium-free Tyrode's solution	40 mL stock I 38 mL stock II 20 mL stock III 1 g glucose 100 mg ascorbic acid ad 1 L distilled water
Stock I (0.2 mM $CaCl_2$)	175 g NaCl 10 g KCl 25 mL $MgCl_2$ 2.22 mL $CaCl_2$ ad 1 L with distilled water
Stock II	50 g/L $NaHCO_3$ ad 1 L with distilled water
Stock III	5.8 g/L Na_2HPO_4 ad 1 L with distilled water
0.02 M $CaCl_2$	0.11 g $CaCl_2$ ad 50 mL with distilled water
10x DMEM	13.3 mg DMEM (powder) ad 10 mL with distilled water sterile filtered
2x DMEM	1 mL 10x DMEM 1 mL Horse serum 0.2 mL CEE 0.1 mL Pen/Strep Ad 5 mL with distilled water sterile filtered

4.1.4 Cell culture media

Table 4.4: Cell culture media

Fibroblast growth medium (NRCF)	DMEM GlutaMAX, 4.5 g/L glucose 10% FCS , 1% Pen/Strep (100x)
Fibroblast growth medium (AMCF)	DMEM/F12 GlutaMAX, high glucose 10% FCS, 1% Pen/Strep (100x) 100 µM ascorbic acid
Non-cardiomyocyte medium (NKM)	DMEM GlutaMAX, 1 g/L glucose 10% FCS (heat inactivated at 56°C for 30min) 1% Pen/Strep (100x)
Serum-free medium	DMEM GlutaMAX, 1 g/L glucose 10% FCS, 1% Pen/Strep (100x)

EHM medium	DMEM, 1g/L glucose, $NaHCO_3$, 11.6% Horse serum 2.3% CEE 1% Pen/Strep (100x)

4.1.5 Kits

Table 4.5: Kits

Kit	Application	Company
Dual-Luciferase reporter assay system	Detection of luminescence	Promega
5x HOT FIREPOL EvaGreen qPCR Mix Plus	qRT-PCR	Solis Biodyne
GoTaq green master mix	PCR	Promega
G-LISA RhoA Activation Assay	Detection of GTP-bound RhoA by luminescence	Cytoskeleton
Lumi-light western blotting substrate	Chemiluminescence protein blot visualization	Roche
Neonatal Heart Dissociation Kit, mouse and rat	Isolation of neonatal cardiac fibroblasts	Miltenyi Biotec
Revert Aid First Strand cDNA Synthesis Kit	RNA reverse transcription into cDNA	Thermo-Scientific
RNeasy Mini Kit	Total RNA isolation	Qiagen
Super signal west femto maximum sensitivity substrate	Chemiluminescence protein blot visualization	Thermo-Scientific

4.1.6 Enzymes

Table 4.6: Enzymes

Enzyme	Company
Collagenase I (245 U)	Worthington
Dispase (5000 U)	Corning
Liberase DH	Roche Applied Science
Trypsin-EDTA 0.05%	Life Technologies
Trypsin 2.5%	Gibco

4.1.7 Antibodies

Table 4.7: Primary antibodies

Primary Antibody against	Dilution		Source	Type/Clone	Cat. No.	Company
	IB	IF				
Acetylated tubulin	1:2000	1:500	mouse	monoclonal/ 6-11B-1	T6793	Sigma-Aldrich
α-actinin	1:2000	1:1000	mouse	monoclonal/ EA-53	A7811	Sigma-Aldrich
α-tubulin	1:2000	not used	mouse	monoclonal/ B-5-1-2	T5168	Sigma-Aldrich
β-actin	1:7500	not used	mouse	monoclonal/ AC-74	A2228	Sigma-Aldrich
c-myc	Not used	1:2500	mouse	monoclonal/ 9E10	M4439	Sigma-Aldrich
c-myc	1:200	1:150	rabbit	polyclonal/ A14	sc-789	Santa Cruz
Cofilin	1:200	not used	rabbit	monoclonal/ D3F9	5175	Cell Signaling
CTGF	1:50	1:200	goat	polyclonal/ L-20	sc-14939	Santa Cruz
ERM (Ezrin/ Radixin/Moesin)	1:1000	not used	rabbit	polyclonal	3142	Cell Signaling
Gm130	not used	1:500	mouse	monoclonal/ 35	610822	Beckton Dickinson
GOPC	not used	1:150	rabbit	polyclonal	HPA024018	Sigma-Aldrich
KDEL	not used	1:200	rabbbit	monoclonal/ EPR12668	176333	Abcam
LAMP-2	not used	1:200	rabbit	polyclonal	HPA029100	Sigma
p63RhoGEF/GEFT	1:500	not used	rabbit	polyclonal	51004-1-AP	Proteintech
PathScan Multiplex Western Cocktail I (P-p90RSK, P-Akt, P-p44/42 MAPK, P-S6, Rab11)	1:200	not used	rabbit	monoclonal	5301	Cell Signaling
P-Cofilin	1:1000	not used	rabbit	monoclonal/ 77G2	3313	Cell Signaling
P-ERM (Ezrin/ Radixin/Moesin)	1:1000	not used	rabbit	monoclonal/ 48G2	3726	Cell Signaling
RhoA	1:200	not used	mouse	monoclonal/ 26C4	sc-418	Santa Cruz
sm-actin	1:2500		mouse	monoclonal 1A4	A5228	Sigma-Aldrich

SRF	not used	1:100	rabbit	polyclonal/ G20	Sc-335	Santa Cruz
Vimentin	1:2000	not used	mouse	monoclonal/ V9	V6630	Sigma-Aldrich
Vinculin	1:2000	not used	mouse	monoclonal/ hVIN-1	V9264	Sigma-Aldrich

Table 4.8: Horseradish peroxidase (HRP)-conjugated secondary antibodies for immunoblotting

Secondary antibody (HRP-coupled) against	Dilution	Source	Catalogue No.	Company
Goat IgG	1:10000	Donkey	sc-2020	Santa Cruz
Mouse IgG	1:10000	Rabbit	A9044	Sigma-Aldrich
Rabbit IgG	1:40000	Goat	A9169	Sigma-Aldrich

Table 4.9: Fluorophore-conjugated secondary antibodies for immunofluorescence

Secondary antibody against	Dilution	Fluorophore	Source	Catalogue No.	Company
Goat	1:1000	AlexaFluor 633	Donkey	A-21028	Life Technologies
Mouse	1:300	AlexaFluor 488	Goat	115-545-003	Jackson Immuno Research
Mouse	1:500	Cy3	Goat	115-165-068	Jackson Immuno Research
Mouse	1:1000	AlexaFluor 568	Goat	A-11004	Life Technologies
Rabbit	1:500	Cy3	Goat	305-165-003	Jackson Immuno Research
Rabbit	1:500	AlexaFluor 594	Goat	111-585-003	Jackson Immuno Research
Rabbit	1:1000	AlexaFluor 633	Goat	A-21070	Life Technologies

Table 4.10: Fluorescence-labeled cell dyes

Fluorescent dyes	Stock concentration	Dilution	Company
DAPI	1 mg/mL	1:1000	Roche
FITC-phalloidin	0.5 mg/mL	1:1000	Sigma-Aldrich
TRITC-phalloidin	0.5 mg/mL	1:1000	Sigma-Aldrich
Wheat germ agglutinin (WGA), AlexaFluor 488 conjugate	1 mg/mL	1:200	Life Technologies
Wheat germ agglutinin (WGA), AlexaFluor 647 conjugate	1 mg/mL	1:200	Life Technologies

4.1.8 Primer

Table 4.11: Designed qRT-Primer used for endpoint PCR and qRT-PCR

Gene	Primer	Sequence (5´ to 3´)	Annealing Temperature (°C)
α-MHC	Forward	CCA ATG AGT ACC GCG TGA A	57.5 °C
	Reverse	ACA GTC ATG CCG GGA TGA T	57.5 °C
ANP (Nppa)	Forward	CAT CAC CCT GGG CTT CTT CCT	63.2 °C
	Reverse	TGG GCT CCA ATC CTG TCA ATC	61.2 °C
β-MHC	Forward	ATG TGC CGG ACC TTG GAA	60 °C
	Reverse	CCT CGG GTT AGC TGA GAG ATC A	60 °C
Biglycan	Forward	CTG AGG GAA CTT CAC TTG GA	58.4 °C
	Reverse	CAG ATA GAC AAC CTG GAG GA	58.4 °C
BNP (Nppb)	Forward	AAG TCC TAG CCA GTC TCC AGA GC	66.6 °C
	Reverse	CTT CAG TGC GTT ACA GCC CAA AC	64.6 °C
Calp1	Forward	CCA GCA TGG CCA AGA CAA AAG	61.2 °C
	Reverse	GGA TCA TAG AGG TGA CGC CG	62.5 °C
Calsequestrin	Forward	GCC CAA CAG TGA AGA GGA G	59.5 °C
	Reverse	TCT AAG AAC TCA TAG CCA TCA GG	60.9 °C
CD31	Forward	AAC CCG TGG AGA TGT CCA GGC CAG C	64.4 °C
	Reverse	ACA CCG TCT CTG TGG CTC TCG TTC CC	64.2 °C
Col1a1	Forward	ACG CCA TCA AGG TCT ACT GC	60.5 °C
	Reverse	ACT CGA ACG GGA ATC CAT CG	60.5 °C
Col3a1	Forward	CCATGACTGTCCCACGTAAGCAC	66.6 °C
	Reverse	GGAGGGCCATAGCTGAACTGAAAAC	67.4 °C
CTGF	Forward	CCG GGT TAC CAA TGA CAA TA	56.4 °C
	Reverse	CAC ACC CCA CAG AAC TTA GC	60.5 °C
Desmin	Forward	GGC GAG GAG AGC AGG ATC AA	62.5 °C
	Reverse	CTG TGT AGC CTC GCT GAC AAC	63.2 °C
FSP-1/S100A4	Forward	TTC AGC ACT TCC TCT CTC TTG GT	62.9 °C
	Reverse	TTC ATC TGT CCT TTT CCC CAG GA	62.9 °C
LGALS3	Forward	ATG CTG ATC ACA ATC ATG G	53.0 °C
	Reverse	CCT GAA ATC TAG AAC AAT CC	54.3 °C
MMP2	Forward	TCCCCCGATGCTGATACTGA	60.5 °C
	Reverse	CCGCCAAATAAACCGGTCCTT	61.2 °C
PBGD	Forward	CCT GAA ACT CTG CTT CGC TG	60.5 °C
	Reverse	CTG GAC CAT CTT CTT GCT GAA	59.5 °C
p63RhoGEF	Forward	AGG GGA GGT GTC CAG AGT GCT G	67.9 °C
	Reverse	CTG GCC TGA CAG GGA GGA GTG T	67.9 °C
RhoA	Forward	GTA GAG TTG GCT TTA TGG GAC AC	62.9 °C
	Reverse	TGG GAT GTT TTC TAA ACT ATC AGG G	62.5 °C
sm22	Forward	GTG AGC CAA GCA GAC TTC CAT	61.2 °C
	Reverse	TGT TGA GGC AGA GAA GGC TTG	61.2 °C

sm-actin	Forward	GAG AAG CCC AGC CAG TCG	60.8 °C
	Reverse	TCC AAC CAT TAC TCC CTG ATG TCT	63.3 °C
sm-MHC	Forward	GGT GAA CGC CCT CAA GAG CA	62.5 °C
	Reverse	CCT CGT TTC CTC TCC TGG TG	62.5 °C
TGF-β	Forward	AGA GCC CTG GAT ACC AAC TA	58.4 °C
	Reverse	TGT TGG TTG TAG AGG GCA AG	58.4 °C
VE-Cadherin	Forward	ACT ATG TGG GAA AGA TCA AGT C	58.4 °C
	Reverse	GAT CTT GCC AGC AAA CTC TC	58.4 °C

Table 4.12: Primer for genotyping

Gene	Primer	Sequence (5´ to 3´)	Annealing Temperature (°C)
Lox1	Forward	CTG GAA TTG CTG CCA GAC TGT AGC	66.9 °C
SDL2	Reverse	CCA CCG CAG CCA AAC TTC TC	62.5 °C
Nrev	Reverse	ATC CTG AGC ATA GCA CAG ATC TGC GG	69.5 °C

4.1.9 Plasmids

Table 4.13: Plasmids

Name	Plasmid	Company
pSRE.L	Luciferase reporter plasmid (“plasmid serum response element luciferase”)	Invitrogen
pRL.TK	Control reporter plasmid (“plasmid renilla luciferase thymidine kinase”)	Invitrogen

4.1.10 Viruses

Table 4.14: Viruses

Virus	Sequences
Ad-CTGF	He et al, 1998
Ad-EGFP	EGFP sequence
Ad-p63RhoGEF	c-Myc-tag; human p63RhoGEF sequence aa 1-580; EGFP
Ad-p63ΔN	c-Myc-tag; human p63RhoGEF sequence aa 295-580; EGFP

4.1.11 Animals

Table 4.15: Animals

Animal	Strain
Mice	Mixed C57/Bl6-J x 129S1 x SvIm-J, inGenious, NY, USA; N2 generation of backcrossing on C57Bl/6-J
Rats	Wistar-Kyoto, own breed

4.1.12 Devices

Table 4.16: Devices

Device	Model	Company
Autoclave	VX-150	Systec
Cell counter	Casy	Roche
Cell counting chamber	Neubauer	Labor Optik
Cell culture incubator	Labotect Incubator C 200	Labotect
Cell sieve	Cell dissociation sieve - tissue grinder kit (250 µm pore size)	Sigma-Aldrich
Centrifuge bench top	Centrifuge 5804 R	Eppendorf
Centrifuge bench top	PCV-2400	Grant-bio
Cell culture centrifuge	Centrifuge 5417 R	Eppendorf
Cell culture centrifuge	Megafuge 3.0R	Heraeus
Chemiluminescence imaging system	ChemiDoc MP	Bio-Rad
Contraction setup	IOA-5301	FMI
Cryotome	Leica CM3050 S	Leica
Double distilled water system	Milli-Q	Millipore
Electric power supply and control (immunoblotting)	Powerpac	Bio-Rad
Electric power supply and control (agarose gel)	Powerpac P25T	Biometra
Freezing Container	Mr. Frosty	Nalgene
Gel electrophoresis chamber (agarose)		Peqlab
Gel electrophoresis chamber (immunoblot)	Mini Protean Tetra Cell 4-gel system	Bio-Rad
Gel imager	GelDoc	Bio-Rad
Heating block	Thermo mixer compact	Eppendorf
Heating plate (magnetic)	RCT basic	Janke u. Kunkel IKA Labortechnik
Homogenizer	Polytron PT 1600E	Kinematica

Immunoblot chamber	Mini Trans-Blot Cell	Bio-Rad
Inverted fluorescence microscope	Axiovert 200	Zeiss
Inverted fluorescence microscope with climate chamber	Olympus IX 81	Olympus
Inverted light microscope	Primovert	Zeiss
Microplate reader for luminescence	GloMax Luminometer	Promega
Microscope camera	CAM-XM10-T-Camera	Olympus
Microscope filter Cy5	BP 635/40	Olympus
Microscope filter DAPI	BP 403/12	Olympus
Microscope filter EGFP	BP 470/20	Olympus
Microscope filter FITC	BP492/18	Olympus
Microscope filter Texas Red	BP 572/23	Olympus
Microscope objective 20x	LUCPLFLN20xPH|0.45	Olympus
Microscope objective 40x	LUCPLFLN40xPH|0.60	Olympus
Microscope objective 60x	PlanApo N60x|1.42 oil	Olympus
Microscope objective 0.8x	NeoLumar S	Zeiss
Microscope objective 10x	EC Plan-Neofluar|0.3	Zeiss LSM 710
Microscope objective 20x	EC Plan-Neofluar|0.5	Zeiss LSM 710
Microscope objective 63x	Plan-Apochromat|1.4 oil	Zeiss LSM 710
Microtome	Leica RM2255	Leica
Multiparameter cell analyzer	Cellavista	Roche
Paraffin embedding machine	Leica EG1150H	Leica
pH meter	WTW	Inolab
Pipettes	Pipetman	Gilson
Plate reader	FlexStation3	Molecular Devices
Phasic stretcher		Internal scientific workshop
Pump	ME2	Vacuubrand
Real-time PCR system	TaqMan 7900HT Fast Real-Time-PCR System	Applied Biosystems
Scale	Portable	Sartorius
Shaker (4°C)	GFL 3025	GFL
Shaker	Vibramax 100	Heidolph
Shaker	GFL 3016	GFL
Special accuracy scale	Research M power	Sartorius
Spectrophotometer	Nanodrop 1000	peqlab
Stereomicroscope	Stemi 2000	Zeiss
Stereomicroscope	SteReo Lumar V.12	Zeiss
Stereomicroscope camera	AxioCam MRC	Zeiss
Sterile workbench	Telstar Bio II A	Prettl
Stimulator	STI 08 Current stimulator	FMI

Stretcher	STI 08 Current stimulator	FMI
Thermocycler	Mastercycler gradient	Eppendorf
Tissue Lyzer II		Qiagen
UV agarose gel imaging system	Gel doc XR	Bio-Rad
UV lamp plate	TI 1	Biometra
Vibratome	Leica VT1000S	Leica
Vortexer	VF 2 Vortexer	Janke u. Kunkel IKA Labortechnik
Water bath	1002	GFL

4.1.13 Software

Table 4.17: Software

Software	Use/Analysis	Company
Amon32	Analysis of contraction measurement	FMI VitroDat 3.52
AxioVision Rel. 4.8	Imaging of EHM/ECT tissue and whole heart sections	Zeiss
BeMon32	Contraction measurement	FMI VitroDat 3.52
Fiji (Image J 5.1)	Evaluation of fluorescence images	National Institutes of Health, USA
GloMax 1.9.2	Luminescence measurement	Promega
GraphPad prism 5.0	Statistical calculations/evaluation and graphical drawing	GraphPad
Image Lab 5.1	Operating the ChemDoc MP system and for semi-quantification of western blots	Bio-Rad
Quantity One 4.6.5	Operating the ChemDoc MP system and for semi-quantification of western blots	Bio-Rad
SDS 2.4	Operating the TaqMan 7900HT Fast Real-Time-PCR System, and its data analysis	Applied Biosystems
SoftMax Pro 5.4	Multi-mode microplate reader measurements	Molecular Devices
Vevo2100 1.6.0	Evaluation of Echocardiography measurements	Vevo
Zen2009	Confocal imaging of cells	Zeiss
Xcellence pro	Operating the Olympus microscopy system for cell imaging	Olympus

4.2 Methods

4.2.1 Animal studies

4.2.1.1 Animal care and experiments

Animal care and mouse experiments were carried out in accordance with the guidelines of The Institutional Animal Aare and Use Committee of LAVES, the Lower Saxony, Germany, State Office for Consumer Protection and Food Safety. Mice were kept on a daily 12 h light/dark cycle with water and food *ad libitum*.

4.2.1.2 Generation of a global p63RhoGEF-knockout line

As a first step, a mouse line containing flox sites on the p63RhoGEF allele was generated by inGenious Targeting Laboratory, Inc. (New York, USA). Using the Cre/*loxP* recombination system, flox sites with putative start codons were integrated flanking exon 1 and 2 of the p63RhoGEF gene located on chromosome 12. At an age of 2 months, heterozygous p63RhoGEF $^{wt/flox}$ mice were shipped and mated with each other to obtain homozygous p63RhoGEF $^{flox/flox}$ mice. In a second step, these mice were mated with animals of an Ella-Cre-line, which express the enzyme Cre-recombinase from early embryonic stadium on, enabling a general knockout of p63RhoGEF. By expression of the Cre-recombinase, exon 1 and 2 were excised at the flanked flox sites resulting in a deletion of the start codon. In order to receive siblings with all three combinations of genoytypes (WT, HET, KO) in further F1 generations, heterozygous p63RhoGEF $^{WT/-}$ mice were mated with each other.
Design of p63RhoGEF-knockout line, verification of the knockout and initial matings of the founder generation were performed by Dr. Christina Würtz, University Medical Center Göttingen.
All mice experiments as well as isolation of mouse adult cardiac fibroblasts (AMCF) were performed using mice from the N2 generation of backcrossing.

4.2.1.3 Genotyping

For genotyping, DNA was extracted from tail or ear biopsies via hot-shot method [172]. For this, biopsies were incubated with alkaline lysis buffer for 1h at 95 °C. The reaction was stopped by adding neutralization buffer, and the extracted DNA was directly used for end-point PCR as described in section 4.2.3.7. For detection of the full length p63WT allele as well as the respective p63KO allele, the following primer combinations were used:

Table 4.18: Designed primer and fragment sizes for genotyping

Primer combination	Fragment and size (bp)		
	WT	HET	KO
Lox 1 x SDL2	345 bp	345 bp	no PCR product
Lox 1 x Nrev	no PCR product	591 bp	591 bp

Genotyping was carried out with the support of technical assistant Beate Ramba.

4.2.1.4 Transverse aortic constriction (TAC) surgery

Ten to twelve-week-old male and female mice (mixed C57/Bl6-J x 129S1 x SvIm-J background) were used for transverse aortic constriction (TAC) or sham surgery. In this process, mice were anesthetized by intraperitoneal (i.p.) injection of Medetomidin (0.5 mg/kg) and Midazolam (5 mg/kg), for pain relief Fentanyl (0.05 mg/kg) was injected. The aortic arch was exposed via median thoracotomy and a constriction between the first and second left carotid artery was created using a 6-0 suture and tied against a 27-gauge needle. Sham surgeries were performed in the same way without constriction of the aorta.
As antagonizing narcotics Atipamezol (2.5 mg/kg) and Flumazenil (0.5 mg/kg) and for post-procedural pain relief buprenorphine (0.05-0.1 mg/kg) were injected subcutaneously (s.c). In addition, all animals received metamizole for pain relief in the drinking water 2 days before and 7 days after surgery. Body weight and physical constitution was monitored daily within the first week after surgery.

4.2.1.5 Echocardiography

Echocardiography was performed before and 1, 2 and 5 weeks after TAC or Sham surgery under 1% isoflurane anaesthesia with a 30 MHz transducer. Cardiac functional parameters were analyzed using the Vevo2100 system (Vevo). Transverse aortic flow velocities were measured by pulse-waved Doppler with a 20 MHz transducer 3 days after surgery and pressure gradients were calculated.

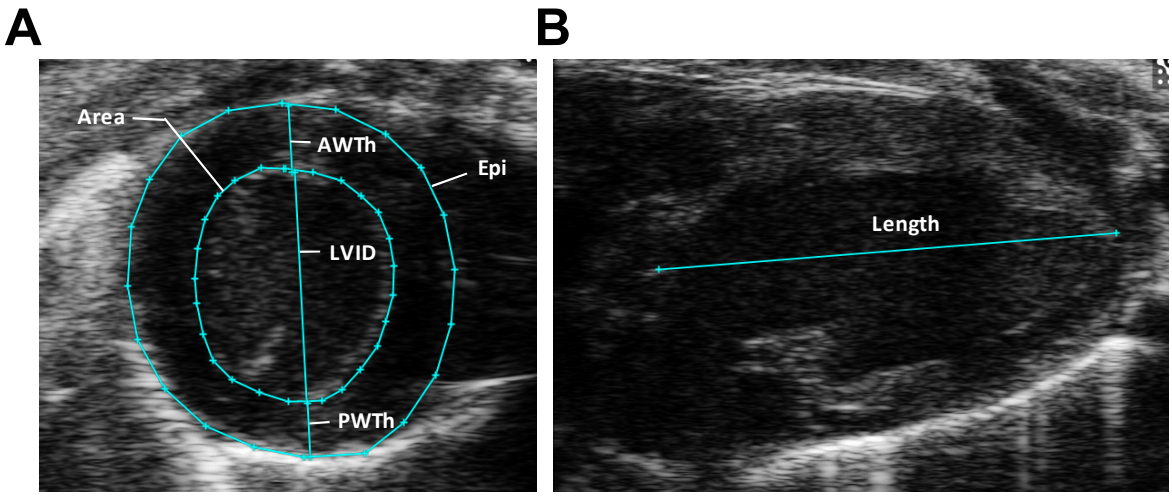

Figure 4.1: Measurements of echocardiography
Exemplified analysis of echocardiography using the Vevo2100 software. (A) Cross-sectional heart of a mouse in systole. (B) Longitudinal section of a mouse heart in systole. Abbreviations of measured parameters: AWTh = Anterior wall thickness, LVID = Left ventricular inner diameter, PWTh = Posterior wall thickness, Area = Area of cross-sectional left ventricular lumen, Epi = Epicardium, Length = Longitudinal axis

Following parameters of echocardiography measurements were obtained and analyzed:

Table 4.19: Directly measured parameters of echocardiography

Abbreviation	Cardiac Parameter	Unit
Area d	Area of cross sectional left ventricular lumen in diastole	mm^2
Area s	Area of cross sectional left ventricular lumen in systole	mm^2
AWTh d	Anterior wall thickness in diastole	mm
AWTh s	Anterior wall thickness in systole	mm
BW	Body weight	g
BT	Body temperature	°C
Epi s	Epicardium in systole	mm^2
HR	Heart rate	beats/min
L d	Axis longitudinal in diastole	mm
L s	Axis longitudinal in systole	mm
LVID d	Left ventricular inner diameter in diastole	mm
LVID s	Left ventricular inner diameter in systole	mm
PWTh d	Posterior wall thickness in diastole	mm
PWTh s	Posterior wall thickness in systole	mm

Table 4.20: Calculated parameters of echocardiography

Abbreviation	Cardiac Parameter	Unit	Calculation
AWThF	Anterior wall thickness fractioning	%	(AWTh d – AWTh s)/ AWTh d * 100
CI	Cardiac index	%	CO/BW * 1000
CO	Cardiac output	%	SV*HR/1000
EF	Ejection fraction	%	(Vol d – Vol s)/ Vol d *100
FAS	Fractional area shortening	%	(Area d – Area s)/ Area d * 100
FS	Fractional shortening	%	(LVID d – LVID s)/ LVID * 100
LVW/BW	Left ventricular weight/body weight	mg/g	LVW/BW
LVW	Left ventricular weight	mg	1.05 * (5/6)* (Epi s * (L s + (AWTh s + AWTh d) /2)) – Area s * L s))
PWThF	Posterior wall thickness fractioning	%	(PWTh d – PWTh s)/ PWTh d * 100
SV	Stroke volume	µL	Vol d – Vol s
Vol d	Volume diastole	µL	(5/6) * (Area d * L d)
Vol s	Volume systole	µL	(5/6) * (Area s * L s)

TAC surgeries and echocardiography was carried out with the help of the SFB 1002 Service Unit (TP S).

4.2.1.6 Organ withdrawal

At the end of the study, mice were sacrificed by cervical dislocation under isoflurane anaesthesia. Organs were quickly excised and either directly fixed with 4% PFA over night for histological analysis and/or immediately frozen in liquid nitrogen and kept at -80 °C for RNA and protein isolation.
In the case of heart samples, the organs were perfused with PBS to remove residual blood and cut axially in two pieces. The upper half of the hearts was used for histological investigations, whereas the apex was used for RNA and/or protein isolation.
In addition, the tibias of the hind legs were prepared and the length measured.

4.2.2 Cell biological methods

4.2.2.1 Isolation of adult mouse cardiac fibroblasts (AMCF)

Cell isolation by collagenase I and dispase digestion

Adult (around 40-60-week-old) female and male mice were anesthetized with isoflurane and sacrificed by cervical dislocation. Chests were opened by cutting the diaphragm and costal arch of the animals and hearts were excised and kept in basal DMEM/F12 on ice. All following steps were carried out under sterile condition at a workbench. To remove the blood, hearts were washed with ice-cold PBS until no further blood was visible. After that, atria were removed, and ventricles were cut into pieces of 1-2 mm^2 in size. The minced tissue was washed with ice-cold PBS until the supernatant remained clear. Then, 2.5 mL pre-warmed digestion buffer per heart was added and incubated for 10 min in a metal block at 37 °C shaking the tubes every 2 min. After sedimentation of the tissue pieces, the supernatant containing the cardiac fibroblasts was collected in a new tube. In order to stop the activity of the collagenase I/dispase enzymes, DMEM/F12 growth medium containing FCS was added and the samples were kept on ice. The above described digestion step was repeated 5-7 times until the tissue was almost completely digested and the supernatant stayed clear. Afterwards, the collected supernatants were centrifuged for 5 min at 1200 rpm at 4 °C, the cell pellet was washed with ice-cold PBS and centrifuged again. Then the cell pellet was resuspended in AMCF growth medium and cells were counted using the CASY cell counting system and seeded in cell culture flasks. After 1 h at 37 °C in an incubator with 5% CO_2, the supernatant was aspirated, cells were washed twice with PBS and AMCF growth medium was added. The next day, cells were washed again once with PBS, and fresh AMCF growth medium was added. The obtained cardiac fibroblasts were further cultivated in a humidified incubator at 37 °C with 5% CO_2 with medium changes every 2-3 days until they reached 70-80% confluency. Cells were then further passaged as described in section 4.2.2.3. For experiments only passage 1 and 2 cardiac fibroblasts were used.

Cell isolation by Langendorff method

Another technique to obtain cardiac fibroblasts is the isolation via Langendorff perfusion. This method is primarily used to isolate cardiomyocytes, but cardiac fibroblasts can also be obtained [173].

In brief, adult male mice were sacrificed under isoflurane anesthesia by cervical dislocation, hearts together with the *Aorta ascendens* were excised, washed and perfused in ice-cold 1x perfusion buffer, and then digested for 10 min at 37 °C with liberase containing digestion buffer. Digestion was stopped by adding BSA-containing stop buffer 1. Hearts were first

mechanically disrupted for 30 sec and then triturated for 2 min. After sedimentation of the cardiomyocytes, the supernatant containing mainly cardiac fibroblasts was collected. Next, the cardiomyocyte pellet was resuspended with stop buffer 2 and incubated for 10 min. Both supernatants were then combined and cells were preplated for 45 to 60 min in AMCF growth medium. Afterwards, the medium was changed and fibroblasts were cultivated in a humidified incubator with 5% CO_2 at 37 °C until confluency was reached.

Cardiac fibroblasts isolated via Langendorff digestion were kindly provided by Sebastian Pasch, Institute of Pharmacology, University Medical Center Göttingen.

4.2.2.2 Isolation of neonatal rat cardiac fibroblasts (NRCF)

Cardiac fibroblasts were isolated from neonatal Wistar rats (postnatal day 0 to 3) following the instructions of the Neonatal Heart Dissociation Kit (gentleMACS, Miltenyi Biotec). Briefly, rats were sacrificed by decapitation and hearts were collected in ice-cold CBFHH buffer. Continuing under sterile conditions, atria were removed and ventricular tissue was cut into pieces of 1-2 mm^2 size and washed two times with CBFHH buffer. Next, the tissue was transferred into two gentleMACS C tubes, and 2.5 mL or 3.75 mL of enzyme mix per tube was added (as shown in table 4.21) and incubated for 15 min at 37 °C.

Table 4.21: Preparation of enzyme mix for digestion of neonatal cardiac cells

Number of rats	Total volume	Enzyme mix 1		Enzyme mix 2		
		Enzyme P	Buffer X	Buffer Y	Enzyme A	Enzyme D
40	5 mL	125 µL	4600 µL	50 µL	25 µL	200 µL
60	7.5 mL	187.5 µL	6900 µL	75 µL	37.5 µL	300 µL

Afterwards, tissue was further disrupted using a gentleMACS Dissociator (h_tumor 3.01). Incubation and dissociation steps were repeated alternating 2-3 times. Digestion was stopped with 7.5 mL of FCS containing NKM medium, and cell suspension was filtered through a mesh of stainless steel with a 250 µm pore size and centrifuged for 20 min at 60 x g. The pelleted cells were resuspended in 20 mL NKM medium, and cell number was determined by using a Neubauer counting chamber. To exclude dead cells, 0.4% trypan blue was added, which stains only non-viable cells.
Freshly isolated cells were either used directly for EHM preparation or seeded at a density of 10^6 cells per 15 cm cell culture dish for 40-45 min to separate fibroblasts from cardiomyocytes. To remove all non-attached cells, the dish was thoroughly rinsed with NKM medium and growth medium was added to the attached fibroblasts. Cardiac fibroblasts were cultivated under humidified condition at 37 °C with 5% CO_2 circulation until cells reached confluency. For experiments only cells from passage 1 and 2 were used.

4.2.2.3 Cultivation and passaging of primary cells

Cardiac fibroblasts were cultivated on cell culture surfaces in a humidified incubator at 37 °C with 5% CO_2 circulation until they reached 70-80% of confluency. For passaging, medium was aspirated, cells were washed with pre-warmed PBS and after removal of PBS, 0.05% pre-warmed trypsin-EDTA was added. Cells were treated with trypsin around 5 min at RT until the majority of cells detached from the bottom surface. The process was assessed by light microscopy. Then, trypsin activity was stopped by adding FCS-containing medium. For cell collection, the surface of the dish was rinsed several times. After centrifugation for 5 min at 300 x g, the cell pellet was resuspended in growth medium containing FCS and counted using the CASY cell counting system. In addition, viability, size and volume of the detached cells were assessed. Cells were seeded for experiments according to the needed cell number, and cultivation was continued in a humidified incubator at 37 °C with 5% CO_2. For immunofluorescence staining, fibroblasts were seeded on glass cover slips coated with collagen (3 mg/mL) diluted 1:100 in PBS.
Prior to any treatment, cells were starved in serum-free medium for 24 h. For this, the medium was aspirated, cells were washed 1-2 times with pre-warmed PBS and low glucose medium without FCS was added (serum-free medium).

4.2.2.4 Deep freezing and thawing of primary cells

For long-term storage of cultivated cardiac fibroblasts, cells of a confluent T75 flask were trypsinized as described above (section 4.2.2.3) and the cell pellet was resuspended in 1 mL growth medium containing 10% DMSO. This cell suspension was transferred into cryotubes and frozen down at -80 °C by the use of Mr. Frosty freezing containers filled with isopropanol, allowing a gradual decrease in temperature with a gentle cooling rate of
-1 °C/min.
In order to re-cultivate the frozen fibroblasts, cells were thawed immediately to room temperature, mixed with an appropriate volume of growth medium and seeded on flasks. The next day, medium was removed and exchanged with fresh growth medium.

4.2.2.5 Adenoviral infection of neonatal rat cardiac fibroblasts (NRCF)

Fibroblasts cultivated in a monolayer were serum-starved and infected with recombinant adenovirus for 24 h to 72 h with a multiplicity of infection (MOI) of around 500-1000. For ECT preparation, the respective viruses were added directly to the mixture prior to the casting of rings. Efficiency of transduction was verified by fluorescence microscopy examination of the co-expressing EGFP as part of the encoding gene sequence.

4.2.2.6 Proliferation Assay

To evaluate the proliferative capacity, AMCF were trypsinized as described in section 4.2.2.3 and counted using the CASY cell-counting system. Cells were seeded on 24-well plates with a density of 10.000 cells per well and cultivated in AMCF growth medium. The next day, cells were washed once with pre-warmed PBS and further cultivated in AMCF growth medium supplemented with or without 10% serum. In addition, cells of one plate (referred as time point t = 0h) were immediately fixed with 4% PFA for 15 min and nuclei were stained with DAPI diluted in PBS (see section 4.1.7) for 30 min in the dark. After three washing steps with PBS, the cell number was determined by nuclei staining using the Cellavista system (Roche). For the following period of cultivation, medium was changed every day. On day 1, 2, 3, 4 and 6 cells were fixed and stained and cell number was assessed as described above. Each sample was run in 4 replicates.

4.2.2.7 Generation of 3D engineered tissue

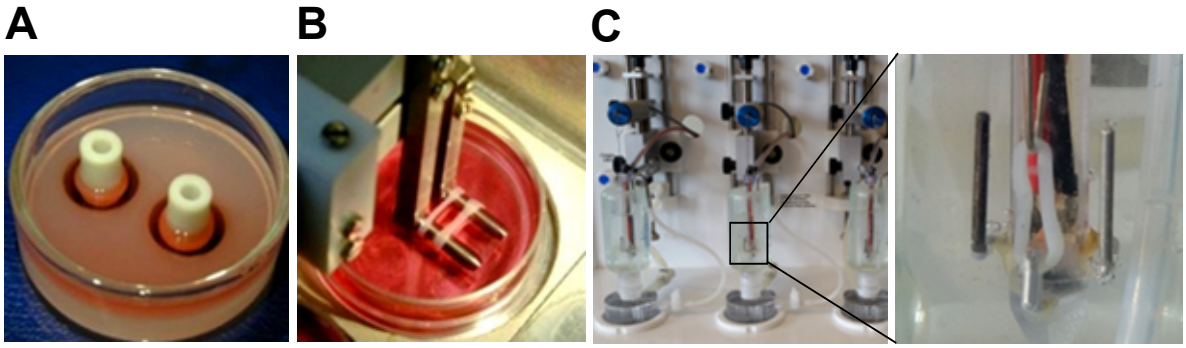

Figure 4.2: Overview of EHM preparation, cultivation and force measurement setup
(A) Example of a rat mouse mold used for casting of the tissue. (B) Image of EHM on a phasic stretcher. (C) Contraction setup (left) and EHM clamped on hooks of an organ bath (right).

<u>Generation of engineered heart muscle (EHM)</u>

EHMs were prepared with 2.5 x 10^6 freshly isolated total heart cells (section 4.2.2.2) and 0.5 x 10^6 adenovirally transduced NRCF (section 4.2.2.5).
All steps of EHM preparation were performed on ice with pre-cooled equipment. First, an equal amount of collagen (table 4.22) and 2x DMEM was mixed and pH was adjusted with 0.1 NaOH until the colour changed from yellow (acidic pH) to a more pink-red colour (neutral pH). Then, matrigel and cells were added, mixed carefully and casted into circular molds. After incubation at 37 °C and 5% CO_2 for 1 h, tissues were covered with EHM medium. The next day, the medium was replaced by fresh EHM medium and further changed every other day for the remaining time of cultivation. After 5 days of culture, the condensed EHMs were transferred on phasic stretchers for 12 consecutive days. EHM tissue was stretched at 1 Hz

for the first 24 h, and then frequency was increased to 2 Hz. Subsequently, contractile force measurements were performed 17 days after casting as described in section 4.2.2.8.

Table 4.22: Master mix for the preparation of one rat EHM

EHM component	Volume (µL) rat molds
Collagen type 1 (0.8 mg/EHM); Stock solution 3.0 mg/mL	280 µL
2x DMEM	280 µL
0.1 NaOH	20 µL
Matrigel	100 µL
Cell suspension: 2.5 x 10^6 total heart cells plus 0.5 x 10^6 virally infected P1 NRCF	220 µL
Total	**900 µL**

Generation of engineered connective tissue (ECT)

ECTs were prepared in a similar way as described for EHMs by mixing only cardiac fibroblasts (1.5 x 10^6 NRCF) with collagen and 2x DMEM in circular molds. For transduction, virus was directly added to the mixture before casting the tissue. After 60 min of condensation growth, medium was added and ECTs were cultivated in molds for 5 consecutive days with medium changes every second day. Stiffness of the tissue was analyzed in an organ bath as described in section 4.2.2.8.

Table 4.23: Master mix for the preparation of one rat ECT

ECT components	Volume (µL) rat molds
Collagen type 1 (1.2 mg/ECT); stock solution 3.0 mg/mL	400 µL
2x DMEM	400 µL
0.2 NaOH	40 µL
Cell suspension	60 µL (1.5 x 10^6 NRCF)
Total	**900 µL**

4.2.2.8 Force measurement of 3D-engineered tissue

Both EHM and ECT were transferred into an organ bath filled with Tyrode's solution constantly kept warm at 37 °C and gassed with 95% O_2 and 5% CO_2. Rings were clamped on hooks connected to a force meter, which were calibrated with a 50 mg weight disk for EHM

or a 500 mg weight disk for ECT. Prior to force, measurement images of the tissues were taken to determine the cross-sectional area.

EHM force measurements

For synchronous contraction of the tissue, EHMs were paced with 2 Hz over the entire term of measurement. First, L_{max} defined by Frank Starling as the length, where the maximal force is generated, was determined for each EHM ring. To do this, EHMs were stepwise (125 µm per step) stretched in the presence of 1.8 mM calcium. As soon as L_{max} was reached, the measurement was stopped, Tyrode's solution was exchanged, and EHM were equilibrated to baseline. Then the contractile force of EHM under increasing calcium concentrations from 0.2 to 3.2 mM was recorded. The minimum (diastolic) force was considered as resting force normalized to the cross-sectional area, whereas the difference between minimal (diastolic) and maximal (systolic) force was defined as force of contraction (FOC) normalized to the cross-sectional area.

ECT force measurement

To evaluate the passive force and hence the stiffness of the tissue, ECTs were stepwise (62,5 µm per step) elongated in the presence of 1.8 mM calcium concentration and the results were presented as resting force normalized to the cross-sectional area.

After measurements, stretch rings were either frozen immediately in liquid nitrogen and kept at -80 °C for RNA and protein isolation or were fixed with 4% paraformaldehyde in PBS overnight at 4 °C for histological analysis. In case of ECT tissue, unstretched rings were also included for further analysis.

4.2.3 Molecular biochemical methods

4.2.3.1 SRF activation assay

To determine the activation of the serum response factor (SRF), neonatal rat cardiac fibroblasts were seeded on 24-well plates, cultivated and starved in serum-free medium for 2 days prior to treatment. For transfection, 0.5 g empty pCMV-Tag3, pCMV-Tag3-p63RhoGEF or pCMV-Tag3-p63ΔN plus 0.4 µg of pSRE.L luciferase reporter plasmid (firefly luciferase)

and 0.1 µg pRL.TL control reporter vector (renilla luciferase) were mixed with Lipofectamine 3000 (Invitrogen) according to the manufacturer's protocol. After incubation for 24 to 48 h, cells were washed with PBS, serum starved for 24 h, pre-incubated with 10 µM CCG1423 for 30 min and treated with 100 nM Ang II for another 24 h. SRF activation was determined by luciferase activity measurement with the Dual-Luciferase reporter assay system (Promega) following the manufacturer's instructions and detected using a luminometer (Glomax). The firefly luciferase activity was normalized to the respective renilla luciferase activity and ratios of untreated controls were set to 1.

4.2.3.2 Isolation of total RNA from monolayer cultured cells

Since RNA is very susceptible to degradation by RNases, all surfaces that could get in contact with RNA samples were thoroughly cleaned beforehand with RNA Zap (Ambion) for an RNase-free environment.
For total RNA isolation from a monolayer culture, cells were seeded on a 6 or 10 cm dish, treated with or without 100 nM of angiotensin II (Ang II) for 3 and 24 h, and harvested by trypsinization (section 4.2.2.3). After centrifugation for 5 min at 300 x g, supernatant was removed and cell pellets were either frozen down at -20 °C for short-term storage or immediately processed for isolation of RNA with the RNeasy Kit (Qiagen) according to the manufacturer's protocol. The RNA was eluted in RNase-free water and the amount of total RNA was assessed by use of a Nanodrop device. For long-term storage RNA was kept at -80 °C.

4.2.3.3 Isolation of total RNA from tissue

For an RNase-free environment, surfaces were cleaned with RNA Zap (Ambion).
Frozen heart tissue was mechanically ground with mortar and pestle in a metal block and constantly cooled down with liquid nitrogen. The powdered hearts were processed with peqGold TriFast (peqLab) in accordance to the manufacturer's protocol. In short, the powdered hearts were dissolved in 1 mL of peqGold TriFast and further disrupted and homogenized using the TissueLyser II (Qiagen) for 90 sec with a speed of 30 Hz with tungsten beads of 5 mm^2 size. The beads were removed, and in order to separate RNA from DNA and protein fraction, chloroform was added and thoroughly mixed. After an incubated period of 10 min and centrifugation for 5 min at 12000 x g, three different phases occurred. The upper aqueous and clear phase containing the RNA was carefully removed and transferred into a new collection tube. For precipitation of the RNA, isopropanol was added, mixed and incubated overnight at -80 °C. The next day, the precipitated RNA was centrifuged for 10 min with 12000 x g at 4 °C, washed twice with 70% ethanol, and resolved in RNase-free water at 55 °C for 10 min. An additional purification step (Clean-up) with an RNeasy Kit was performed following the instructions of the manufacturer (Qiagen). RNA was eluted in

RNase-free water and concentration was determined with the Nanodrop. For long-term storage RNA was kept at -80 °C.

4.2.3.4 Formaldehyde agarose gel electrophoresis

RNA is very susceptible to degradation by RNases. To check the level of degraded RNA isolated from heart tissue, FA gel electrophoresis was performed. For this purpose, a 1.2% agarose gel with RNase-free water, 37% formaldehyde, and ethidium bromide was cast. For sample preparation, RNA was mixed with 5x RNA loading buffer, incubated for 5 min at 65 °C, and was loaded along with a DNA marker ladder on the gel. FA gel electrophoresis was performed at 120 V for 45-60 min in 1x FA gel running buffer. Intact Ribosomal RNA was visualized by UV exposure using the GelDoc XR device and images were taken with the Quantity One programme.

4.2.3.5 cDNA synthesis

The cDNA was synthesized by reverse transcription of isolated total RNA using the RevertAid First Strand cDNA Synthesis Kit (Thermo Scientific). The master mix for a single reaction contained the following components:

Component	**Volume (µL)**
Template 150 - 500 ng	
Oligo dT	1 µL
ad H_2O	12 µL

For annealing of the oligonucleotides, the mixture was incubated for 5 min at 65 °C, cooled down on ice, and buffer, nucleotides, RNase inhibitor as well as enzyme were added.

Component	**Volume (µL)**
5x Reaction buffer	4 µL
dNTPs	2 µL
RI (Ribolock)	1 µL
Reverse Transcriptase	1 µL

Synthesis of cDNA was performed for 60 min at 42 °C followed by a termination step of the reaction for 5 min at 70 °C. cDNA reaction was stored at -20 °C or was directly used for endpoint-PCR/qRT-PCR.

4.2.3.6 Endpoint polymerase chain reaction (PCR)

To analyze the expression of cell type-specific marker, an endpoint PCR was performed. To do this, cDNA samples were diluted 1:20, the respective primers (stock solution 100 pmol) were diluted 1:10 and mixed with the ready-to-use GoTaq Master Mix containing Taq DNA Polmerase, dNTPs, $MgCl_2$ and buffer for efficient amplification of DNA templates (Promega). The mixture of one reaction is shown below:

Table 4.24: Reaction mixture for endpoint PCR

Component	Volume (µL)
Template cDNA (1:20)/DNA from genotyping	1 µL/2 µL
Forward primer (stock solution 100 pmol) (1:10)	1 µL
Reverse primer (stock solution 100 pmol) (1:10)	1 µL
GoTaq Green Master Mix	10 µL
ad H_2O	20 µL

Exponential amplification of a specific DNA fragment was performed in a Mastercycler gradient device using the following programme:

Table 4.25: PCR programme for endpoint PCR

No.	Step	Temperature (°C)	Time	Repitition
1	Initialization	94 °C	3 min	1 time
2	Denaturation	94 °C	30 sec	30 times
3	Annealing	56 °C	30 sec	
4	Elongation	72 °C	2 min	
5	Final elongation	72 °C	5 min	1 time
6	Final hold	4 °C	∞	

After this, the PCR product was separated by size via DNA agarose gel electrophoresis (section 4.2.3.7).

4.2.3.7 Agarose gel electrophoresis

For separation and detection of an amplified PCR product of a specific size, the PCR reaction was loaded on a DNA agarose gel. For preparation of a gel, agarose was mixed with 1x TAE buffer and heated until the agarose was dissolved. The viscous solution was cooled down to approximately 50 °C, ethidium bromide was added, and the gel was cast. After solidification, the gel was transferred into a gel electrophoresis chamber and covered with 1x TAE buffer.

Gel electrophoresis was performed at 120 V for 45-60 min depending on the expected size of the DNA fragment. DNA bands were visualised by UV exposure using the GelDoc XR device, and images were taken with the Quantity One software application.

4.2.3.8 Quantitative real-time polymerase chain reaction (qRT-PCR)

For quantitative analysis of an expressed gene on mRNA level, qRT-PCR was performed using the 5x HOT FIREPol Eva Green qPCR Plus Kit (Solis BioDyne), according to the manufacturer's instructions. Each cDNA sample was diluted 1:20 and run in four replicates. For each primer pair, a standard curve using a pool of all cDNAs was included. For each gene, a master mix was prepared as shown in table 4.26 and scaled up to the required number of samples. The experiment was performed in a Micro-Amp optical reaction 384 plate (Applied Biosystems) with 1 µL of the diluted cDNA and 19 µL of the master mix per well. After loading of all samples, the plate was sealed with a Micro-Amp optical adhesive film and centrifuged for 5 min at 300 x g.

Table 4.26: Reaction mixture for qRT-PCR

Component	Volume (µL)
Forward primer (10 pmol)	1 µL
Reverse primer (10 pmol)	1 µL
5x HOT FIREPol Eva Green qPCR Plus Kit	4 µL
H_2O	13 µL

The reaction was performed using TaqMan 7900HT Fast Real-Time-PCR instrument, according to the programme depicted in table 4.27. Relative cDNA amount was calculated by SDS 2.4 software with the help of a standard curve and normalized to the housekeeping gene porphobilinogen deaminase (PBGD).

Table 4.27: qRT-PCR programme

No.	Step	Temperature (°C)	Time	Repitition
1	Initialization	95 °C	10 min	1 time
2	Denaturation	95 °C	15 sec	40 times
	Annealing	60 °C	20 sec	
	Elongation	72 °C	40 sec	
3	Denaturation	95 °C	15 sec	1 time
	Melting curve start (Ramp rate: 1.6°C/sec)	60 °C	15 sec	
	Melting curve end	95 °C	15 sec	

4.2.4. Histological methods

4.2.4.1 Sample preparation, embedding and sectioning of ECT and EHM

ECT and EHM tissue were fixed in 4% PFA in PBS overnight. The next day, tissues were washed once with PBS and 70% ethanol and embedded in a 6- or 12-well plate with 2% agarose solved in 1x TAE buffer. After solidification at 4 °C over night, a block of tissue and agarose was cut out, fixed with superglue (Uhu) on a magnetic disk, and positioned in a container filled with ice-cold PBS. Slices of 100 µm thickness were cut in automatic modus at a speed of 6 and frequency of 10 using a Leica vibratome (Leica). During sectioning, the container was permanently cooled with ice. Tissue slices were transferred into PBS filled well plates and stored at 4 °C until proceeding further with immunofluorescence staining (section 4.2.5.2).

4.2.4.2 Sample preparation and embedding of heart tissue

Excised hearts were fixed with 4% PFA overnight at 4 °C on a rotating shaker and washed twice with PBS. For tissue embedding, two different techniques were performed as described below.

Paraffin-embedding

In order to embed hearts in hydrophobic paraffin, water inside of the tissue was removed by stepwise increase of ethanol concentration and toluol treatment. All incubation steps of the "ascending" ethanol series were performed at 4 °C on a rotating shaker for the period of time shown in table 4.28.

Table 4.28: Incubation steps of "ascending" ethanol series

Reagent	Incubation time (min)
70% ethanol	72 hours
80% ethanol	30 min
90% ethanol	30 min
96% ethanol	60 min
96% ethanol	30 min
100% ethanol	60 min
100% ethanol	30 min
Toluol/ethanol (1:1)	15 min
Toluol	60 min
Toluol	30 min

After toluol treatment, hearts were transferred into preheated liquid paraffin and kept at 65 °C over night. The next day, hearts were fixed in embedding molds with fresh preheated liquid paraffin, cooled down on ice, and solidified at 4 °C over night. Until preparation of sections, paraffin-tissue blocks were further kept at 4 °C.

Cryo-embedding

After fixation with 4% PFA and washing twice with PBS, hearts were transferred into 30% sucrose solution and kept at 4 °C until the organ, when fully infused with the solution, had moved to the bottom of the tube. After this, hearts were put in a 1:1 mixture of 30% sucrose and O.C.T. compound (Sakura), kept again at 4 °C until the organ had reached the bottom, and were subsequently transferred into O.C.T. solution and incubated at 4 °C over night. Finally, hearts were embedded in cryo molds with O.C.T. compound, which was constantly cooled down on a metal block with liquid nitrogen until it had become solid. Cryo molds were kept and stored at -20 °C until crytome sectioning (section 4.2.4.3).

4.2.4.3 Sectioning of heart tissue (microtome and cryotome)

Microtome sectioning

Heart tissue embedded in paraffin was cut with a microtome (Zeiss), preparing cross-sectional slices of 7-10 µm thickness. During sectioning, paraffin block and collecting tray were cooled with ice-cold PBS. Single slices were transferred briefly into 37 °C pre-warmed distilled water and after unfolding, slices were transferred on glass slides, dried over night at room temperature, and further stored in slide boxes at RT.

Cryotome sectioning

In O.C.T. solution embedded hearts were sectioned using a crytome (Zeiss). Cross-sectional slices with a thickness of 100 µm were prepared. During the course of sectioning, all material and chamber were permanently cooled at -20 °C and slices were immediately transferred on glass slides and kept at -20 °C until further processing.

4.2.4.4 Immunohistochemistry (IHC) and immunofluorescence staining of heart tissue

Paraffin-sections

Prior to any staining of paraffin-embedded tissue sections, a deparaffinization procedure was performed to remove the hydrophobic paraffin and to moisturize the dried sections for aqueous dye and antibody incubation. All steps of the "descending" ethanol series were performed at RT for the period of time shown in table 4.29.

Table 4.29: Incubation steps of "descending" ethanol series

Reagent	Incubation time (min)
Histol	10 min
Histol	10 min
100% ethanol	5 min
100% ethanol	5 min
96% ethanol	5 min
96% ethanol	5 min
80% ethanol	5 min
70% ethanol	5 min
Bidest. H_2O	5 min
PBS	5 min

For detection of collagen within the tissue, IHC staining was performed. To do this, a Fast Green/Sirius Red dye (Chondrex) was used and incubated for 30 min in a humidified chamber to prevent dehydration of heart sections. Afterwards, the dye was removed and slides were washed with distilled water, mounted, and dried overnight at RT. Preservation was carried out in the Institute of Pathology, UMG Göttingen. To prevent desiccation of the sections during long-term storage, slides were additionally sealed with nail polish.

To evaluate the cross-sectional area of cardiomyocytes, heart sections were stained with wheat germ agglutinin (WGA), visualizing glycosylated proteins of the ECM. To do this, deparaffinized sections were stained with WGA and DAPI (for concentration see section 4.1.7) diluted in PBS for 30-60 min, washed 3 times with PBS, and mounted with Fluoromount (Sigma). For long-term storage, slides were sealed with nail polish and kept at 4 °C protected from light.

Cryo-sections

Heart tissue embedded in O.C.T. medium were briefly thawed at room temperature, washed 5 min in PBS and stained for collagen with Fast Green/Sirius Red dye or for ECM with WGA and DAPI as described above.

4.2.5 Immunofluorescence

4.2.5.1 Preparation and staining of monolayer cells

Cells seeded on a 12-well plate with or without covers slips were fixed with 4% PFA for 15 min at room temperature, washed 3 times with PBS followed by permeabilization of the cell membrane with 0.2% of the detergent Triton X-100 solved in PBS for 3 min. Again, cells were rinsed 3 times with PBS. Blocking of free binding sites was carried out for 1 h using Roti-block (Roth). Thereafter, incubation with the first antibody diluted in PBS was performed at 4 °C overnight on a shaking plate. Continuing the next day, the solution was apirated, cells were washed 3 times with PBS, and second antibody incubation was conducted for 1 h at room temperature in the dark along with fluorophore-labelled Phalloidin or WGA and DAPI. After washing with PBS 3 times, cells cultured on plastic surface were stored in PBS at 4 °C in the dark. Cells seeded on glass cover slips were mounted with Fluoromount (Sigma), sealed with nail polish, and stored at RT protected from light until imaging.

4.2.5.2 Preparation and staining of ECT and EHM 3D tissue

Longitudinal sections obtained from 3D engineered tissue were simultaneously blocked with Roti-block (Roth) and permeabilized with 0.2 Tween X-100 at 4 °C over night. First and fluorocrome-labeled second antibody were each incubated at 4°C overnight in blocking/permeabilization buffer, and fluorophor-coupled Phalloidin or WGA and DAPI were incubated for 1 h at RT in the dark. Between every staining period, tissues were washed 3 times with PBS. Finally, agarose was removed and tissue sections were mounted with Fluoromount (Sigma) and sealed with nail polish the day after. Until microscopy analysis, samples were stored at RT in the dark.

4.2.6 Protein biochemical methods

4.2.6.1 Preparation of protein samples from monolayer cells for SDS-PAGE

For protein analysis, cells were seeded on 6-well plates, cultivated until 90% confluency, and treated as indicated. All steps of cell lysate preparation were performed with pre-cooled solutions and equipment on ice. First, conditioned medium was collected, then cells were rinsed twice with PBS, lysed and scraped off with an adequate volume of GST-Fish buffer (250 µL/6-well for NRCF or 150 µL/6-well for AMCF) containing 1x phosphatase and

protease inhibitor (PhosSTOP and cOmplete, Roche). In case of AMCF, cell lysates from 2 to 3 single 6-wells were pooled. To remove cell debris, lysates were centrifuged for 10 min at 14000 x g at 4 °C and the supernatants were transferred into new reaction tubes. For SDS-PAGE, 4x SDS loading buffer without glycerol was added to the lysate fraction. Medium samples were mixed with 4x loading buffer with glycerol. Samples were incubated for 5 min at 95 °C in a heating block, cooled down briefly on ice, shortly centrifuged and kept cooled until gel electrophoresis. Native cell lysates and conditioned medium without loading buffer were immediately snap-frozen in liquid nitrogen and kept at -20 °C for short-term and at -80° for long-term storage.

4.2.6.2 Preparation of protein samples from 3D tissue for SDS-PAGE

Frozen EHM, ECT and heart tissue were mechanically ground with mortar and pestle in a metal block that was constantly cooled down with liquid nitrogen. Ice-cold GST-Fish-buffer containing 1x phosphatase and protease inhibitor (PhosSTOP and cOmplete, Roche) were added to the powdered tissue and homogenized using a Polytron (Kinematica). After this, protein lysates were centrifuged and SDS-PAGE samples were prepared as described above (section 4.2.6.1).

4.2.6.3 Discontinuous sodium dodecyl sulfate polyacrylamide gel electrophoresis (SDS-PAGE)

For detection of proteins, lysate samples obtained from 2D or 3D (EHT/ECT) cell culture and heart tissue (see section 4.2.6.1 and 4.2.6.2) were first separated by size according to Laemmli et al. [174]. Depending on the corresponding size of the proteins, SDS polyacrylamide gels with a concentration between 8 and 15% were cast (see table 4.3) or commercially available gradient gels (Bio-Rad) were used. Samples and a protein standard ladder were loaded onto a gel, and SDS gel electrophoresis was performed with an electrical current of 200 V in 1x SDS-PAGE electrophoresis buffer. The run was stopped as soon as the loading front reached the bottom line of the gel.

4.2.6.4 Immunoblotting

Proteins separated by SDS-PAGE were transferred onto a nitrocellulose membrane by voltage application of 100 V for 60 min. For improved transfer, ice-cold blotting buffer was used and constantly kept chilled with the help of a frozen thermal pack inside the chamber. Afterwards, efficiency and equality of the protein transfer were assessed by Ponceau S staining of the membrane for approximately 5 min. The solution was aspirated and the membrane washed with distilled water 3-4 times to remove staining residues until single

bands became visible. The membrane was cut for individual protein sizes and washed once with TBS-T. To cover all putative free binding sites on the proteins, the membrane was blocked with Roti-block for 60 min at RT on a shaking plate. Incubation with the first antibody in concentrations depicted in table 4.7 was performed over night at 4 °C.
The next day, the antibody solution was removed and membrane was washed 3 times with TBS-T for 5 min each before the second HRP-coupled antibody used in concentration shown in table 4.8 in TBS-T was incubated for 60 min at room temperature. Antibodies were always diluted in TBS-T and incubated on a shaker. After the second antibody incubation, the membrane was washed again 3 times with TBS-T and kept in distilled water. Finally, detection of proteins was assessed by the measurement of chemiluminescence. To do so, the membrane was covered with HRP-substrate solutions and signals were recorded using the VersaDoc Imaging system. For highly abundant proteins, Lumi Light (Roche) was used, whereas for lower expressed proteins, the more sensitive reagent Super signal west Femto (Thermo Scientific) was chosen. Semi-quantitative protein analysis was performed with the Image Lab 5.1 software.

4.2.7 Statistical analysis

All results are presented as means ± SEM. Data were analyzed by 1way or 2way ANOVA, followed by Bonferroni's Multiple Comparison Test when comparing 3 or more groups or by an unpaired t-test in order to compare 2 groups. P-values of less than 0.05 were considered statistically significant.

5 Results

5.1 The relevance of p63RhoGEF expression in the pathophysiology of cardiovascular diseases

5.1.1 Expression of p63RhoGEF and CTGF is up-regulated during afterload-induced cardiac remodeling

To investigate the role of p63RhoGEF under pathophysiological conditions of cardiac diseases, tissue from an animal study with female mice subjected to transverse aortic constriction (TAC), as an afterload- and pressure-induced disease model, was used to analyze p63RhoGEF expression. Heart samples were collected 1 week after surgery, when the left ventricular hypertrophy as indicated by left ventricular weight to tibia length ratio (LVW/TL) was increased by 22% and a significant 4.9-fold increase in myocardial fibrosis in the perivascular region was observed [175]. Immunoblot analysis revealed that expression of p63RhoGEF and CTGF was elevated by 2.2-fold and 6.6-fold, respectively, in TAC animals compared to sham group (Figure 5.1). This change was independent of the used normalization marker used vimentin or calsequestrin.

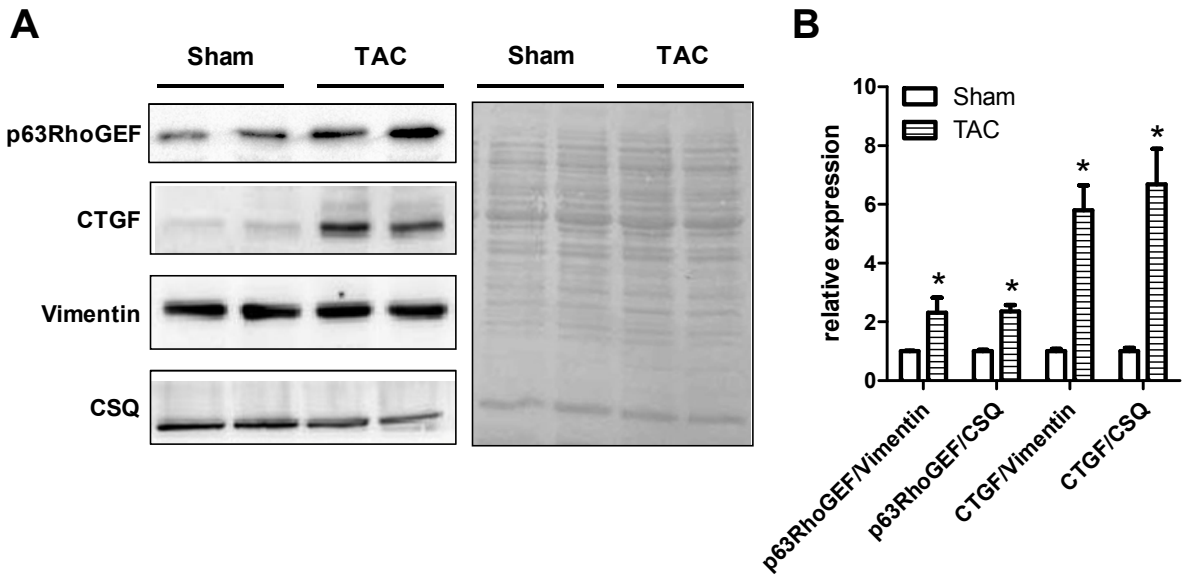

Figure 5.1: Expression of p63RhoGEF and CTGF in murine hearts after TAC
Heart samples from female mice subjected to transverse aortic constriction (TAC) or sham surgery were lysed in GST-Fish buffer 7d after operation. (A) Representative immunoblots (left) and Ponceau staining (right) of p63RhoGEF, CTGF, vimentin and calsequestrin-2 (CSQ) are shown. (B) Quantification of p63RhoGEF and CTGF expression normalized to vimentin and calsequestrin relative to sham group. Values are given as means ± SEM, n=6; *$p < 0.05$ vs. sham.

In addition to the TAC model, shunt surgeries as a preload- and volume-induced cardiac model were performed [175]. While these mice developed a left ventricular hypertrophy similar to TAC animals, no elevated amount of fibrotic tissue was observed one week after intervention. Protein expression of p63RhoGEF and CTGF was analyzed one week after shunt and showed only a moderately 1.5-fold and 1.9-fold rise respectively in comparison to TAC (Figure 5.2).

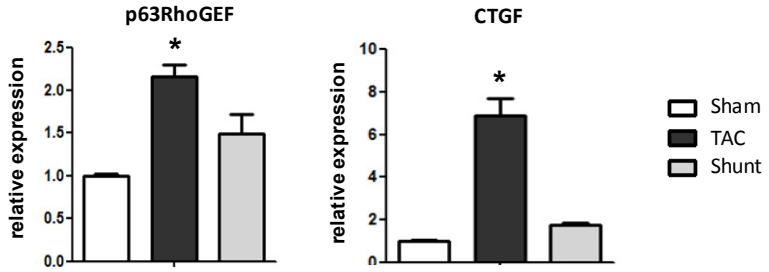

Figure 5.2: Comparison of p63RhoGEF and CTGF expression after TAC and shunt intervention
Heart samples from female mice subjected to TAC, shunt or sham surgery were lysed in GST-Fish buffer 7d after operation. Quantification of p63RhoGEF and CTGF expression normalized to calsequestrin and relative to sham group are shown. Values are given as means ± SEM, n=6; *p < 0.05 vs. sham.

This data suggest that p63RhoGEF and CTGF expression seems to be more relevant for afterload-dependent cardiac remodeling than for preload-induced processes.

5.1.2 p63RhoGEF expression correlates with CTGF expression and cardiac function during afterload-induced cardiac remodeling

To further elucidate the influence of p63RhoGEF and CTGF, a second mouse study was performed in which male and female mice were subjected to TAC or sham surgery. Over a time period of 5 weeks after surgery, mice developed a more severe hypertrophic phenotype with an increase in LVW/BW by 70% accompanied by a 25% reduction in ejection fraction (EF) and a rise in systolic (Vs) as well as diastolic volume (Vd) in the left ventricle by 62% and 31%, respectively (Figure 5.3 A).

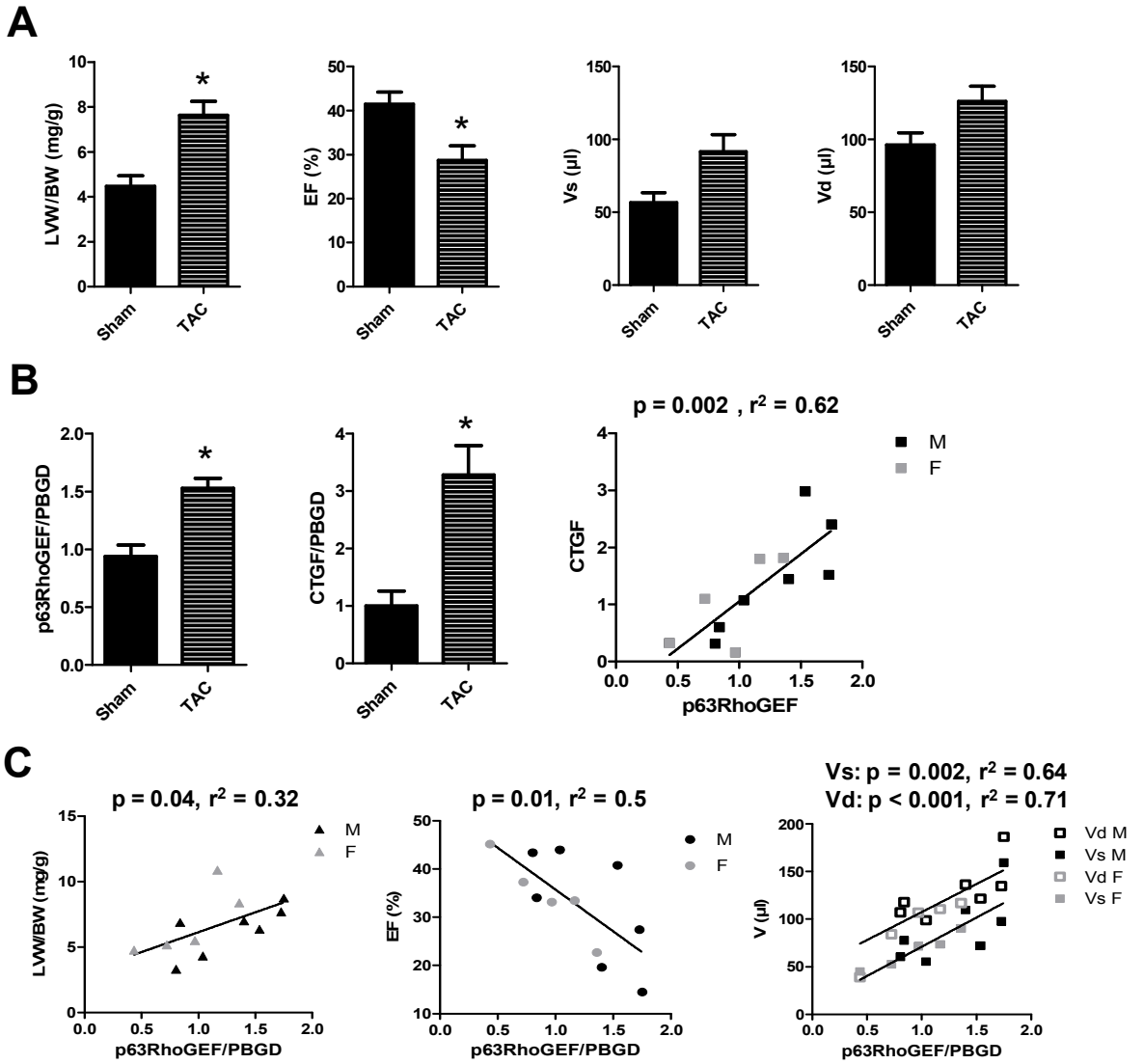

Figure 5.3: Analysis of cardiac parameter and p63RhoGEF expression after TAC

Male and female mice (10-12 weeks old) were subjected to TAC or sham surgery for 5 weeks. (A) Left ventricular dimension (given as ratio to the body weight, LVW/BW), ejection fraction (EF), and ventricular volume in systole (Vs) and diastole (Vd) were analyzed by echocardiography. Values are given as means ± SEM, n=4 (sham) and n=8 (TAC), *p < 0.05 vs. sham. (B-C) RNA was isolated from male and female hearts of TAC and sham-operated mice and expression of p63RhoGEF and CTGF was assessed by qPCR and normalized to the housekeeping gene PBGD. Correlation between p63RhoGEF and CTGF (B) and correlation of cardiac parameters (LVW/BW, EF, Vs and Vd) to p63RhoGEF expression is shown (C). The p and r^2 values are depicted above the graphs.

Analysis of heart samples by qPCR showed a 1.5- and 3.3-fold higher expression of p63RhoGEF and CTGF in TAC-operated mice compared to the sham group. Importantly, in both male and female mice, a positive correlation between p63RhoGEF expression and CTGF expression could be determined (Figure 5.3 B). Likewise, p63RhoGEF expression correlates positively with LVW/BW, Vs, and Vd, but negatively with EF (Figure 5.3 C).

5.2 Cellular function of p63RhoGEF in neonatal cardiac fibroblasts

Previous data investigating the role of p63RhoGEF in cardiac fibroblasts clearly demonstrated that p63RhoGEF expression regulates the Ang II-dependent RhoA activation, as well as CTGF expression and secretion (see chapter 3). To further establish the function of p63RhoGEF in the underlying mechanism of auto- and paracrine signaling in cardiac fibroblasts, involvement of the serum-response factor in the signaling cascade as well as localization of p63RhoGEF was examined.

5.2.1 p63RhoGEF regulates the activation of the serum response factor (SRF)

The serum response factor (SRF) is an abundant transcription factor and thereby a downstream target of many pathways involved in cell-cycle regulation, apoptosis, cell growth and differentiation [176]. The SRF regulates the expression of immediate early genes and is involved in the organization of the actin cytoskeleton. To investigate whether SRF plays a role in the downstream signaling of p63RhoGEF, NRCF were transfected with either a construct for p63RhoGEF overexpression or the dominant negative p63ΔN construct blocking the signaling cascade downstream of $G\alpha_{q/11}$ (Figure 5.4). SRF activity was assessed by luciferase gene reporter measurements (as described in section 4.2.3.1) in the absence or presence of Ang II.

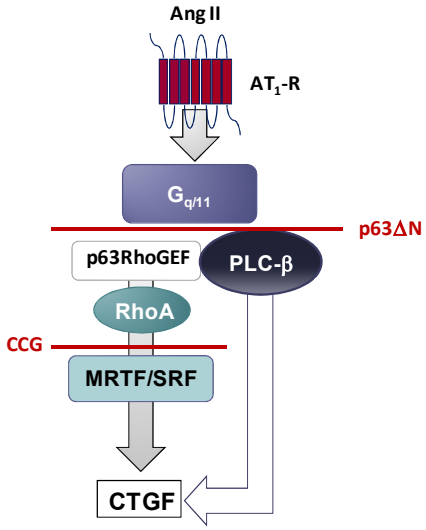

Figure 5.4: Schematic overview of the Ang II-dependent-p63RhoGEF-RhoA signaling cascade and targets for intervention

Abbreviations: Ang II (angiotensin II), AT_1R (angiotensin II receptor subtype 1), MRTF (myocardin-related transcription factor), SRF (serum response factor), CTGF (connective tissue growth factor), PLC-β (phospholipase C-β), p63ΔN (dominant negative N-terminal truncated p63RhoGEF construct), CCG-1423 (MRTF/SRF inhibitor).

Stimulation of control NRCF with Ang II resulted in a significant 1.5-fold increase in SRF activity (Figure 5.5). Overexpression of p63RhoGEF increased SRF activity significantly by 1.7-fold, and treatment with Ang II further raised the activity up to 4-fold compared to control condition. In contrast, blocking of the $G\alpha_{q/11}$ pathway by p63ΔN almost completely inhibited the SRF activation in presence of Ang II, demonstrating that p63RhoGEF is involved in the Ang II-dependent activation of the SRF.

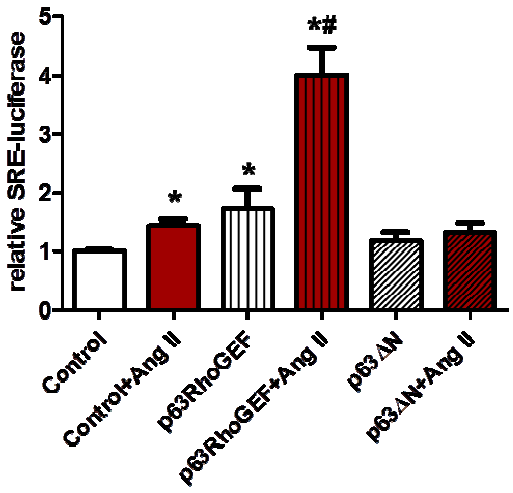

Figure 5.5: Effect of p63RhoGEF on the SRF activation
NRCF were co-transfected with pCMV-control, pCMV-p63RhoGEF, pCMV-p63ΔN plus pSRE.L and pRL.TK, serum starved for 24 h and stimulated with 100 nM Ang II for another 24 h. Ratios of firefly/renilla luciferase measurements are normalized to control, and values are shown as means ± SEM, n = 4-6, *$p < 0.05$ vs. control, $^{\#}p < 0.05$ vs. control + Ang II.

5.2.2 p63RhoGEF regulates CTGF expression and secretion via the serum response factor

To validate the involvement of the SRF in the p63RhoGEF-dependent CTGF regulation, the SRF inhibitor CCG-1423 was implemented in the experiments. In detail, CCG-1423 binds to the myocardin-related transcription factor (MRTF), a co-factor of the SRF. In doing so, it prevents the translocation of the MRTF/SRF complex into the nucleus, where the SRF otherwise binds to the serum response element (SRE) in the promotor region of its potential target genes (Figure 5.4) [177, 178].
First, SRF activity was investigated in NRCF after stimulation with Ang II or serum for 24 h and in combination with or without prior CCG treatment for 1 h. Similar to the result seen in Figure 5.5, Ang II stimulation increased the SRF activity by 2-fold, while serum led to an approximately 15-fold increase in SRF activity (Figure 5.6 A). Although treatment of cardiac fibroblasts with the inhibitor CCG blocked the Ang II-dependent SRF activation, the level of SRF activity in CCG-treated cells was significantly higher compared to the control. Moreover, CCG treatment followed by stimulation with serum resulted in an even higher increase in

SRF activity compared to fibroblasts treated only with serum. These data suggest that the MRTF is involved in the Ang II-dependent SRF activation, but other co-factors must also be considered to be involved in SRF activation.

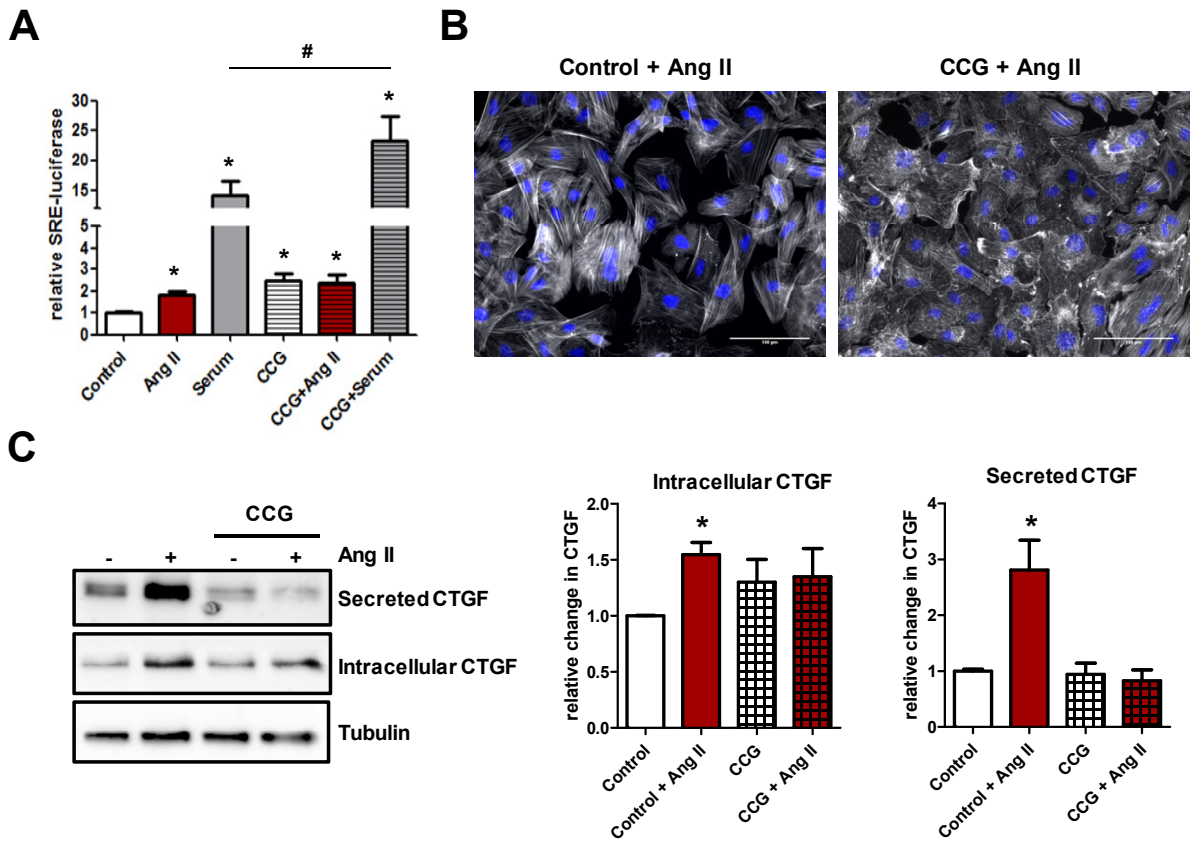

Figure 5.6: Effect of SRF activity on the p63RhoGEF-dependent CTGF regulation
(A) NRCF were co-transfected with pSRE.L and pRL.TK, serum-starved for 24 h and pre-incubated with 10 µM CCG-1423 for 1h. Afterwards, cells were treated with serum or 100 nM Ang II for additional 24 h. Ratios of firefly/renilla luciferase measurements are normalized to control and values are shown as means ± SEM, n = 4, *p < 0.05 vs. control, #p < 0.05 vs. serum. (B-C) NRCF were pre-treated with 10 µM CCG-1423 for 1 h and stimulated with 100 nM Ang II for 24 h. The actin cytoskeleton was stained with FITC-phalloidin and nuclei with DAPI. Scale bar 100 µm. (B) Cell lysates and conditioned medium were collected and the amounts of intracellular and secreted CTGF were determined by immunoblot (C). Representative immunoblots (left) and protein quantification (right) are shown. Values are given as means ± SEM, normalized to tubulin and relative to control, n = 5, *p < 0.05 vs. control.

Next, the influence of MRTF/SRF inhibition on the organization of the actin cytoskeleton was determined. Control NRCF formed typically thick actin fibers, so-called stress fibers, upon Ang II stimulation, whereas treatment with CCG for 1 h followed by stimulation with Ang II for 24 h resulted in a clear disassembly of the actin stress fibers (Figure 5.6 B).

Finally, the effect of the MRTF/SRF inhibition on the regulation of CTGF as a downstream target was investigated. Immunoblot analysis revealed that 24 h of Ang II stimulation led to a 1.6- and 2.8-fold increase of intracellular and secreted level of CTGF, respectively. Treatment with CCG blocked the Ang II-dependent CTGF secretion, reducing it to its basal level, whereas only a slight decrease in the intracellular amount of CTGF of CCG-treated cells compared to Ang II stimulated control NRCF was detected (Figure 5.6 C).

5.2.3 p63RhoGEF localizes at intracellular membrane structures involved in secretion

Finally, localization of p63RhoGEF in cardiac fibroblasts was examined. For this purpose, NCRF were adenovirally infected with a c-myc tagged construct allowing the detection of overexpressed p63RhoGEF in the cell via a specific anti-c-myc-antibody. In addition, viral transduction of fibroblasts was verified by EGFP fluorescence. Confocal imaging revealed that p63RhoGEF localizes close to WGA-stained membranes rich in glycosylated proteins and with the trans-Golgi network (Figure 5.7 A, E), both membrane structures that are highly involved in the secretory machinery of mammalian cells. In addition, co-localization of p63RhoGEF with CTGF was detected (Figure 5.7 F), whereas localization with lysosomes, the endoplasmatic reticulum and cis-Golgi membranes could be excluded (Figure 5.7 B, C, D).

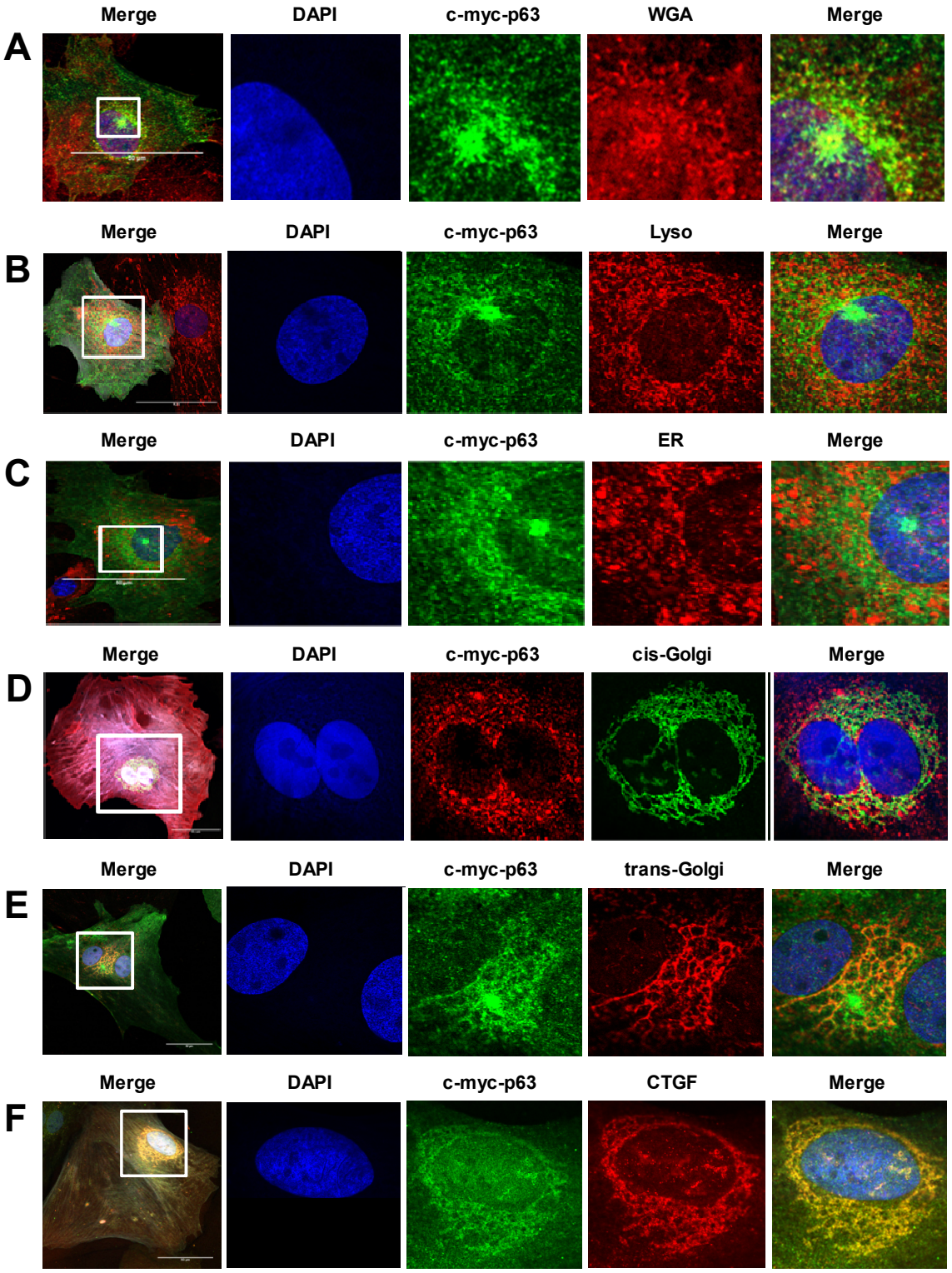

Figure 5.7: Localization of p63RhoGEF in cardiac fibroblasts

NRCF were transduced with Ad-p63RhoGEF for 24 h, fixed and stained for confocal imaging. Adenoviral transduction was verified by EGFP fluorescence. Fibroblasts were stained for p63RhoGEF (c-myc), glycosylated membrane proteins (WGA) (A), and lysosomes (Lamp2) (B), endoplasmatic reticulum (ER; KDEL) (C), cis-Golgi network (GM130) (D), trans-Golgi network (GOPC) (E) and CTGF (F). Nuclei were stained with DAPI. Representative merged images and magnifications of the nuclear region are shown. Scale bar 50 µm. *(Stainings and confocal imaging was performed together with Sebastian Pasch, Institute of Pharmacology and Toxicology, University Medical Center Göttingen.)*

Interestingly, staining of p63RhoGEF in NCRF (Figure 5.8 A) as well as AMCF (Figure 5.9 A) showed a very distinct punctual accumulation near or on top of the nuclei. Co-staining with acetylated tubulin, the main component of primary cilia, revealed that p63RhoGEF is localized within the transition zone and basal body of a primary cilium (Figure 5.8 B). Z-stack recording of the nuclear region (Figure 5.9 B) could confirm the localization of p63RhoGEF close to the nucleus and not inside it.

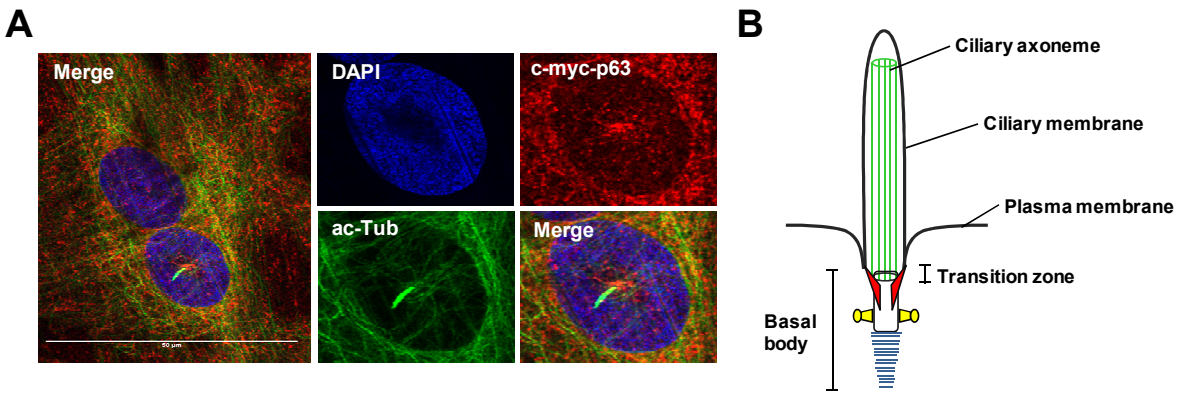

Figure 5.8: Analysis of p63RhoGEF localization with primary cilia
(A) NRCF were transduced with Ad-p63RhoGEF for 24 h, fixed and confocal imaging was performed. Adenoviral transduction was verified by EGFP fluorescence and fibroblasts were stained for p63RhoGEF (c-myc) and acetylated tubulin (ac-Tub). Nuclei were stained with DAPI. Scale bar 50 µm. (B) Schematic illustration of a primary cilium (modified according to Seeley and Nachury, 2010). *(Stainings and confocal imaging was performed together with Sebastian Pasch, Institute of Pharmacology and Toxicology, University Medical Center Göttingen.)*

Beside the function as mechanoreceptors, primary cilia are supposed to be specialized compartments for secretion [179, 180] and in line with the described localization of p63RhoGEF at trans-Golgi membranes, an active participation of p63RhoGEF in the regulation of secreted factors, as e.g. CTGF might be conceivable.

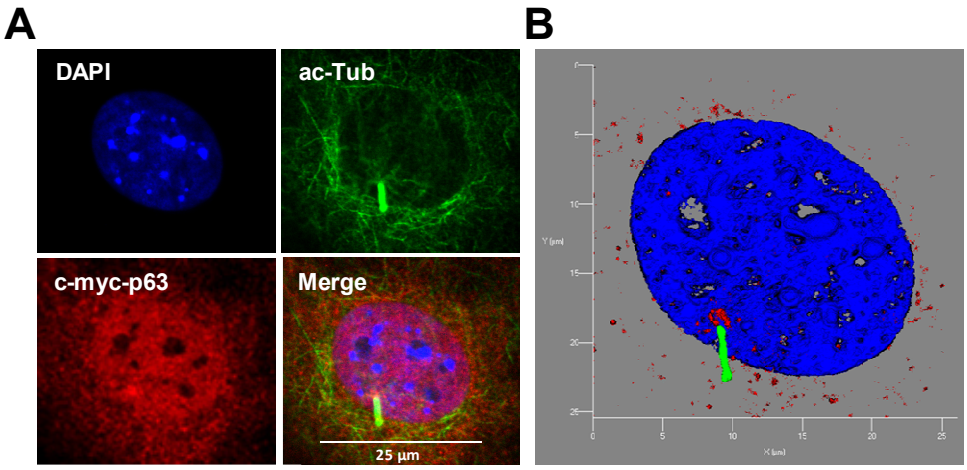

Figure 5.9: Localization of p63RhoGEF with primary cilia
AMCF were transduced with Ad-p63RhoGEF for 24 h, fixed and confocal imaging was performed. (A-B) Adenoviral transduction was verified by EGFP fluorescence and fibroblasts were stained for p63RhoGEF (c-myc) and acetylated tubulin (ac-Tub). Nuclei were stained with DAPI. Scale bar 25 µm. (B) Computational 3D image of the nuclear region based on z-stack recordings.

5.3 Influence of p63RhoGEF and its downstream effector CTGF on viscoelastic and contractile properties of 3D engineered tissue

To manifest the importance of p63RhoGEF expression in auto- and paracrine signaling of cardiac fibroblasts in effecting tissue properties and thereby contractile performance of cardiomyocytes, experiments using 3D engineered tissue models were carried out.

5.3.1 p63RhoGEF regulates viscoelastic properties of engineered connective tissue (ECT)

In a first experimental setup, ECTs consisting mainly of collagen and neonatal cardiac fibroblasts with the respective p63RhoGEF encoding adenovirus were generated, and passive force, as an indicator for the rigidity of a tissue, was measured (for detailed description - see section 4.2.2.7 and 4.2.2.8).

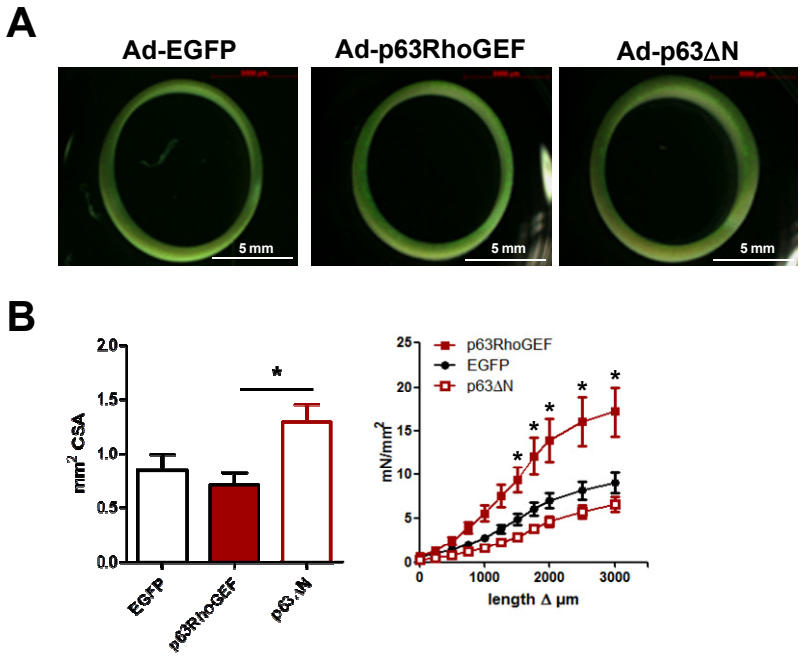

Figure 5.10: Effect of p63RhoGEF expression on viscoelastic properties of ECT
NRCF, collagen, and the respective adenovirus (Ad-EGFP, Ad-p63RhoGEF, Ad-p63ΔN) were mixed and cultivated for 5 days. (A) Representative images of ECT. Scale bar 5 mm. (B) ECTs were elongated stepwise in an organ bath and passive force was detected. Shown are the cross sectional area (CSA) (left graph) and measured forces normalized to CSA (right graph) as means ± SEM, n = 4-5, 10-22 ECT were measured each, *p < 0.05 vs. EGFP.

Overexpression of p63RhoGEF significantly enhanced rigidity of the tissue accompanied by a slight decrease of the cross-sectional area (CSA), whereas in ECTs containing p63ΔN transduced fibroblasts, the stiffness was reduced compared to EGFP ECTs (Figure 5.10 B). In line with this, p63ΔN ECTs were less condensed (Figure 5.10 A), and the cross-sectional area of these tissues was increased by approximately 40% (Figure 5.10 B). Protein lysates of unstretched and stretched ECT samples were prepared, and expression of CTGF was analyzed by immunoblot. In unstretched tissue overexpressing p63RhoGEF, the overall amount of CTGF was elevated by 2.2-fold compared to the EGFP control, while in p63ΔN ECTs the CTGF level was unchanged (Figure 5.11 A). After stretching, p63RhoGEF ECT showed a significant 75% decrease in CTGF content, arguing for enhanced secretion of CTGF during mechanical elongation of the tissue (Figure 5.11 B). In contrast, in stretched p63ΔN ECTs, the level of CTGF was increased after tensile force measurement. Independent from the stretching condition, sm-actin was increased when p63RhoGEF was overexpressed in the tissue, pointing to a more pronounced myofibroblast character of the NRCF within these tissues.
Taken all together, these results emphasize the contribution of p63RhoGEF in regulating viscoelastic tissue properties by mechanically induced stress and confirm the regulation of CTGF secretion in a matrix-surrounded environment.

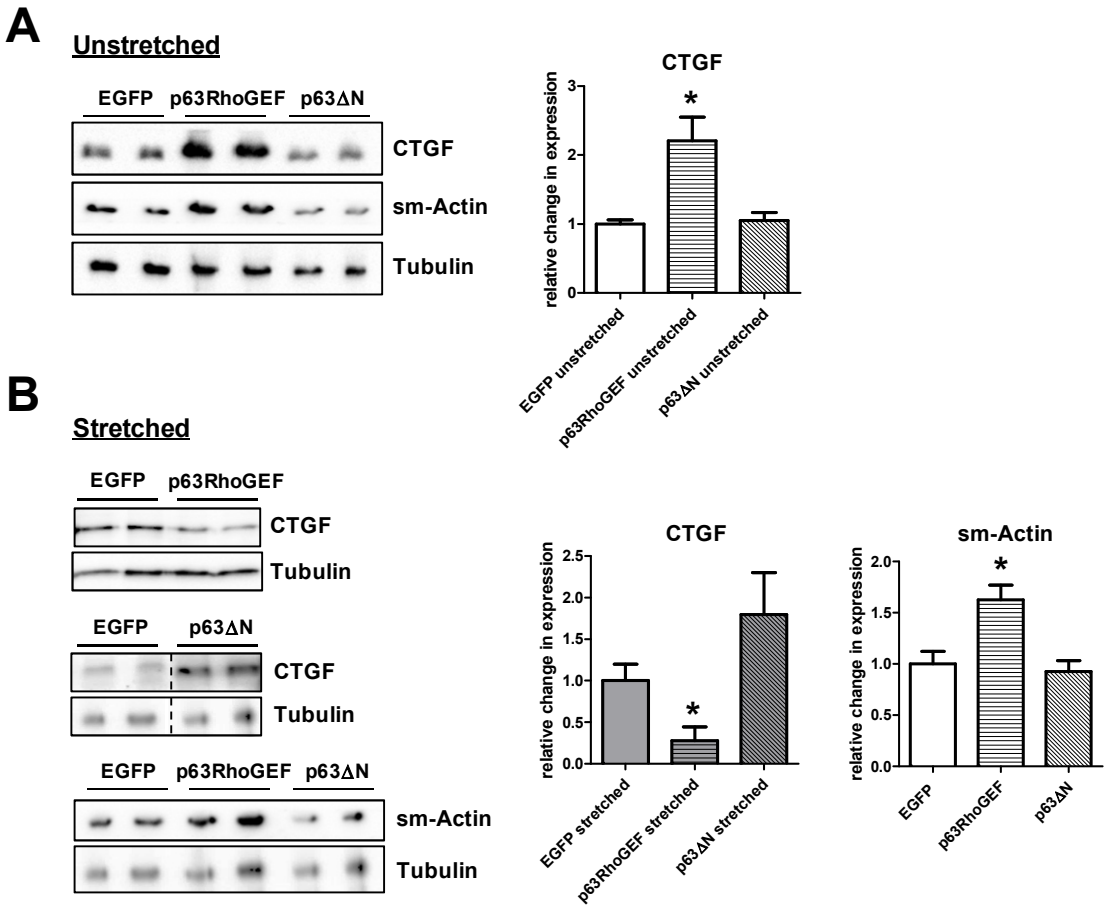

Figure 5.11: Impact of p63RhoGEF on CTGF expression and secretion in ECT
NRCF, collagen, and respective adenovirus (Ad-EGFP, Ad-p63RhoGEF, Ad-p63ΔN) were mixed and incubated for 5 days. (A) Unstretched and (B) stretched ECTs were minced, and lysates were used for immunoblot analysis. Representative immunoblots (left) and quantification of CTGF and sm-Actin (right) are shown. Values are given as means ± SEM, normalized to tubulin and relative to EGFP, n = 3 with 2-6 replicates each, *p < 0.05 vs. EGFP.

5.3.2 CTGF overexpression does not influence stiffness properties of ECTs

Based on literature, CTGF was found to be upregulated in diverse fibrotic diseases and was therefore widely accepted as a profibrotic factor [52]. Recent published studies showed conflicting data on the function of CTGF within the heart, from being cardioprotective, detrimental or without any influence regarding cardiac diseases [90, 181, 182]. In this context, the influence of CTGF expression on viscoelastic properties was examined by generation of ECT with adenovirally infected cardiac fibroblasts (Ad-CTGF). The overexpression of CTGF did not alter the rigidity of the tissue and showed only a minimal reduction in CSA compared to control infected ECTs (Figure 5.12). Thus, CTGF might not be the relevant factor causing an increase in tissue stiffness in the p63RhoGEF expressing ECTs.

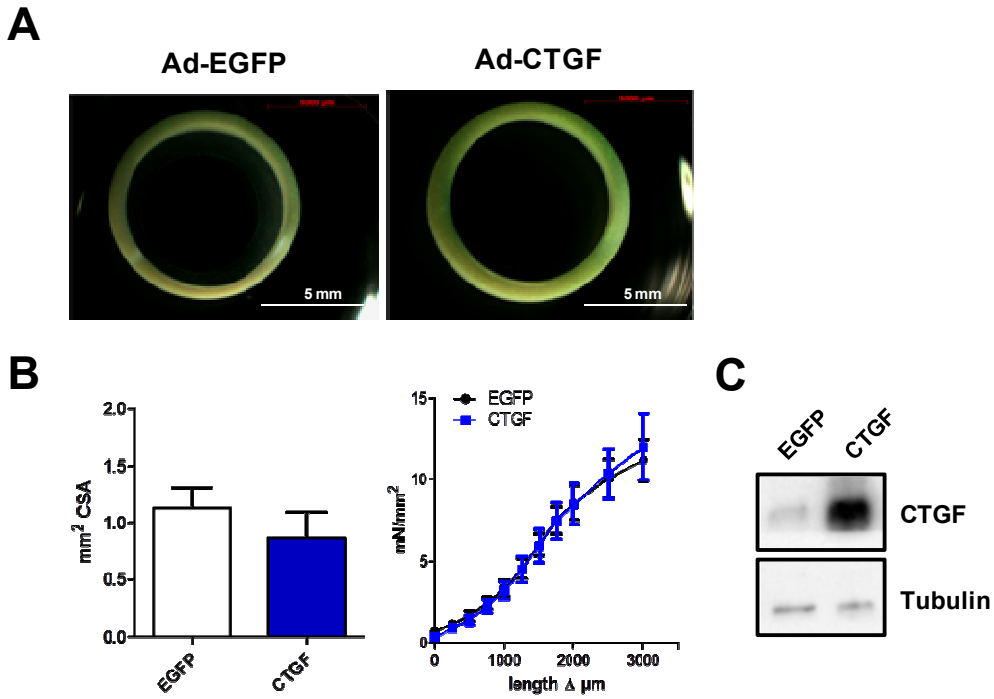

Figure 5.12: Influence of CTGF expression on viscoelastic properties of ECT
NRCF, collagen, and the respective adenovirus (Ad-EGFP and Ad-CTGF) were mixed and incubated for 5 days. (A) Representative images of ECTs. Scale bar 5 mm. (B) ECTs were elongated stepwise in an organ bath, and passive force was detected. Shown are the cross sectional area (CSA) (left) and measured forces normalized to CSA (right) as means ± SEM, n = 3, with a minimum of 6 ECTs in total. (C) ECTs were minced, and lysates were subjected to immunoblot analysis. Representative immunoblot of CTGF and tubulin are shown.

5.3.3 Inhibition of the SRF activation leads to a decreased stiffness of ECTs

As data from 2D culture experiments demonstrated a MRTF/SRF-dependent regulation of CTGF, the influence of the MRTF/SRF inhibition by CCG was also examined in 3D engineered tissue. Similar to the effect observed with the inhibition of $G\alpha_{q/11}$ by the use of the p63ΔN construct (Figure 5.10), treatment with CCG led to a reduction in tissue rigidity, which was, however, not significant and accompanied by an increased CSA (Figure 5.13 A, B). On protein level, the amount of CTGF in the tissue after stretch was 2.7-fold higher, with CCG treatment pointing to reduced secretion and/or increased expression of CTGF. Inhibition of the SRF activity via the MRTF had no effect on the expression of sm-actin in these tissues. This indicates that MRTF/SRF activity plays a role in the regulation of tissue rigidity, and it further substantiates that CTGF is not a regulatory factor for tissue stiffness.

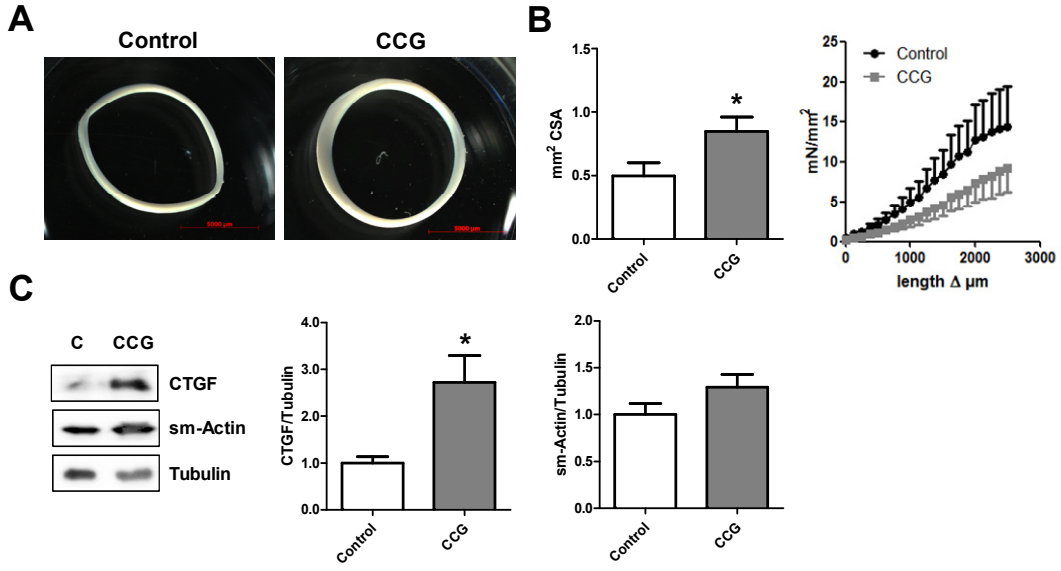

Figure 5.13: Effect of the SRF-dependent regulation of CTGF on viscoelastic properties of ECT
NRCF and collagen were mixed and incubated in the presence or absence of 10 µM CCG-1423 for 5 days. (A) Representative images of ECT. Scale bar 5 mm. (B) ECTs were elongated stepwise in an organ bath, and passive force was detected. Shown are the cross sectional area (CSA) (left) and measured forces normalized to CSA (right) as means ± SEM, n = 3, 9-10 ECT were measured each, *p < 0.05 vs. control. (C) Stretched ECTs were minced and lysates were subjected to immunoblot analysis. Representative immunoblots (left) and quantification of CTGF and sm-Actin (right) are shown. Values are given as means ± SEM, normalized to tubulin and relative to control, n = 3 with 3-4 replicates, *p < 0.05 vs. control.

5.3.4 p63RhoGEF expression in cardiac fibroblasts regulates contractility of engineered muscle tissue (EHM)

For further evidence that p63RhoGEF is involved in auto- and more importantly paracrine signaling in cardiac fibroblasts and thus could effect the function of other cell types, e.g. the contractility of cardiomyocytes, NCRF transduced with p63RhoGEF or the $G\alpha_{q/11}$ inhibiting p63ΔN adenovirus was added to a mixture of isolated heart cells in a 1:5 ratio, and engineered heart muscle tissue (EHM) were cast. Cultivation of these tissues was performed as described in section 4.2.2.7.
First, equal distribution of infected NRCF was confirmed by EGFP detection (Figure 5.14 A, 5.15 A). In addition, α-actinin staining of cardiomyocytes displayed a distinct striated pattern of the sarcomeres as proof for cardiomyocyte maturation within the tissue. It could be ruled out that cardiomyocytes were transduced by the respective virus, as no EGFP signal was visible in these cells.
Isometric force measurement revealed that overexpression of p63RhoGEF increased the resting tension, comparable to the diastolic force generated in a heart, indicating higher rigidity of the tissue. In contrast, the twitch tension was likewise elevated at a different

calcium concentration, pointing to a better contractile performance of the cardiomyocytes in the EHM (Figure 5.14 B). Immunoblot analysis showed a CTGF increase of about 80%, while sm-actin on the protein level was unchanged (Figure 5.14 C).

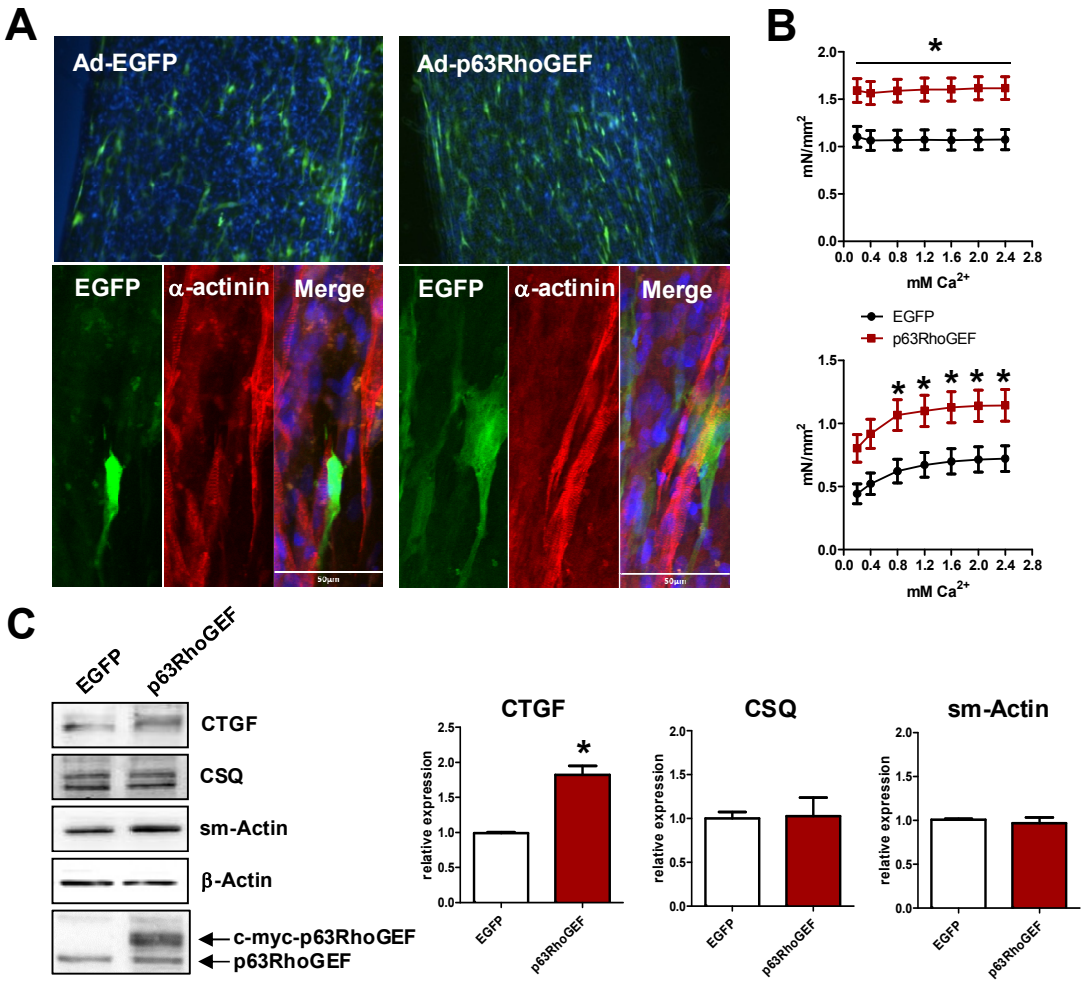

Figure 5.14: Impact of p63RhoGEF overexpression in cardiac fibroblasts on contractile function and CTGF expression of EHM

NRCF were transduced with Ad-EGFP and Ad-p63RhoGEF for 24 h and added to cardiac cells for EHM preparation. (A) Representative images of Ad-EGFP EHM (left) and Ad-p63RhoGEF (right) by confocal microscopy are shown. EGFP expression was detected in sections of EHM to ensure equal distribution of modified fibroblasts. Cardiomyocytes were visualized by α-actinin and nuclei by DAPI staining. (B) Analysis of resting force (top graph) and contractile force (bottom graph) of EHM normalized to cross sectional area at different calcium concentrations is depicted. Shown are means ± SEM, n = 3-5, 15-20 EHM per group were analyzed, *p < 0.05 vs. EGFP. (C) Homogenized EHMs were used for immunoblot analysis. Representative immunoblots are shown. The expression of CTGF, calsequestrin-2 and sm-actin were normalized to β-actin and given relative to Ad-EGFP EHM. In addition, p63RhoGEF was detected by c-myc-tag and specific antibody. Values are given as means ± SEM, n = 7-10, *p < 0.05 vs. EGFP.

Interestingly, when p63RhoGEF overexpressing adenovirus was added after tissue condensation on day 2 of cultivation, mainly cardiomyocytes of the EHM were infected (Figure 5.15 A) and no change in either resting tension or twitch tension was measured. (Figure 5.15 B). Immunoblot analysis revealed an elevated level of CTGF, which was, however, not significant (Figure 5.15 C). Thus, the improved contractility seems to be rather an effect of paracrine signaling initiated by p63RhoGEF expression in cardiac fibroblasts.

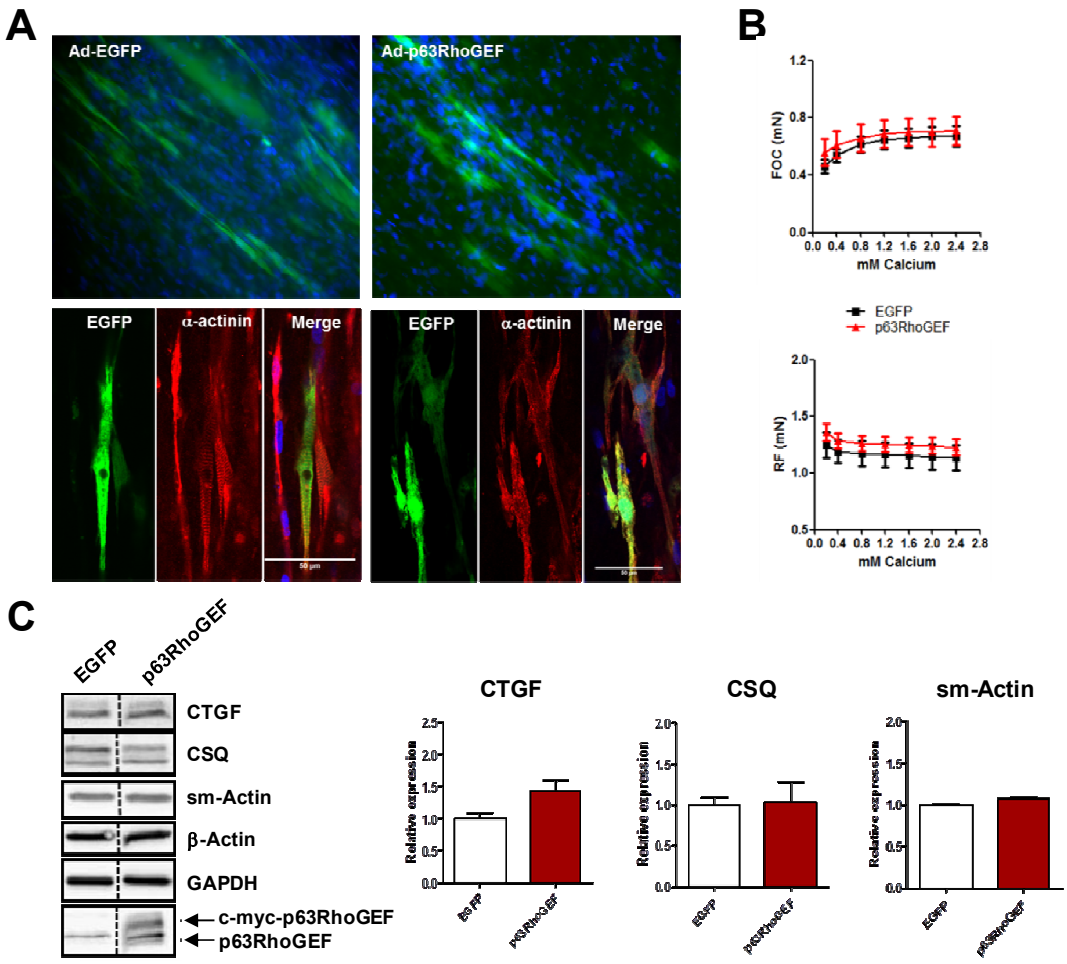

Figure 5.15: Influence of p63RhoGEF overexpression in cardiomyocytes on contractile function and CTGF expression of EHM

EHM were prepared with freshly isolated cardiac cells from neonatal rats and transduced with Ad-EGFP or Ad-p63RhoGEF after tissue condensation on day 2. After cultivation and phasic stretch for 7 days, EHM were used for contraction analysis. (A) Representative images of Ad-EGFP (left) and Ad-p63RhoGEF (right) EHM by confocal microscopy are shown. Adenovirally infected cells were detected in sections of EHM by EGFP expression. Additionally, cardiomyocytes were visualized by α-actinin and nuclei by DAPI staining. (B) Analysis of contractile force (FOC; top graph) and resting force (RF; bottom graph) of EHM at different calcium concentrations is depicted. Shown are means ± SEM, n = 4, with a total of 12-16 EHM per condition were analyzed. (C) Homogenized EHMs were used for immunoblot analysis. Representative immunoblots are shown. The expression of CTGF, calsequestrin-2, and sm-actin were normalized to β-actin and given relative to control-transduced EHM. In addition, p63RhoGEF was detected by c-myc-tag and specific antibody. Values are given as means ± SEM, n = 12-16.

EHM supplemented with p63ΔN-infected NRCF showed adverse effects as described previously for the overexpression of p63RhoGEF in EHM, presenting a lower resting tension accompanied by reduced twitch tension (Figure 5.16 B). CTGF as well as sm-actin were decreased by about 50% on protein level (Figure 5.16 C).

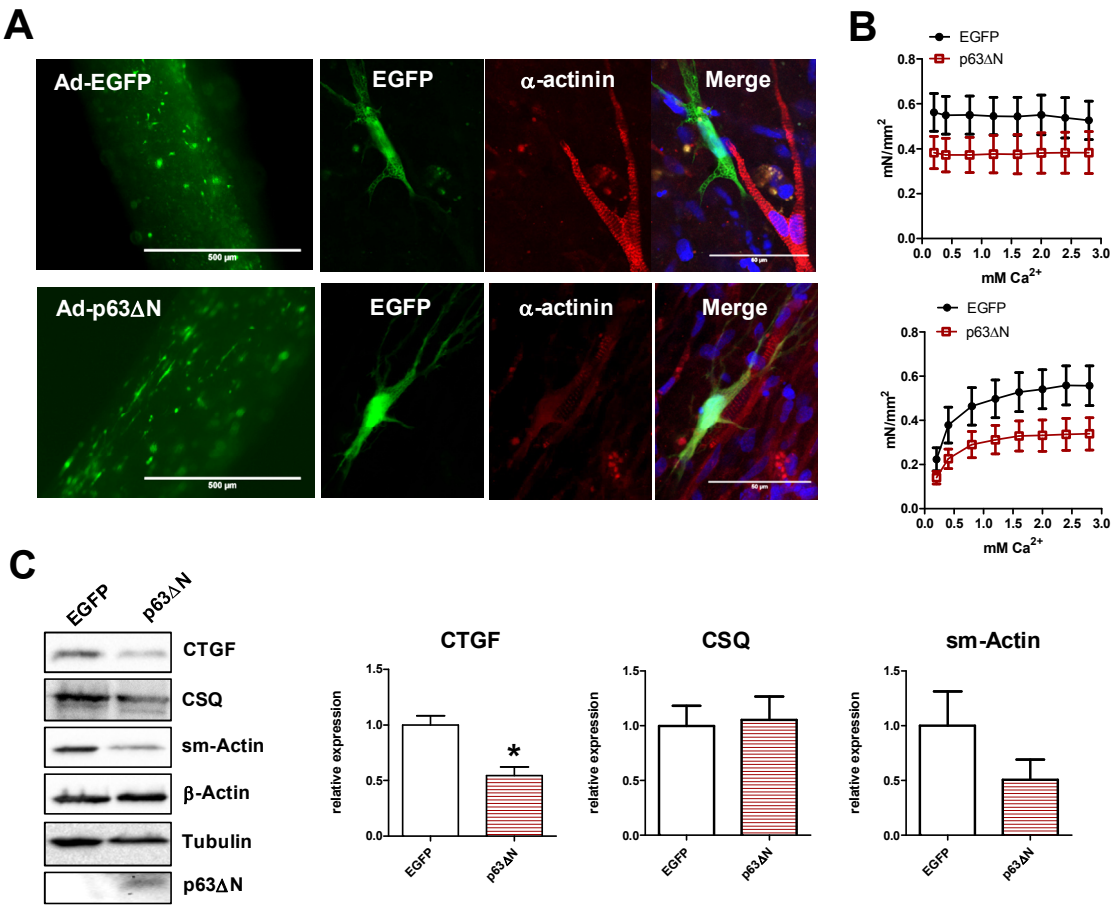

Figure 5.16: Impact of p63RhoGEF inhibition in cardiac fibroblasts on contractile function and CTGF expression of EHM

NRCF were transduced with Ad-EGFP and Ad-p63ΔN for 24 h and added to cardiac cells for EHM preparation. (A) Representative images of Ad-EGFP EHM (upper panel) and Ad-p63ΔN (lower panel) by confocal microscopy are shown. EGFP expression was detected in sections of EHM to ensure equal distribution of modified fibroblasts. Cardiomyocytes were visualized by α-actinin and nuclei by DAPI staining. (B) Analysis of resting force (top graph) and contractile force (bottom graph) of EHM normalized to cross sectional area at different calcium concentrations is depicted. Shown are means ± SEM, n = 3-5, 15-20 EHM per group were analyzed. (C) Homogenized EHMs were used for immunoblot analysis. Representative immunoblots are shown. The expression of CTGF, calsequestrin-2, and sm-actin were normalized to β-actin and given relative to Ad-EGFP EHM. In addition, p63ΔN was detected by c-myc-antibody and tubulin by specific antibody. Values are given as means ± SEM, n = 7-10, *p < 0.05 vs. EGFP.

In conclusion, p63RhoGEF expression in cardiac fibroblasts clearly regulates contractile and viscoelastic properties in 3D engineered heart tissue and affects CTGF expression and secretion in these tissues.

5.4 Impact of the genetic deletion of p63RhoGEF in pressure overload-induced processes of cardiac remodeling

So far, 3D experiments revealed that p63RhoGEF expression in cardiac fibroblasts regulates contractility and stiffness of engineered heart tissue. Overexpression of p63RhoGEF in EHM increased both contractility and tissue stiffness, while blocking the $G\alpha_{q/11}$-pathway by the use of p63ΔN led to reduced contractile function and rigidity. Preliminary data in TAC mice demonstrated that p63RhoGEF expression is changed in pressure overload-dependent processes, and its up-regulation correlates with the deterioration of cardiac function. Therefore, the impact of a reduced and complete loss of p63RhoGEF expression in mice under healthy and pathological conditions of the heart was investigated.

5.4.1 Mice with a global p63RhoGEF knockout are viable and fertile

Due to the lack of a suitable approach to establish a mouse line with a fibroblast-specific deletion of p63RhoGEF at that time, a mouse line with a global knockout of p63RhoGEF was generated. For this purpose, flox-sites were integrated in the genome flanking exon 1 and 2 of the p63RhoGEF allele (Figure 5.17 A). These $p63^{flox/flox}$-mice were then mated with animals of an EIIa-Cre-line, which express the Cre-recombinase from early embryonic stadium on, resulting in a flox site-directed excision of exon 1 and 2; thus the start codon is removed by the Cre-recombinase. In order to receive homozygous $p63RhoGEF^{-/-}$-knockout animals in the next generations, heterozygous p63RhoGEF $^{WT/-}$ mice were mated with each other.

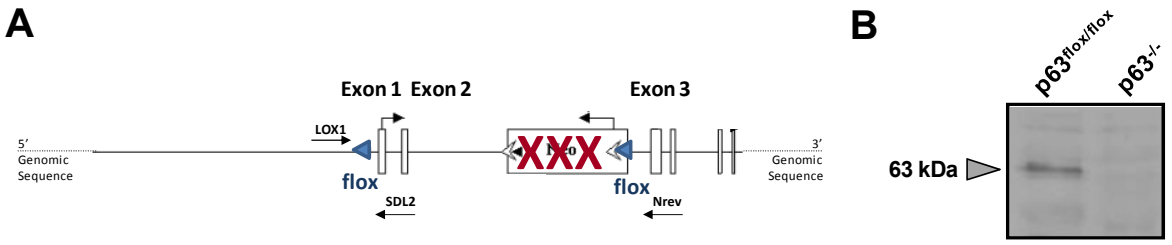

Figure 5.17: Strategy for the generation of p63RhoGEF knockout mice
(A) Schematic illustration of the p63RhoGEF genomic sequence with exon 1 and 2 flanked by flox sites for the generation of a p63RhoGEF knockout allele. In addition, the binding sites of the respective primer for genotyping are shown. (B) Verification of p63RhoGEF deletion in the heart by immunoblot analysis.

To prove the homozygous knockout (-/-) on genomic level, genotyping was performed as described in section 4.2.1.3. For verification of the knockout on protein level, heart samples were lysed and immunoblotting was performed. Detection with a specific antibody against

p63RhoGEF demonstrated a clear absence of a 63 kDa protein in knockout mice compared to mice carrying the homozygous floxed allele (Figure 5.17 B).
For further experiments, mice with a homozygous (KO) as well as heterozygous (HET) knockout of p63RhoGEF were implemented. As control group, wild-type littermates (WT) were used. All mice were viable and fertile and showed no abnormal phenotype under basal conditions.

5.4.2 Partial deletion of p63RhoGEF influences cardiac function at basal condition

To evaluate the influence of the genetic deletion of p63RhoGEF in the heart, cardiac performance was analyzed under basal condition by echocardiography. Analysis of cardiac parameter revealed that the ratio of the left ventricular weight to body weight (LVW/BW) was unchanged in male and female mice regardless of the genotype (Figure 5.18 A). In contrast, contractile parameters were considerably impaired in the heterozygous groups. As a marker for contractility, the fractional area shortening (FAS) was reduced by 10% and, significantly by 15% in HET male and female mice, respectively, showing a similar trend for the ejection fraction (EF) depicted in Table 5.1. Accompanied by this, the systolic volume (Vol s) (Figure 5.18 A) and left ventricular inner diameter (LVID s) (Table 5.1), indicators of changes in the left ventricular lumen, were elevated significantly in HET male and by trend in HET female mice. Interestingly, no difference was observed between the KO group and the WT group (Figure 5.18 A, Table 5.1).

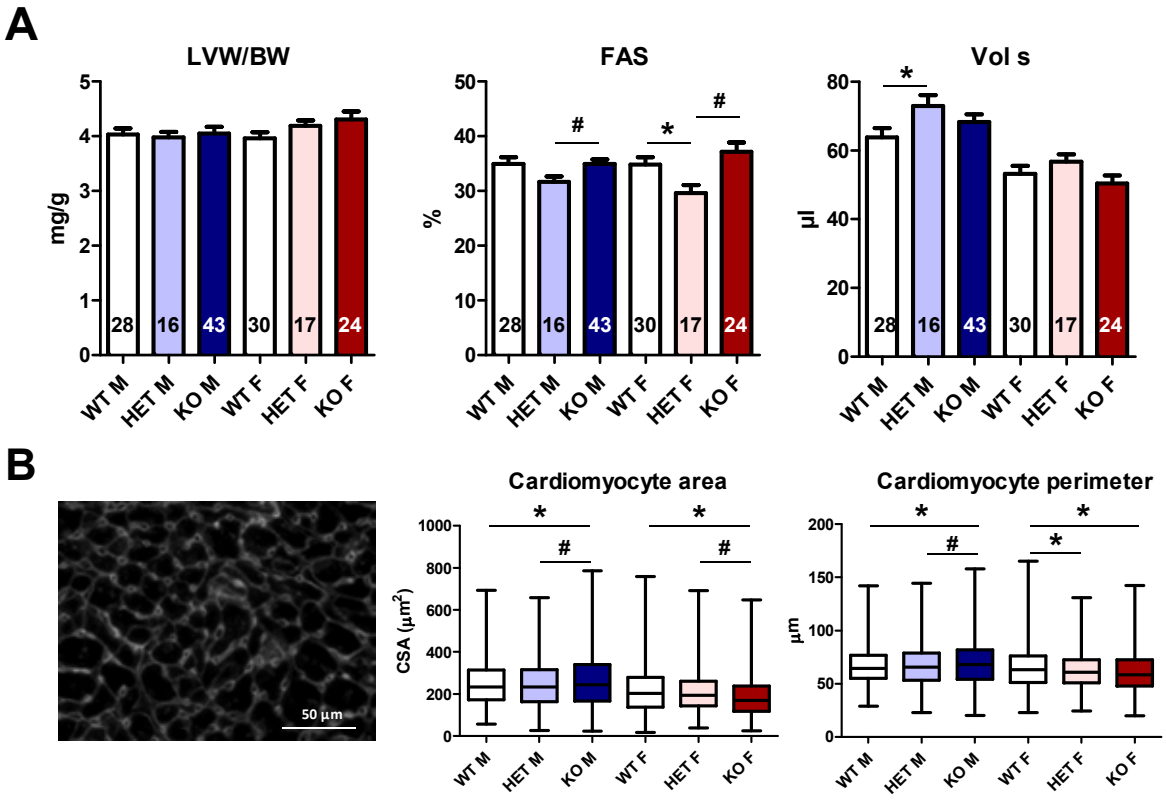

Figure 5.18: Impact of the genetic deletion of p63RhoGEF *in vivo*

(A) Evaluation of basal cardiac function in 10-12 week old mice by echocardiography. Shown are left ventricular weight per body weight (LVW/BW), fractional area shortening (FAS), and systolic volume (Vol s). Values are given as means ± SEM, *p < 0.05 vs. WT group, #p < 0.05 vs. KO group by ANOVA or two conditions by unpaired t-test. The n-numbers are annotated in the respective bars. (B) Glycosylated proteins of ECM were visualized by staining with WGA. A representative image is shown as an example (left), scale bar 50 µm. Cardiomyocyte area (middle) and perimeter (right) of cross-sectional heart sections were analyzed (CSA = cross-sectional area). Results are shown as median with maximal and minimal value, n = 6-10 with more than 200 cells per heart, *p < 0.05 vs. WT group, #p < 0.05 vs. KO group by ANOVA or two conditions by unpaired t-test.

On a cellular level, the dimension of cardiomyocytes in cross-sections of the heart was determined. Morphometric analysis exhibited an increased cardiomyocyte area and perimeter in KO male mice, whereas in KO female mice, both parameters are decreased. In the HET groups, no alteration to the control WT group regarding the cell area of cardiomyocytes was observed (Figure 5.18 B).

Table 5.1: Analysis of basal characterization by echocardiography

Parameter	WT M	HET M	KO M	WT F	HET F	KO F
n	28	16	43	30	17	24
HR (beats/min)	435.9 ± 7.32	442.1 ± 9.28	435.8 ± 5.66	434.3 ± 8.28	433 ± 8.77	449.8 ± 9.39
BW (g)	25.88 ± 0.45	26.68 ± 0.37	27.14 ± 0.32 *	20.81 ± 0.35	19.85 ± 0.36	20.9 ± 0.47
LVW/BW (mg/g)	4.04 ± 0.11	3.98 ± 0.1	4.05 ± 0.12	3.96 ± 0.12	4.19 ± 0.1	4.31 ± 0.15
FAS (%)	34.94 ± 1.21	31.68 ± 1.02 #	34.92 ± 0.86	34.84 ± 1.36	29.59 ± 1.47 *	37.13 ± 1.72
EF (%)	41.33 ± 1.3	38.06 ± 1.13 #	41.39 ± 0.84	40.66 ± 1.34	37.11 ± 1.36	42.74 ± 1.61
Vol s (µL)	63.86 ± 2.65	72.9 ± 3.19 *	68.28 ± 2.23	53.25 ± 2.26	56.67 ± 2.26	50.45 ± 2.29
Vol d (µL)	108.4 ± 3.3	117.5 ± 4.5 *	118.8 ± 3.46 *	89.03 ± 2.62	89.78 ± 2.48	88.23 ± 2.56
LVID s (mm)	3.71 ± 0.07	3.95 ± 0.08 *	3.76 ± 0,06	3.45 ± 0.08	3.57 ± 0.08	3.43 ± 0.09
LVID d (mm)	4.63 ± 0.07	4.8 ± 0.08	4.75 ± 0.06	4.28 ± 0.06	4.32 ± 0.06	4.32 ± 0.08
CI (%)	771.3 ± 29.96	722.9 ± 36.3	792.8 ± 28.51	753.1 ± 33.19	734.2 ± 32.91	825.6 ± 36.59
CO (%)	19.7 ± 0.91	20.25 ± 1.3	21.51 ± 0.81	15.59 ± 0.67	14.55 ± 0.67	17.26 ± 0.84

Abbrevations: n = number; HR = heart rate; BW = body weight; LVW/BW = left ventricular weight/body weight; FAS = fractional area shortening; EF = ejection fraction; Vol s = systolic volume; Vol d = diastolic volume; LVID s = left ventricular inner diameter in systole; = LVID d = left ventricular inner diameter in diastole; CI = cardiac index; CO = cardiac output; *$p < 0.05$ vs. WT group, $^{\#}p < 0.05$ vs. KO group by ANOVA or two conditions by unpaired t-test.

5.4.3 Partial genetic deletion of p63RhoGEF leads to deterioration of contractility along with increased dilation in male mice after TAC

Next, the impact of the reduced and lost expression of p63RhoGEF under pathophysiological condition was investigated. For this, male and female mice were subjected to either TAC or sham surgery and were monitored over a time period of 5 weeks. Analysis of echocardiography showed that in all male and female groups, the transverse aortic flow velocity given as the gradient increased equally, from 5-8 mmHg (sham group) to an average of 70 mmHg (Table 5.2, Figure 5.19 and 5.20) 3 days after surgery.

Table 5.2: Gradients measured by a pulse-waved Doppler 3 days after TAC surgery

Para-meter	WT M		HET M		KO M		WT F		HET F		KO F	
	Sham	TAC	Sham	TAC	Sham	TAC	Sham	TAC	Sham	TAC	Sham	TAC
n	7	12	9	6	11	22	8	11	7	7	9	14
Gradient (mmHg)	6,08 ± 0,99	73,00 ± 4,42 *	5,67 ± 0,51	68,92 ± 7,41 §	8,923 ± 2,39	68,96 ± 3,9 ¥	3,967 ± 0,8	69,10 ± 4,15 *	4,856 ± 0,71	66,77 ± 7,2 §	3,38 ± 0,29	67,16 ± 5,51 ¥

*p < 0.05 vs. WT basal group, §p < 0.05 vs. HET basal group, $^{¥}$p < 0.05 vs. KO basal group by ANOVA or two conditions by unpaired t-test.

As a result of the TAC surgery, mice of all groups developed severe hypertrophy with a significant doubling of the LVW/BW from around 4 mg/g to 8 mg/g within 5 weeks (Figure 5.19 and 5.20, upper panel) with the strongest effect seen already after 1 week.

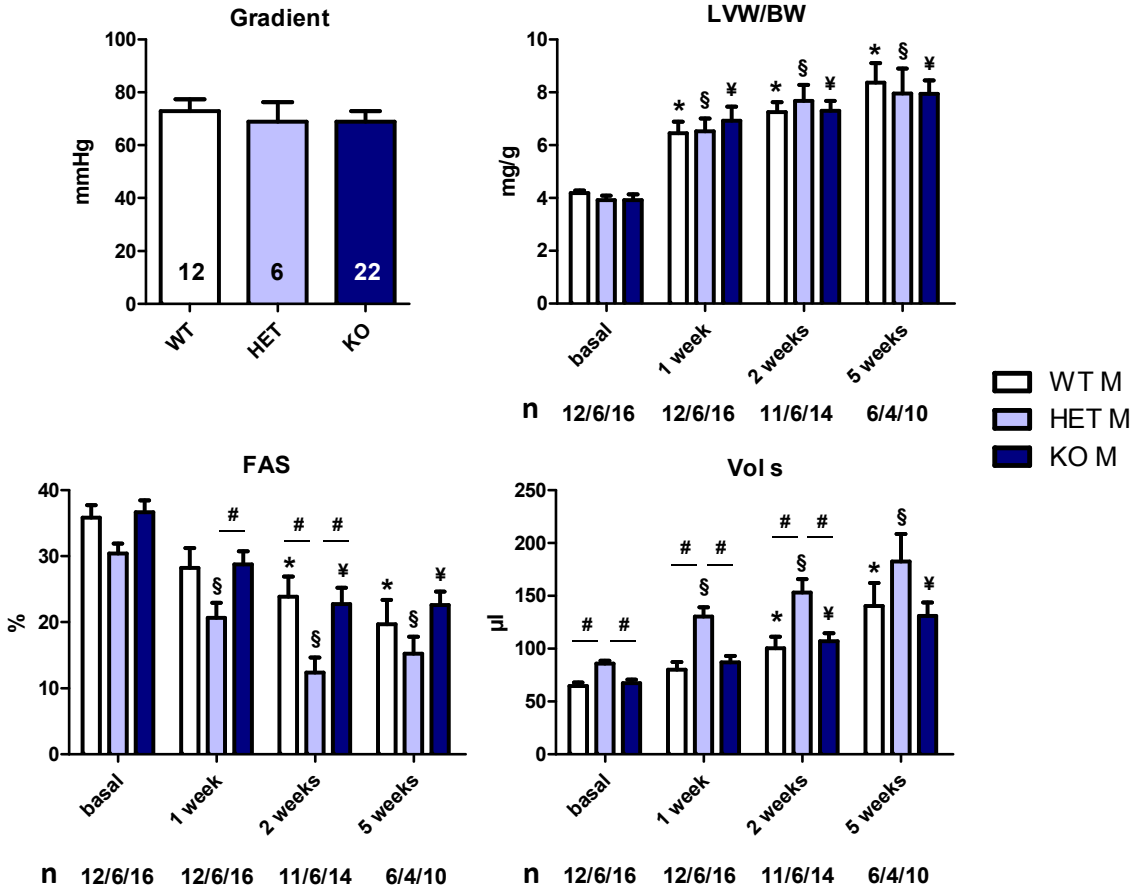

Figure 5.19: Influence of the genetic deletion of p63RhoGEF in male mice on cardiac function after TAC
Evaluation of cardiac parameter after transverse aortic constriction (TAC) by echocardiography. Shown are pressure gradient, left ventricular weight per body weight (LVW/BW), fractional area shortening (FAS), and systolic volume (Vol s) of male mice. Values are given as means ± SEM, *p < 0.05 vs. WT basal group, §p < 0.05 vs. HET basal group, $^{¥}$p < 0.05 vs. KO basal group, $^{#}$p < 0.05 vs. WT and/or KO group by ANOVA or two conditions by unpaired t-test.

Along with the progression of hypertrophy, male mice showed clear worsening of contractile properties and transition to a dilative cardiac phenotype, with the most pronounced impairment in the HET male group.

Within 5 weeks after surgery, the FAS decreased gradually by approximately 45% in all male groups, while the systolic volume was doubled compared to basal level (Figure 5.19 lower panel). Moreover, the EF also declined by approximately 40%, and the systolic LVID elevated by 28% (Table 5.3). Although the change in parameter progressed at a similar rate over the monitored time, the predisposed heterozygous male mice displayed the most severe deterioration of contractility, characterized by an overall decrease in FAS to 15% and EF to 21%, accompanied by an earlier transition to a dilative left ventricular phenotype depicted as a high increase in systolic volume and LVID up to 162 µL and 5.2 mm, respectively (Table 5.3). As already observed under basal conditions, the KO male group revealed a very similar response to pressure overload as the WT group.

Table 5.3: Analysis of cardiac parameters by echocardiography in male mice with TAC surgery
Abbrevations: 1 w = 1 week after TAC, 2 w = 2 weeks after TAC, 5 w = 5 weeks after TAC

Para-meter	WT M				HET M				KO M			
	basal	1 w	2 w	5 w	basal	1 w	2 w	5 w	basal	1 w	2 w	5 w
n	12	12	11	6	6	6	6	4	16	16	14	10
HR (beats/ min)	455.4 ± 14.4	487.8 ± 15.5	491.1 ± 19.9	527.7 ± 11.3	447 ± 14.5	489.5 ± 18.9	491.8 ± 12.3	492.5 ± 26.2	430.5 ± 8.99	463.8 ± 14.6	480 ± 10.6	499.3 ± 14.7
BW (g)	27,04 ± 0,22	27,38 ± 0,39	28,25 ± 0,43	27,55 ± 1,07	27,75 ± 0,2	26,43 ± 0,78	26,22 ± 0,99	27,45 ± 1,09	26,99 ± 0,55	26,21 ± 0,72	27,70 ± 0,6	28,77 ± 0,61
LVW/BW (mg/g)	4.29 ± 0.1	6.45 ± 0.43 *	7.25 ± 0.37 *	8.37 ± 0.74 *	3.91 ± 0.17	6.53 ± 0.49 §	7.68 ± 0.61 §	7.95 ± 0.95 §	3.852 ± 0.23	6.53 ± 0.51 ¥	7.15 ± 0.36 ¥	7.94 ± 0.51 ¥
FAS (%)	35.85 ± 1.86	28.24 ± 2.96 *	23.84 ± 3.06 *	19.67 ± 3.73 *	30.4 ± 1.53	20.7 ± 2.24 §	12.37 ± 2.29 §, # WT/KO	15.22 ± 2.57 §	36.68 ± 1.76	28.76 ± 1.99 ¥	22.74 ± 2.52 ¥	22.59 ± 2.07 ¥
EF (%)	42.62 ± 1.94	34.84 ± 2.96	30.77 ± 3.15	24.35 ± 3.86 *	36.44 ± 1.41	27.14 ± 2.64	18.77 ± 2.46 §, # WT/KO	20.76 ± 3.54	42.7 ± 1.68	34.9 ± 1.97	28.41 ± 2.44 ¥	27.18 ± 2.26 ¥
Vol s (µL)	64.66 ± 3.1	80.18 ± 7.2	100.5 ± 10.85	140.6 ± 21.62 *	82.41 ± 4.038 §, # WT/KO	121.6 ± 11.3 # WT	142 ± 15.15 §, # WT/KO	161.6 ± 27.84 §	67.24 ± 3.34	87.2 ± 6.09	107.3 ± 7.51 ¥	131 ± 12.62 ¥
Vol d (µL)	112.3 ± 2.59	121.7 ± 7. 46	141.9 ± 9.95 *	181.2 ± 20.73 *	129.6 ± 5.39 # WT	161.2 ± 11.73 §, # WT	173.3 ± 15.57 §	200.6 ± 26.63 §	117.5 ± 5.17	132.7 ± 7.34	148.5 ± 8.03 ¥	178 ± 13.3 ¥
LVID s (mm)	3.68 ± 0.09	3.9 ± 0.15	4.13 ± 0.18 *	4.74 ± 0.36 *	4.16 ± 0.13 §, # WT	4.8 ± 0.22 §, # WT/KO	5.0 ± 0.28 §, # WT/KO	5.23 ± 0.36	3.76 ± 0.09	4.13 ± 0.13 ¥	4.35 ± 0.14 ¥	4.79 ± 0.24 ¥
LVID d (mm)	4.66 ± 0.05	4.61 ± 0.11	4.77 ± 0.11	5.24 ± 0.24 *	5.01 ± 0.12 # WT	5.37 ± 0.21 §, # WT	5.29 ± 0.22 # WT	5.68 ± 0.28 §	4.74 ± 0.09	4.88 ± 0.12	5.07 ± 0.12 ¥	5.42 ± 0.2 ¥
CI (%)	807.6 ± 52.14	734.6 ± 56.49	708 ± 44.36	785.2 ± 84.36	765.3 ± 61.24	818.2 ± 78	591.1 ± 72.71	692.6 ± 35.04	807.8 ± 58.1	806 ± 54.4	712.7 ± 61.02	817.3 ± 70.88
CO (%)	21.86 ± 1.47	20.05 ± 1.54	19.97 ± 1.22	21.37 ± 1.78	21.24 ± 1.74	21.67 ± 2.22	15.42 ± 1.72 §, # WT	18.98 ± 1.07	21.7 ± 1.47	21.1 ± 1.5	19.85 ± 1.74	23.42 ± 2.0

Abbrevations: n = number; HR = heart rate; BW = body weight; LVW/BW = left ventricular weight/body weight; FAS = fractional area shortening; EF = ejection fraction; Vol s = systolic volume; Vol d = diastolic volume; LVID s = left ventricular inner diameter in systole; = LVID d = left ventricular inner diameter in diastole; CI = cardiac index; CO = cardiac output; *$p < 0.05$ vs. WT basal group, $^{§}p < 0.05$ vs. HET basal group, $^{¥}p < 0.05$ vs. KO basal group, $^{\#}p < 0.05$ vs. WT and/or KO group by ANOVA or two conditions by unpaired t-test.

In female mice, the overall effect of the pressure overload increase was less prominent than in the corresponding male mice, resulting in an approximately 21% decline in FAS and EF as well as a 45-50% and 15-20% increase in systolic volume and LVID, respectively, within 5 weeks after TAC intervention. Additionally, the adverse effects seen in the HET male mice were less pronounced in the female HET group, showing only small differences in FAS and systolic volume compared to the female WT group (Figure 5.20; Table 5.4). Comparison of KO female and WT female mice again displayed a similar response to pressure overload, confirming the results observed in the male groups.
These findings suggest that female mice in general can adapt to the increased afterload by TAC surgery better than male mice.

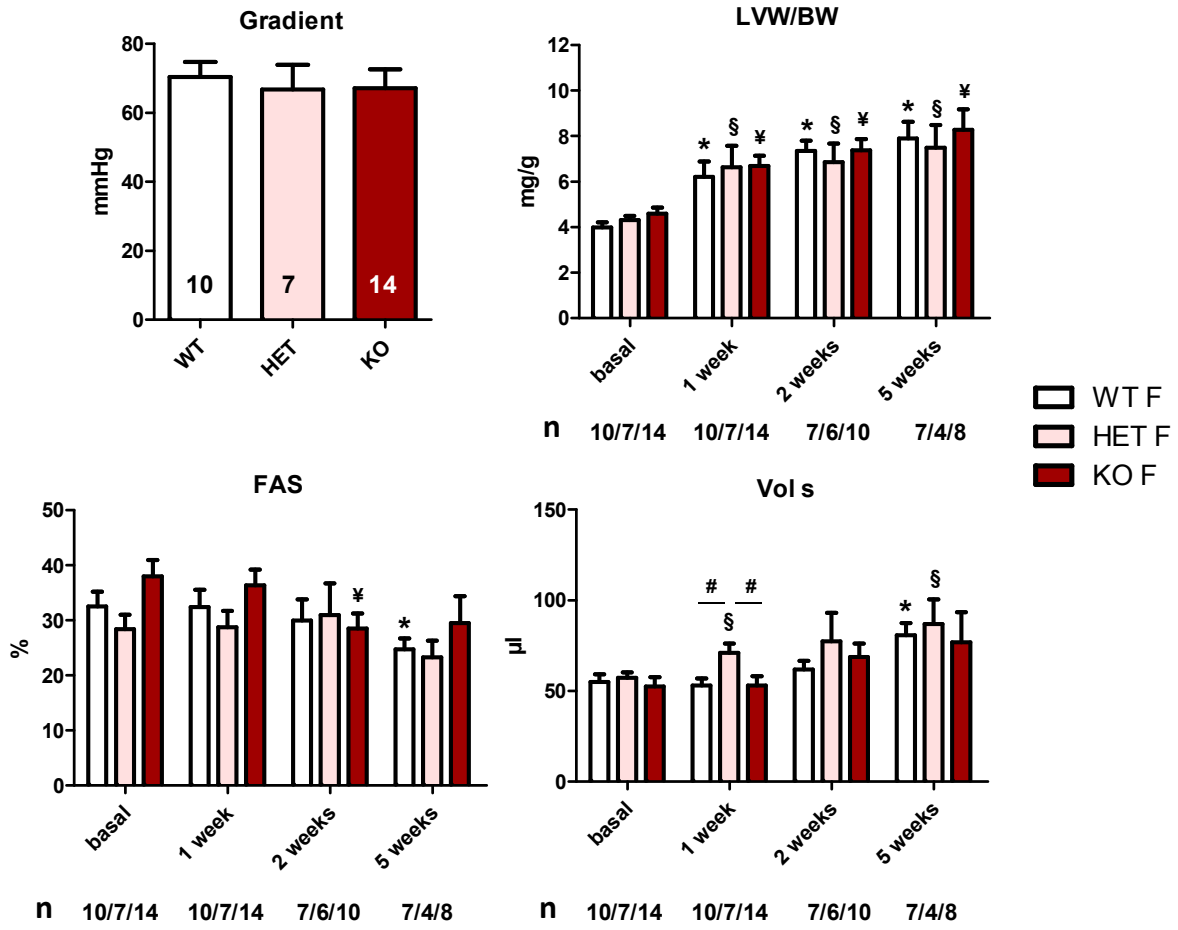

Figure 5.20: Influence of the genetic deletion of p63RhoGEF in female mice on cardiac function after TAC
Evaluation of cardiac parameter after transverse aortic constriction (TAC) by echocardiography. Shown are pressure gradient, left ventricular weight per body weight (LVW/BW), fractional area shortening (FAS) and systolic volume (Vol s) of female mice. Values are given as means ± SEM, *p < 0.05 vs. WT basal group, §p < 0.05 vs. HET basal group, $^{¥}$p < 0.05 vs. KO basal group, $^{\#}$p < 0.05 vs. WT and/or KO group by ANOVA or two conditions by unpaired t-test.

Table 5.4: Analysis of cardiac parameters by echocardiography in female mice with TAC surgery
Abbrevations: 1 w = 1 week after TAC, 2 w = 2 weeks after TAC, 5 w = 5 weeks after TAC

Para-meter	WT F				HET F				KO F			
	basal	1 w	2 w	5 w	basal	1 w	2 w	5 w	basal	1 w	2 w	5 w
n	10	10	8	7	7	7	6	4	14	14	10	8
HR (beats/ min)	428.7 ± 12.1	470.5 ± 16.18	506.5 ± 12.81	520.4 ± 8.07	433.4 ± 13.77	444.6 ± 19.23	470.7 ± 9.89	449.8 ± 24.42	447.1 ± 10.41	477,9 ± 10.8	505.9 ± 13.1	485.6 ± 18.41
BW (g)	20,99 ± 0,79	21,23 ± 0,7	21,75 ± 0,7	22,31 ± 0,64	19,61 ± 0,52	19,37 ± 0,73	21,17 ± 1,79	20,30 ± 1,54	20,39 ± 0,39	20,71 ± 0,33	21,32 ± 0,43	22,24 ± 0,44 ¥
LVW/BW (mg/g)	4.0 ± 0.22	6.21 ± 0.68 *	7.35 ± 0.45 *	7.91 ± 0.72 *	4.31 ± 0.19	6.63 ± 0.94 §	6.86 ± 0.82 §	7.5 ± 1.0 §	4.59 ± 0.26	6.689 ± 0.46 ¥	7.38 ± 0.5 ¥	8.28 ± 0.91 ¥
FAS (%)	32.51 ± 2.65	32.38 ± 3.19	29.92 ± 3.84	24.75 ± 2.0 *	28.39 ± 2.59	28.73 ± 3.01	30.94 ± 5.74	23.27 ± 3.0	37.96 ± 2.98	36.3 ± 2.89	28.53 ± 2.68 ¥	29.53 ± 4.81
EF (%)	38.73 ± 2.6	38.88 ± 3.09	35.03 ± 3.64	28.95 ± 2.38 *	36.34 ± 2.38	35.71 ± 2.9	36.05 ± 5.96	28.92 ± 4.05	43.8 ± 2.76	41.2 ± 2.76	33.45 ± 2.7 ¥	34.5 ± 4.83
Vol s (µL)	54.95 ± 4.26	52.89 ± 3.89	61.76 ± 4.82	80.65 ± 6.79 *	57.29 ± 2.89	71.1 ± 4.98 §, # WT/KO	77.27 ± 15.85	86.89 ± 13.58 §	52.46 ± 5.16	53.12 ± 4.95	68.66 ± 7.554	76.78 ± 16.66
Vol d (µL)	89.46 ± 5.57	85.73 ± 2.79	95.36 ± 5.68	124.8 ± 12.08 *	90.08 ± 3.67	109,9 ± 3.74 §, # WT/KO	114.6 ± 14.4	120.9 ± 13.2 §	92.42 ± 7.24	88.92 ± 5.58	109.4 ± 10.46	129.2 ± 20.45
LVID s (mm)	3.53 ± 0.14	3.49 ± 0.12	3.36 ± 0.13	4.28 ± 0.2 *	3.57 ± 0.08	3.71 ± 0.14	3.7 ± 0.41	4.05 ± 0.24 §	3.49 ± 0.14	3.36 ± 0.15	3.75 ± 0.28	4.03 ± 0.38
LVID d (mm)	4.3 ± 0.08	4.14 ± 0.09	4.13 ± 0.1	4.89 ± 0.13 *	4.36 ± 0.07	4.45 ± 0.12 # WT	4.39 ± 0.3	4.71 ± 0.14 §	4.34 ± 0.12	4.23 ± 0.13	4.39 ± 0.17	4.75 ± 0.26
CI (%)	691.9 ± 95.43	721.8 ± 43.4	775.4 ± 78.91	827.8 ± 82.42	728.3 ± 67.48	853 ± 63.06	851.9 ± 85.9	763.3 ± 101.9	872.9 ± 72.9	821.6 ± 59.95	841.7 ± 76.63	843.4 ± 62.92
CO (%)	14.85 ± 1.41	15.34 ± 0.86	16.83 ± 1.91	18.33 ± 1.67	14.3 ± 1.42	17.29 ± 1.35	17.54 ± 1.45	15.34 ± 2.05	17.82 ± 1.57	17.09 ± 1.3	17.9 ± 1.68	18.68 ± 1.3

Abbrevations: n = number; HR = heart rate; BW = body weight; LVW/BW = left ventricular weight/body weight; FAS = fractional area shortening; EF = ejection fraction; Vol s = systolic volume; Vol d = diastolic volume; LVID s = left ventricular inner diameter in systole; = LVID d = left ventricular inner diameter in diastole; CI = cardiac index; CO = cardiac output; *$p < 0.05$ vs. WT basal group, $^{§}p < 0.05$ vs. HET basal group, $^{¥}p < 0.05$ vs. KO basal group, $^{\#}p < 0.05$ vs. WT and/or KO group by ANOVA or two conditions by unpaired t-test.

Finally, the echocardiography parameters of the sham groups are given in table 7.1 for male and in table 7.2 for female mice (see appendix). No impact of the sham surgery was found.

5.4.4 Genetic deletion of p63RhoGEF expression has no major influence on afterload induced hypertrophy

At the endpoint of 5 weeks after TAC or sham surgery, hearts were collected for further histological investigations. As a hypertrophic response to the afterload induction, the excised hearts of TAC mice showed a prominent increase in the heart weight to tibia length ratio (HW/TL) of approximately 70-80% in all male groups and to a slightly lesser extent in female mice groups compared to the respective sham group, confirming the results obtained by echocardiography analysis (Figure 5.21).

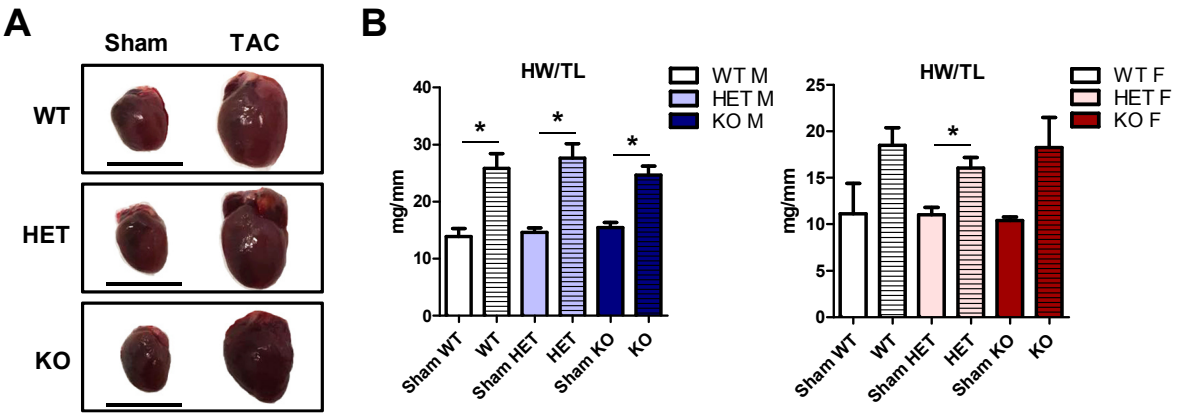

Figure 5.21: Influence of p63RhoGEF expression on afterload-induced hypertrophy
Evaluation of hypertrophic hearts 5 weeks after transverse aortic constriction (TAC). (A) Representative images of excised hearts from male mice. Scale bar 1 cm. (B) Analysis of male (left) and female (right) heart weight (HW) normalized to tibia length (TL) is depicted. Values are given as means ± SEM, male n = 4-10, female n = 3-8, *p < 0.05 vs. respective sham group by ANOVA or two conditions by unpaired t-test.

To further verify the observed hypertrophy of the hearts on a cellular level, the cross-sectional area (CSA) of ventricular cardiomyocytes were determined and showed a significant rise in cell size after TAC (Figure. 5.22 A). In all TAC male groups the cardiomyocyte area was increased by 160 ± 5.5 µm^2 compared to the respective sham groups (Figure 5.22 B; upper panel). In the female mice, the cross-sectional area of cardiomyocytes was elevated by about 64.7 ± 3.6 µm^2 in the WT as well as KO TAC group and, with 165.4 ± 5.5 µm^2, even more in HET female mice compared to the sham group (Figure. 5.22 B, lower panel). Amongst the TAC groups, cardiomyocytes in KO male hearts

reached the largest cross-sectional area (median 384.5 µm^2), whereas KO female mice displayed the smallest cardiomyocyte size (median 223.1 µm^2) in cross-sections of the left ventricle.

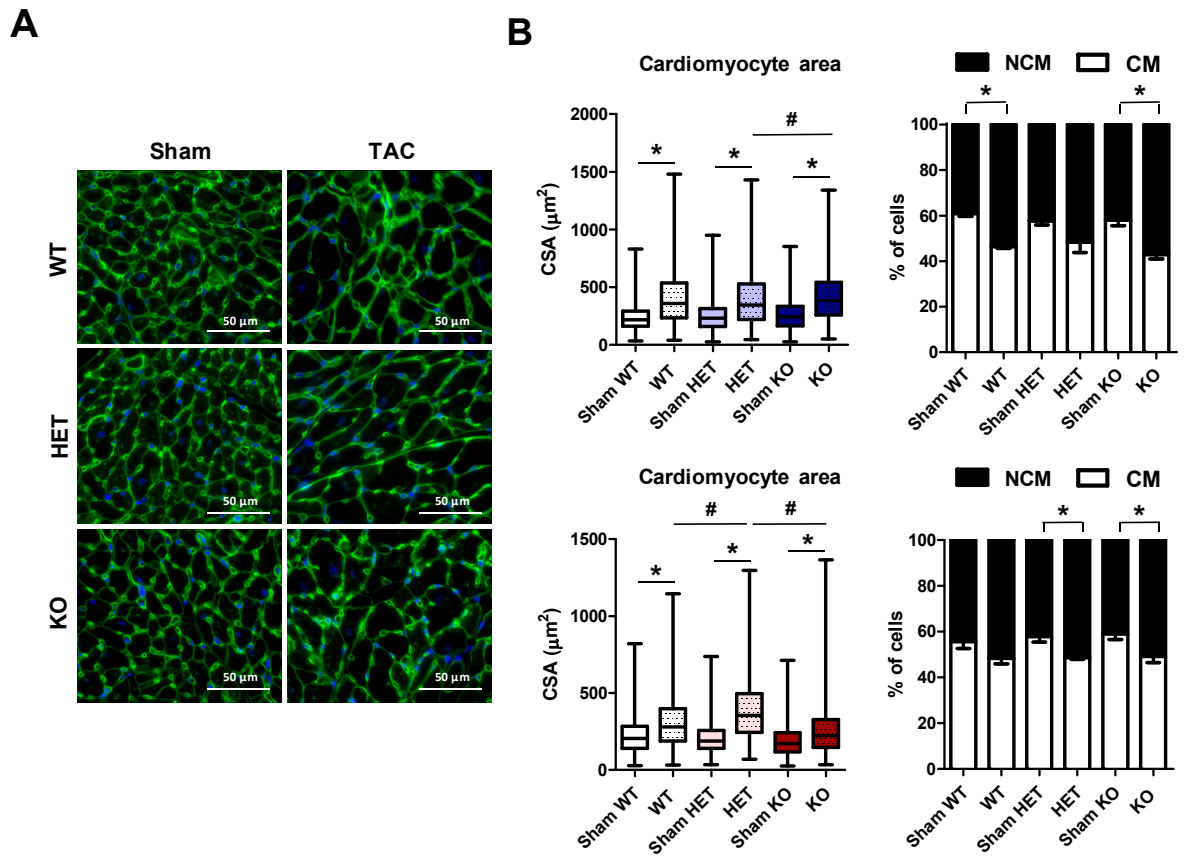

Figure 5.22: Evaluation of cardiomyocyte area and cell distribution after TAC
Analysis of hypertrophy and heart cell composition 5 weeks after transverse aortic constriction (TAC). Cross-sectional heart sections were prepared, and ECM was visualized by staining glycosylated proteins of the ECM with wheat germ agglutinin (WGA). Nuclei were stained using DAPI. (A) Representative images of sham and TAC hearts from male mice are depicted. Scale bar 50 µm. (B) Cross-sectional area (CSA) of cardiomyocytes from male (upper panel) and female (lower panel) hearts were determined. In addition, the ratio between cardiomyocytes (CM) and non-cardiomyocytes (NCM) were analyzed by cell and nuclei counting. Results are given as median with maximal and minimal value, male n = 4-9, female n = 3-7, *$p < 0.05$ vs. respective sham group, $^{\#}p < 0.05$ vs. WT/KO group by ANOVA or two conditions by unpaired t-test.

Furthermore, the distribution of cardiomyocytes (CM) and non-cardiomyocytes (NCM) within the cross-sections of the hearts was assessed by cardiomyocyte and nuclei counting (Figure 5.22 A). In sham-operated mice, the percentage of CM and NCM was around 60% to 40%, respectively, while the proportion was shifted after TAC leading to a 50% : 50% distribution, independent of gender and genotype (Figure 5.22 B). Whether this alteration is

due to enhanced cell death of cardiomyocytes and/or proliferation by the non-cardiomyocyte population was not further elucidated.
In summary, the hypertrophic growth of the heart reflected by LVW/BW, HW/TL and cardiomyocyte size was similar in all analyzed animals. Moreover, no difference in the proportion of CM and NCM was found.
On a molecular level, the expression of hypertrophy-associated marker in tissue of the left ventricle was determined by qPCR. Natriuretic peptides, such as ANP and BNP, are highly secreted by heart muscle cells in response to excessive stretching of the heart and high blood volume and are considered to be cardioprotective. The expression of ANP was significantly increased by about 17-fold and 20-fold in WT and KO animals after TAC, whereas the HET group revealed only an 8.5-fold up-regulation compared to the respective sham group. For BNP a 7.5-fold up-regulation in WT was found after TAC, while in the HET and KO group it was less increased compared to the WT group (Figure 5.23).

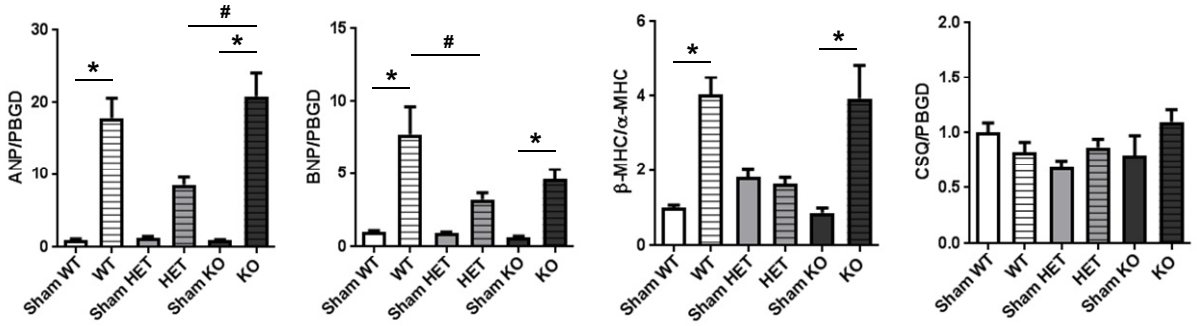

Figure 5.23 Impact of p63RhoGEF expression level on the regulation of hypertrophy-associated factors
Evaluation of gene expression 5 weeks after transverse aortic constriction (TAC). RNA was isolated from male and female hearts of TAC and sham operated mice, cDNA was synthesized, and expression of respective markers was assessed by qPCR. Values were normalized to the housekeeping gene PBGD and are given as means ± SEM, n = 4-10, *$p < 0.05$ vs. Sham group, $^{\#}p < 0.05$ vs. WT/KO by ANOVA or two conditions by unpaired t-test. Abbrevations: ANP = atrial natriuretic peptide, BNP = brain natriuretic peptide, β-MHC = β-myosin heavy chain, CSQ = calsequestrin.

The ratio of the contractile isoform of the myosin heavy chain α-MHC and β-MHC showed a 4-fold up-regulation in the WT and KO TAC animals. In contrast, the ratio was already 2-fold higher in the HET sham group by trend compared to the WT sham animals and was not further up-regulated in the HET group after TAC. No significant changes on mRNA level were detected for calsequestrin.
All together, no major difference in the up-regulation of molecular marker of cardiac growth in KO and WT TAC animals was found. In the HET group, the cardioprotective marker ANP and BNP were less up-regulated, and the β-isoform of myosin heavy chain was not increased after TAC induction.

5.4.5 Partial expression of p63RhoGEF decreases fibrosis in TAC animals by trend

Next to hypertrophy, the influence of reduced and loss of p63RhoGEF expression on the appearance of fibrotic tissue due to pressure overload was assessed. Staining of cross-sections of hearts for collagen, the main component of the ECM, revealed that the amount of fibrotic tissue was reduced in the HET TAC group of male and female mice in comparison to the WT TAC groups, however not significantly (Figure 5.24 A, B). In WT and KO TAC animals the level of collagen deposition in the perivascular as well as interstitial regions was massively increased.

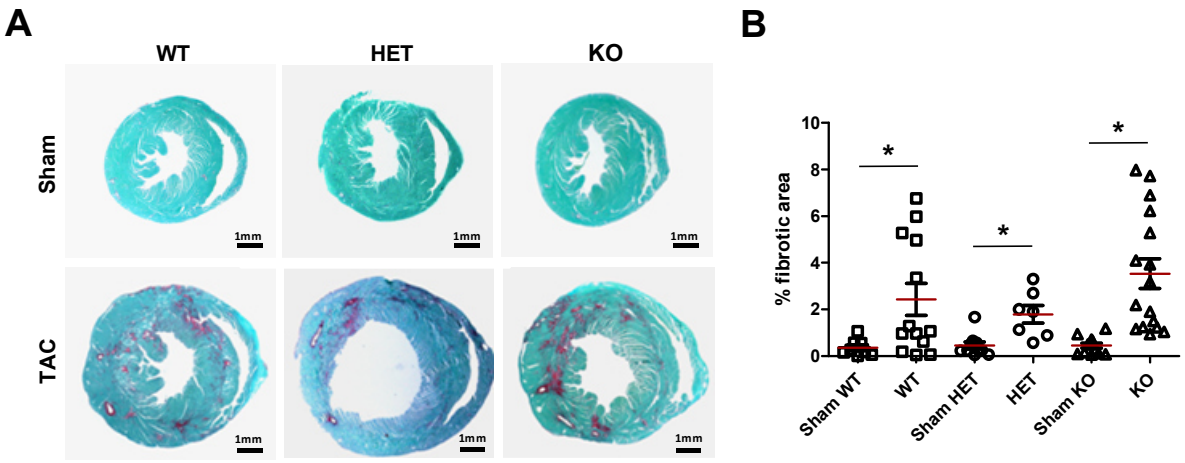

Figure 5.24: Impact of p63RhoGEF expression on myocardial fibrosis
Evaluation of fibrotic tissue 5 weeks after transverse aortic constriction (TAC). Cross-sectional heart sections were stained with Fast Green (non-collagen in green) and Sirius Red (collagen in red). (A) Representative images of sham and TAC male hearts are shown. Scale bar 1 mm. (B) Amount of collagen was analyzed in male and female hearts using Image J and is given in percent, *p < 0.05 vs. sham group by ANOVA or two conditions by unpaired t-test.

Notably, the KO mice displayed a clear overall increase in collagen deposition in comparison to the respective sham group, while in the WT group, two subgroups emerged. As described, one subgroup developed elevated levels of fibrosis ranging from 3-7% of collagen per cross-sectional area, whereas in the other subgroup, the collagen amount remained within the same range (below 1%) as in the respective sham group.
To further validate these findings on a molecular level, expression of fibrosis-associated marker was investigated by quantitative RT-PCR. In general, most of these factors were highly up-regulated after TAC (Figure 5.25).
The myofibroblast marker sm-Actin was already approximately 2-fold and 3-fold up-regulated in the sham animals of the HET and KO groups, respectively. In the WT and HET animals a similar increase in sm-actin was observed after TAC, while in the KO TAC group no further up-regulation occurred. Collagen type 1 (Col1a1) was increased 5-fold and 4-fold in WT and HET animals after TAC, respectively, while the KO group displayed a slightly higher

increase on mRNA level. Collagen type 3 (Col3a1) was increased 4-fold in both the HET and KO TAC groups, with a slightly lower amount of mRNA in the WT group.

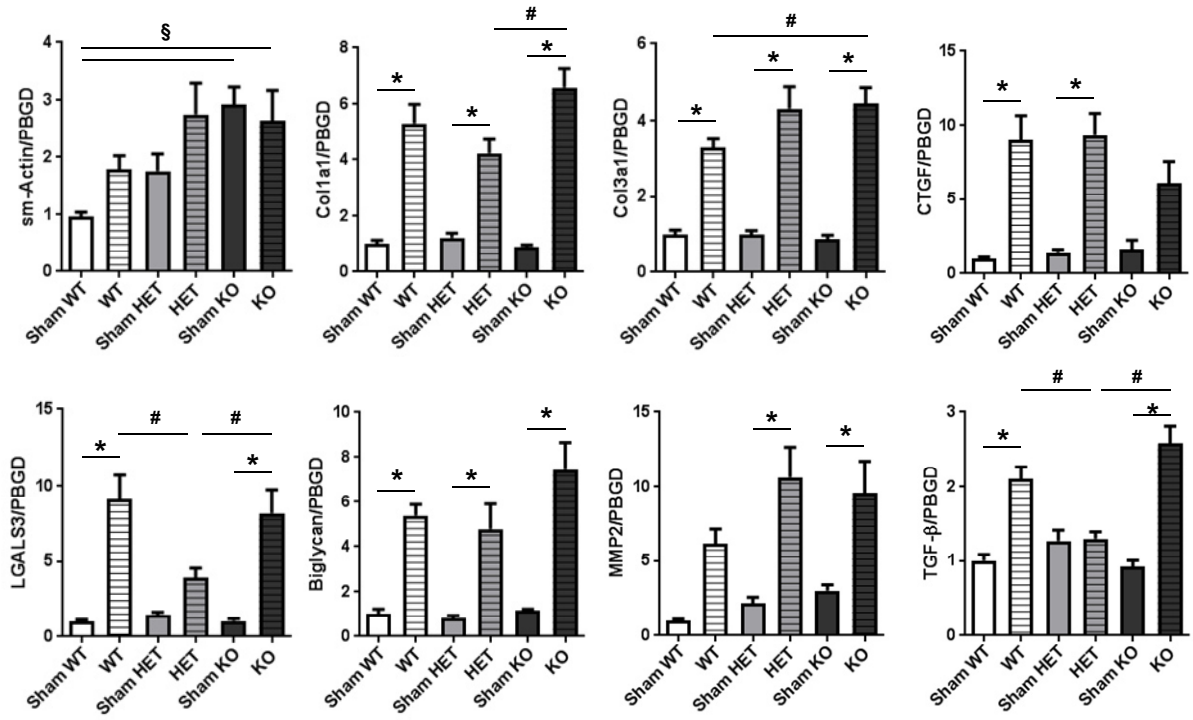

Figure 5.25: Impact of p63RhoGEF expression level on the regulation of fibrosis-associated factors
Evaluation of fibrotic factors 5 weeks after transverse aortic constriction (TAC). RNA was isolated from male and female hearts of TAC and sham operated mice, cDNA was synthesized, and expression of fibrotic markers was assessed by qPCR. Values were normalized to the housekeeping gene PBGD and are given as means ± SEM, n = 4-10, *$p < 0.05$ vs. sham group, $^{\#}p < 0.05$ vs. WT/KO, $^{\S}p < 0.05$ vs. WT Sham by ANOVA or two conditions by unpaired t-test. Abbrevations: sm-Actin = smooth muscle-Actin**,** Col1a1 = collagen type 1, Col3a1 = collagen type III, LGALS3 = galectin-3, biglycan, MMP2 = matrix metalloproteinase 2, TGF-β = transforming growth factor-β, CTGF = connective tissue growth factor**.**

In contrast, the β-galactoside binding lectin LGALS3 showed a 7- to 8-fold rise on mRNA level in KO and WT TAC animals, but was significantly less increased in the HET group. Biglycan, a proteoglycan involved in collagen fibril assembly, displayed similar elevated levels for the WT and HET TAC group, with an even higher increase in the KO TAC group. For MMP2, a matrix degrading proteinase, already an up-regulation in the HET and KO Sham group in a dose-dependent manner was found to have reached a 2.5-fold increase in the KO Sham group. After TAC, MMP2 was approximately 10-fold up-regulated in both HET and KO animals, while the WT group showed a less increased level. CTGF increased by approximately 9-fold in WT and HET TAC groups and was slightly less up-regulated in the KO animals after TAC. Interestingly, TGF-β showed similarly elevated mRNA levels in the WT and KO TAC groups, whereas no increase in the HET group after TAC was detected.

The results obtained from the histological staining of collagen and the expression profile of fibrotic marker point to a changed regulation of the ECM turnover in the HET mice after TAC that was different from the WT group. Thus, reduction of p63RhoGEF expression might have a beneficial effect on afterload-induced fibrosis.

5.4.6 The knockout of p63RhoGEF increases the mortality in male mice in afterload induced cardiac disease

Comparison between KO and WT groups after TAC surgery showed no huge difference in cardiac performance within the 5 weeks of monitoring. Furthermore, hypertrophy and fibrosis were established in a similar way. Interestingly, a dramatic increase in mortality was observed among KO male mice within the first two weeks after TAC leading to a survival rate of less than 60% (Figure 5.26).

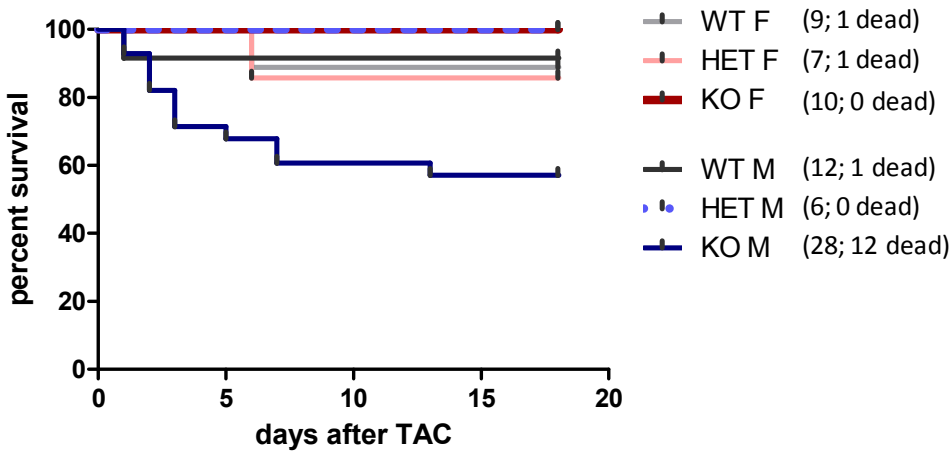

Figure 5.26: Impact of p63RhoGEF knockout on survival rate after TAC
Kaplan-Meier survival rate over a time period of 3 weeks after TAC is shown. WT F n = 9, HET F n = 7, KO F n = 10, WT M n = 12, HET M n = 6, KO M n = 28.

To elucidate possible reasons that might have led to this impaired survival in afterload-dependent cardiac disease, underlying processes of cardiac remodeling were examined more closely. Heart samples from KO male mice, which had to be sacrificed, were used for evaluation on the histological level. Analysis of the cross-sectional area and perimeter of cardiomyocytes revealed a significant decrease in cell size and perimeter compared to basal KO mice and WT mice. In contrast, 2 weeks after TAC, the cardiomyocyte area and perimeter were already increased, showing a hypertrophic response due to pressure overload (Figure

5.27 B). In addition, no change in the proportional distribution of cardiomyocytes (CM) and non-cardiomyocytes (NCM) was detected in the sacrificed male mice keeping a 60% CM to 40% NCM ratio like the basal KO and WT group.

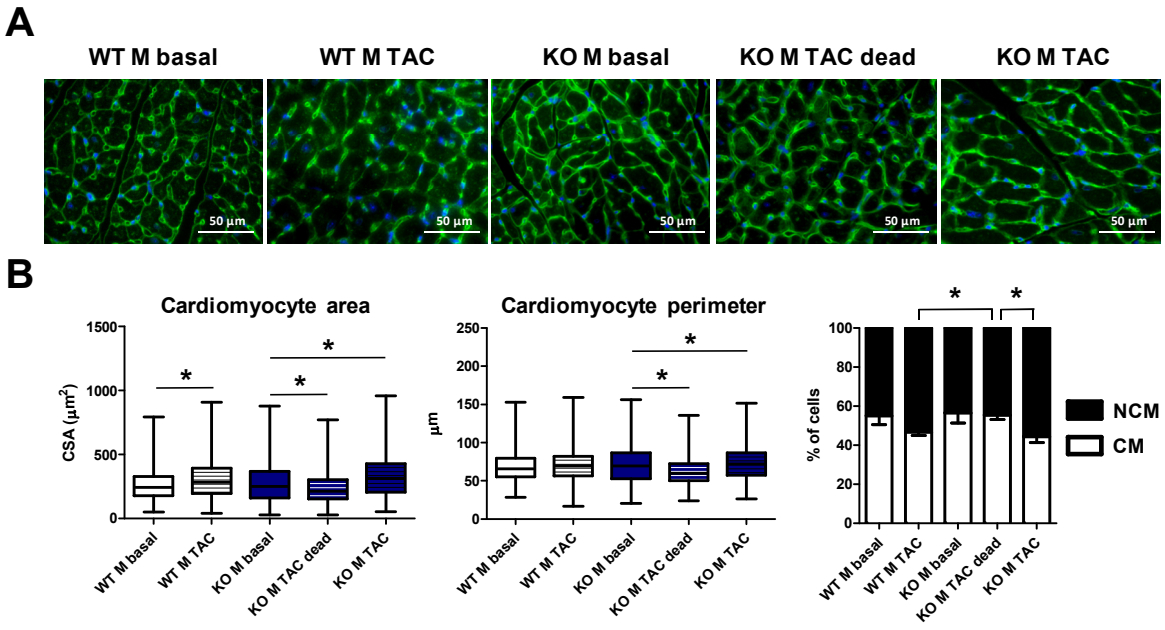

Figure 5.27: Analysis of cardiomyocyte area and cell distribution in the context of increased mortality in KO male mice after TAC

Analysis of hypertrophy and heart cell composition within 2 weeks after transverse aortic constriction (TAC). Cross-sectional heart sections were prepared from male mice before TAC surgery (WT M basal and KO M basal), 2 weeks after TAC surgery (WT M TAC and KO M TAC), and sacrificed male mice between 2-7 days after TAC (KO M dead). The ECM was visualized by staining glycosylated proteins of the ECM with wheat germ agglutinin (WGA) for glycosylated proteins of the ECM. Nuclei were stained using DAPI. (A) Representative images of basal and TAC hearts from WT and KO male mice are depicted. Scale bar 50 µm. (B) Cardiomyocyte area (left) and perimeter (middle) of cross sectional heart sections were analyzed. In addition, the ratio between cardiomyocytes and non-cardiomyocytes was analyzed by cardiomyocyte and nuclei counting (right). n = 3-6 with more than 200 cells per heart *$p < 0.05$ vs. respective basal group by ANOVA or two conditions by unpaired t-test.

For this reason, extensive hypertrophy and changes in cell proportions can be excluded as putative factors influencing the death rate shortly after TAC.

Likewise, the amount of fibrosis by analysis of collagen as well as the WGA amount was examined and revealed no excessive fibrotic response in the sacrificed mice compared to KO and WT male mice 2 weeks after TAC. Rather, the amount was similar to the basal KO group shortly after TAC intervention (Figure 5.28).

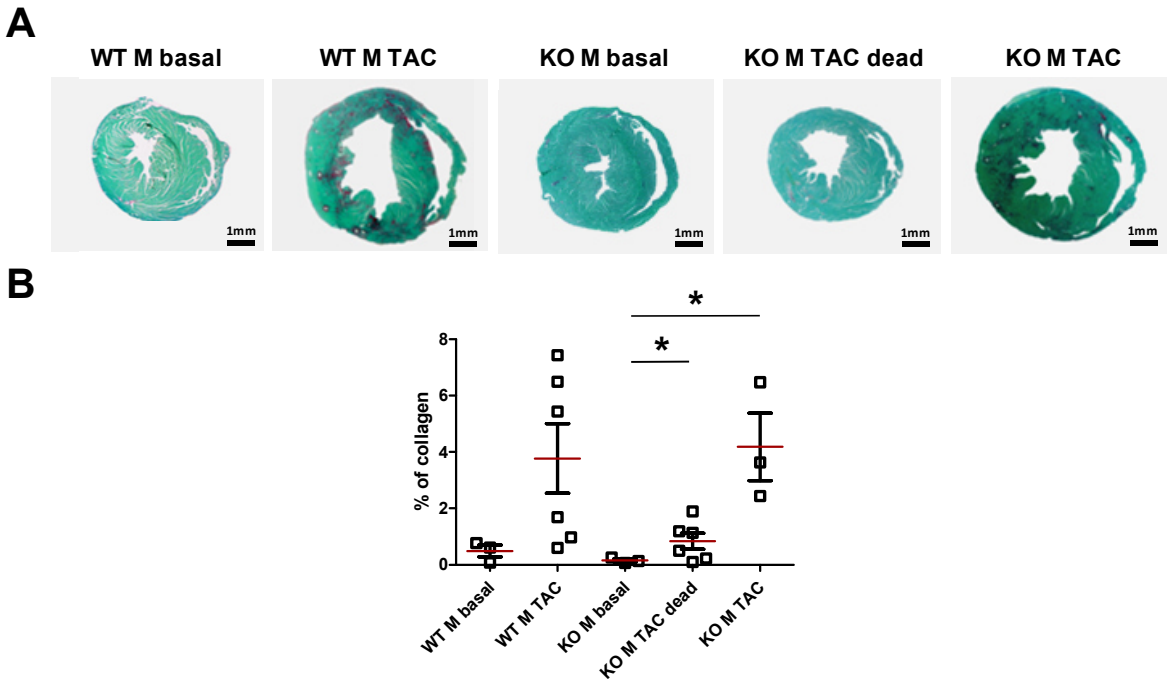

Figure 5.28: Evaluation of fibrosis in the context of increased mortality in KO male mice
Evaluation of fibrotic tissue in short term after transverse aortic constriction (TAC). Cross-sectional heart sections were prepared from male mice before TAC surgery (WT M and KO M basal), 2 weeks after TAC surgery (WT M TAC and KO M TAC), and sacrificed male mice between 2-7 days after TAC (KO M dead) and stained with Fast Green (non-collagen in green) and Sirius Red (collagen in red). (A) Representative images of basal and TAC male hearts are shown. Scale bar 1 mm. (B) Amount of collagen was analyzed using Image J and is given in percent, *p < 0.05 vs. sham group by ANOVA or two conditions by unpaired t-test.

In summary, the data obtained regarding the role of p63RhoGEF *in vivo* in healthy and under pathophysiological condition argue for an ambivalent role of p63RhoGEF.

The partial deletion of p63RhoGEF, especially in case of the male group, display a pre-disposed cardiac phenotype with an impaired cardiac function characterized by a decrease in contractility together with a dilative heart geometry due to an increased lumen of the left ventricle. Upon induction of pressure-overload using the TAC model, these phenotype is worsening over time, leading to extremely poor cardiac performance among these mice. The reduced expression had no major effect on the development of hypertrophy in cardiomyocytes, but it diminished the amount of fibrosis by trend.

The general knockout of p63RhoGEF in mice led to a phenotype similar to that described for the WT mice, arguing for compensatory mechanisms that occur for the loss of p63RhoGEF expression. As a result, in the first instance, KO mice showed no major difference in cardiac function and associated processes at basal and under pressure-load condition in comparison to the WT control. Nonetheless, KO male mice depicted a higher mortality rate within the first 2 weeks after TAC. Neither hypertrophy nor fibrosis was detected in the sacrificed KO mice within this time window, thereby ruling out a direct contribution regarding the increased death rate shortly after TAC.

5.5 Influence of the genetic deletion of p63RhoGEF in adult mouse cardiac fibroblasts

Finally, the effect of the genetic deletion of p63RhoGEF in adult cardiac fibroblast was investigated. For this purpose, fibroblasts were isolated from female and male mice with an age of 40-60 weeks and mixed equally for cultivation.

5.5.1 Genetic deletion of p63RhoGEF has no effect on the myofibroblast phenotype of isolated cells, but might influence the reorganization of the actin cytoskeleton

First, characterization of the isolated adult mouse cardiac fibroblasts (AMCF) was carried out. Since the method of isolation does not include a further purification step to separate the cardiac fibroblasts from other fast-attaching cardiovascular cells e.g. smooth muscle cells, which show a similar morphological phenotype in culture, the homogeneity of fibroblasts within the population was assessed by marker expression on mRNA level. Endpoint RT-PCR revealed that regardless of the genotype, AMCF strongly express (myo-) fibroblast-associated marker FSP-1 (fibroblast specific protein 1) and Col1a1 (collagen type 1) (Figure 5.29). In addition, sm-actin (smooth muscle actin) is similarly expressed on mRNA level. The smooth muscle-associated calcium binding protein Calp1 (calponin 1) was detected in all genotypes at low level. None of the other smooth muscle cell markers such as smMHC (smooth muscle myosin heavy chain), desmin, or sm22 (smooth muscle protein) was detected, and the endothelial markers VE-cadherin (vascular endothelial cadherin) and CD31 (PECAM-1) were also absent.
Analysis of the expression profile suggests that, independent of the deletion of p63RhoGEF, isolated cardiac fibroblast displays a pronounced myofibroblast phenotype in culture, and contamination by other non-myocyte cell types were low.

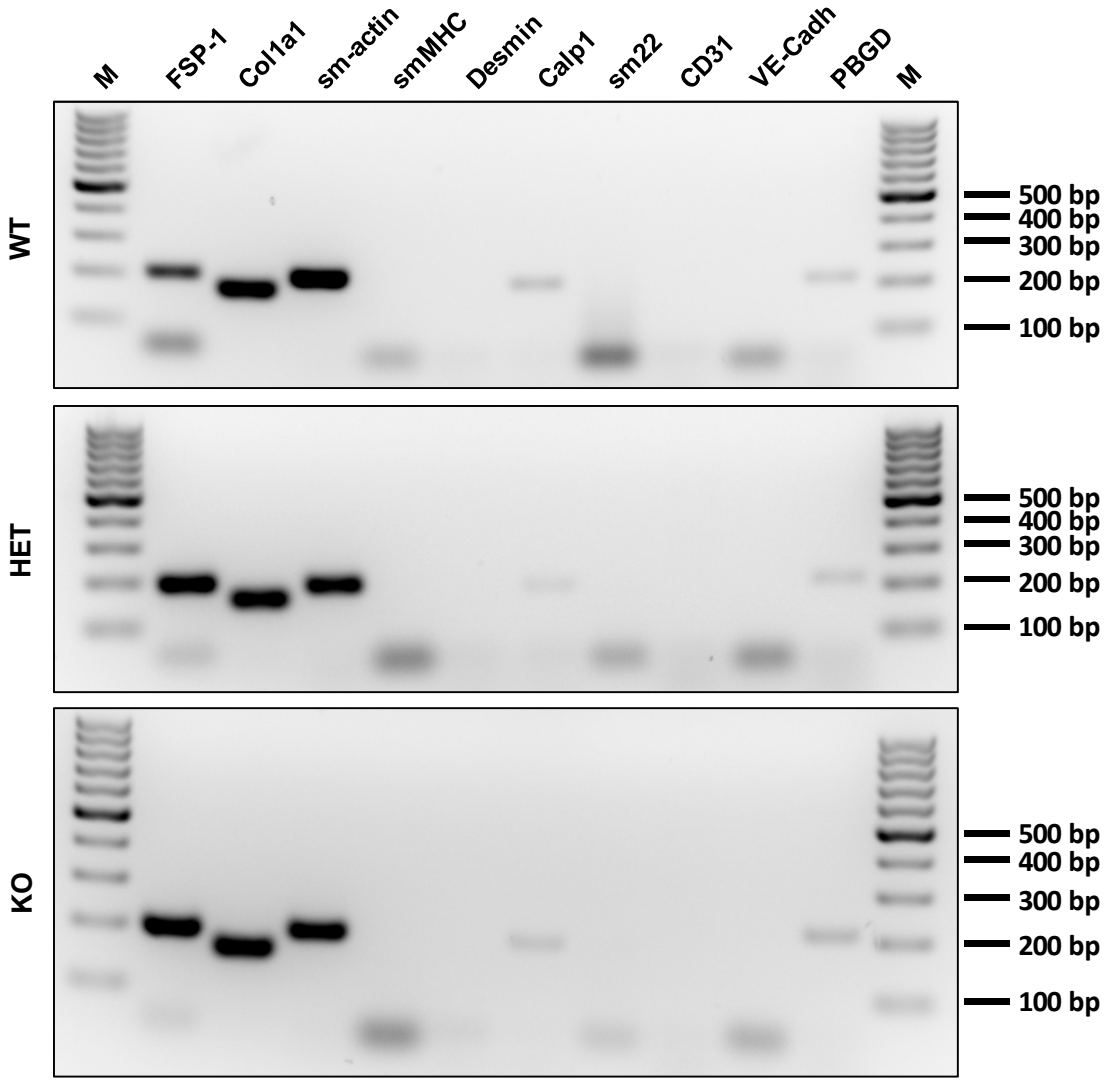

Figure 5.29: Evaluation of marker expression in AMCF

Cardiac fibroblasts isolated from adult p63RhoGEF wildtype (WT), heterozygous (HET), and knockout mice (KO) were cultivated, RNA was isolated, and cDNA was synthesized. Endpoint RT-PCR was performed using fibroblast/myofibroblast (FSP-1, Col1a1), smooth muscle cell (sm-actin, smMHC, Desmin, Calp1, sm22), and endothelial (CD31, VE-Cad) specific marker. As a housekeeping gene, porphobilinogen deaminase (PBGD) was included. Abbrevations: FSP1 = fibroblast specific protein 1, Col1a1 = collagen type 1, sm-actin = smooth muscle actin, smMHC = smooth muscle myosin heavy chain, Calp1 = Calponin 1, sm22 = smooth muscle protein 22, VE-Cad = VE-cadherin, CD31 = PECAM1. Representative PCR of 3-4 replicates is shown.

Next, the morphology of AMCF was examined. For this, cultured and serum-starved cells were fixed and stained for actin structures with fluorescent-labelled phalloidin. On a planar cell culture dish, adult fibroblasts showed a flat, widespread morphology and formed thick actin fibers, so-called stress fibers, which is a typical feature of a myofibroblast character (Figure 5.30 A). Analysis of the surface area revealed that the cell area can vary from 4000-40000 μm^2, with the majority of cells ranging in a smaller fraction between 4000 and 12000 μm^2 (Figure 5.30 B). Regarding the genotype, no difference was observed, but in general AMCF appear to be quite heterogeneous in cell area and extent of stress-fiber formation.

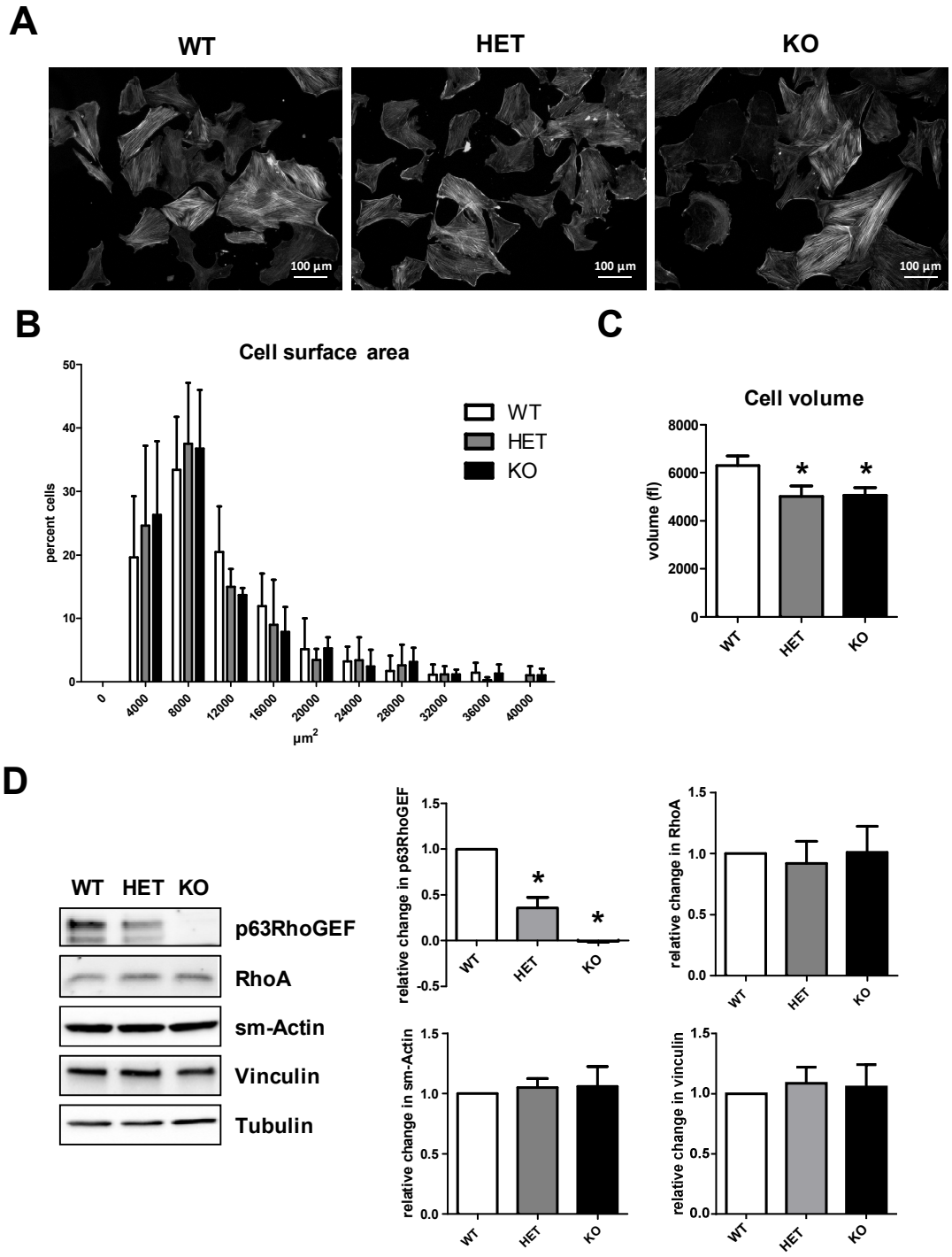

Figure 5.30: Morphometric analysis and protein expression of isolated AMCF

Cardiac fibroblasts were isolated from WT, HET and KO adult mice and cultivated. (A) Representative images of actin-stainings of AMCF after 48 h of serum-free cultivation. Scale bar 100 µm. (B) Analysis of cell surface area of cardiac fibroblasts cultivated for 48 h under serum-free condition, n =5. (C) Size measurement of detached cardiac fibroblasts by low voltage field resistance measurements (CASY). Values are given as means ± SEM, n= 16-22, *p < 0.05 vs. WT by ANOVA or two conditions by unpaired t-test. (D) Cardiac fibroblasts isolated from adult mice were cultivated and serum-starved for 24 h prior to the experiment. Protein lysates were collected and immunoblot analysis was performed. Representative immunoblots (left) and quantification of proteins (right) are shown. Given are means ± SEM normalized to tubulin, n=4 (p63RhoGEF), n=12 (RhoA), n = 8 (Vinculin) n = 7 (sm-actin), *p < 0.05 vs. WT group.

Apart from the cell surface area, the volume of detached cells was assessed by voltage-field measurements depicting a significant 20% decline in cell volume in HET and KO AMCF (Figure 5.30 C). Therefore, expression of cytoskeletal proteins was examined by immunoblot analysis. Regardless of the genotype, expression of sm-actin, tubulin and the focal adhesion protein vinculin was unchanged (Figure 5.30 D).
In addition, the genetic deletion of p63RhoGEF could be validated on protein level using a specific antibody against p63RhoGEF. While in the HET AMCF the expression of p63RhoGEF was reduced significantly, more than 50% compared to the WT fibroblasts, in the KO AMCF no expression was detectable. Interestingly, the amount of total RhoA expression was not altered by the deletion of its upstream activator.

To investigate a possible effect of the genetic deletion on downstream targets of p63RhoGEF-RhoA signaling, the impact of ROCK (Rho-associated protein kinase) activity was examined. In particular, phosphorylation of the ROCK targets cofilin as well as proteins of the ERM family (ezrin, radixin, moesin) were determined. While cofilin controls the reorganisation of actin filaments, proteins of the ERM complex serve as a crosslink between actin filaments and the plasma membrane.

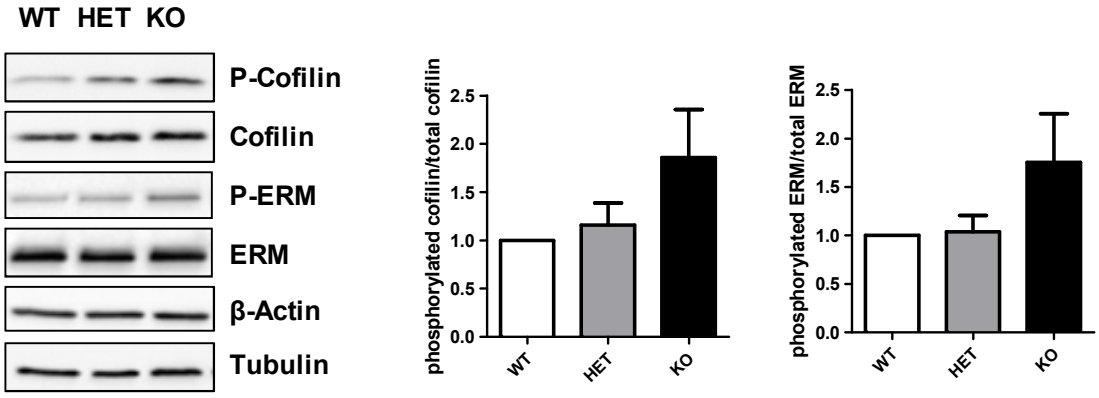

Figure 5.31: Influence of the genetic deletion of p63RhoGEF on ROCK targets
Cardiac fibroblasts isolated from adult mice were cultivated and serum-starved for 24 h. Protein lysates were prepared and immunoblot analysis was performed. (A) Representative immunoblots (left) and quantification of cofilin and ezrin/radixin/moesin (ERM) (right) are shown. In addition, β-Actin and tubulin were included for equal protein loading. Ratios of phosphorylated and unphosphorylated cofilin and ERM are given as means ± SEM and relative to WT group, n = 5-6.

As immunoblot analysis indicated, both targets showed elevated phosphorylation levels in p63RhoGEF KO cells, which was, however, not significant (Figure 5.31). In the HET AMCF, no change in comparison to the WT cells was detected.

In summary, isolated AMCF in culture display a prominent myofibroblast phenotype by strong expression of sm-actin and collagen type 1 accompanied by a strong stress fiber formation, which is independent of the genotype. While no major effect of the p63RhoGEF deletion on general expression of cytoskeletal protein and the total RhoA amount was seen, the knockout of p63RhoGEF led to increased phosphorylation and thereby activation of ROCK targets involved in actin reorganization.

5.5.2 Genetic deletion of p63RhoGEF increases CTGF expression and up-regulates sm-actin, TGF-β as well as collagen in AMCF

As the fact that p63RhoGEF regulates the expression and secretion of CTGF was demonstrated in neonatal cardiac fibroblasts by gain- and loss-of-function studies, the impact of the genetic deletion on CTGF in adult cardiac fibroblasts was examined.
On basal level, CTGF was significantly increased by 2-fold in KO AMCF compared to the WT control, while no difference in cardiac fibroblasts with the partial deletion was observed. Upon treatment with angiotensin II for 3 h, an up-regulation by around 2-fold in WT and HET AMCF was detected, whereas the strongest effect was seen in the KO AMCF with a 6-fold increase in CTGF mRNA (Figure 5.32 A). After 24 h of angiotensin II incubation, this effect was reversed to its unstimulated level independent of the genotype of the cells, suggesting that prolonged stimulation with Ang II has no additional effect on CTGF up-regulation. This is in line with the fact that CTGF, as an immediate early gene, is rapidly and transiently up-regulated.

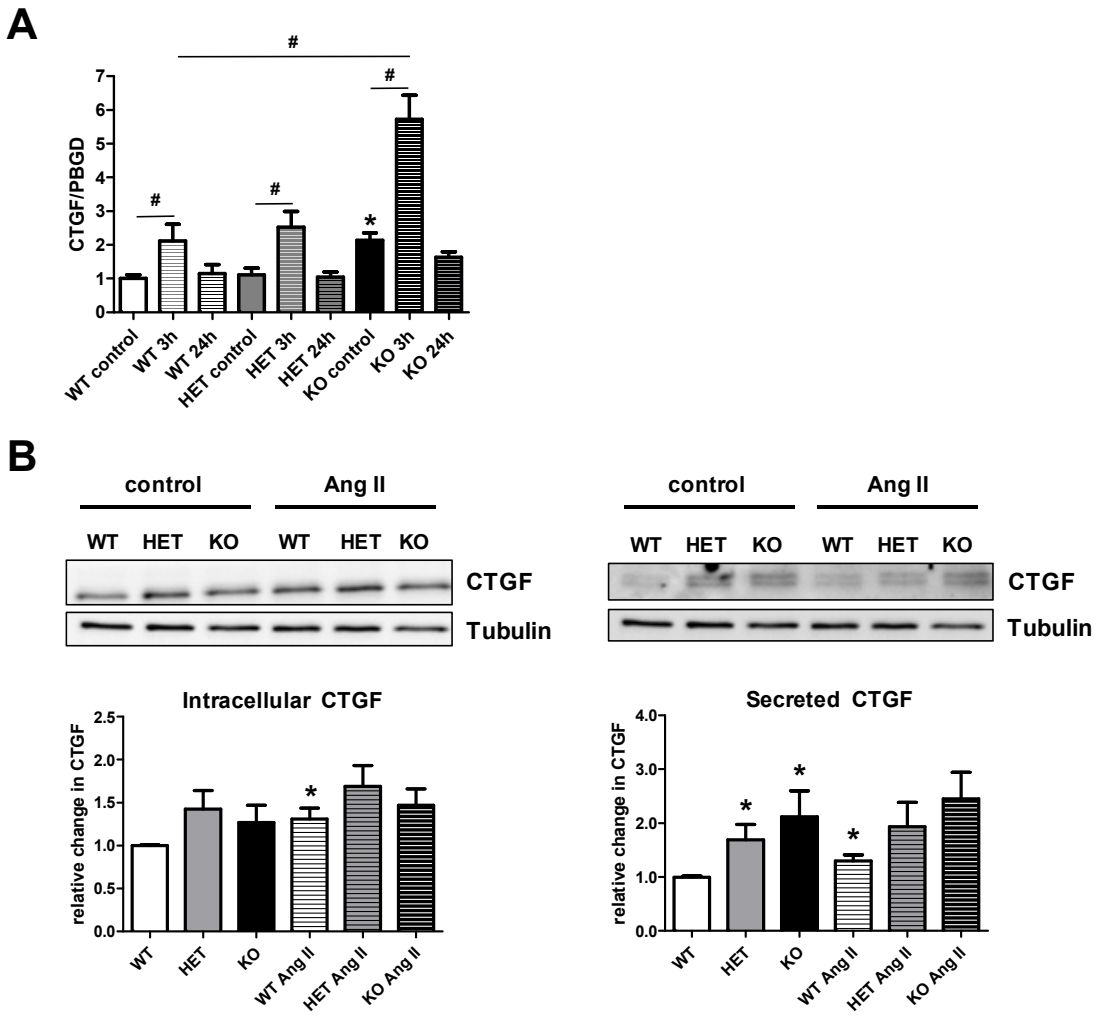

Figure 5.32: Evaluation of the genetic deletion of p63RhoGEF on CTGF expression in AMCF
Cardiac fibroblasts isolated from adult mice were cultivated and serum-starved for 24 h prior to the experiments. (A) AMCF were treated for 3 h and 24 h with 100 nM Ang II, and total RNA was isolated, cDNA synthesized, and qPCR was performed. Values were normalized to the house-keeping gene PBGD and are given relative to WT group. Results are shown as means ± SEM n = 3-8, *p < 0.05 vs. WT control, #p < 0.05 vs. respective control group/WT 3h by ANOVA or two conditions by unpaired t-test. (B) AMCF were treated for 24 h with 100 nM Ang II, and conditioned media and protein lysates were collected. Immunoblot analysis was performed. Representative immunoblots (upper panel) and quantification of intracellular and secreted CTGF (lower panel) are shown. Values are given as means ± SEM, normalized to tubulin and relative to WT group, n = 5, *p < 0.05 vs. WT by ANOVA or two conditions by unpaired t-test.

On protein level, deletion of p63RhoGEF had no effect on the intracellular level of CTGF under control condition, but led to a significantly higher secretion, 1.75 and 2 fold, of CTGF in HET and KO cells, respectively. Stimulation with angiotensin II for 24 h resulted in a 30% rise in intracellular and secreted CTGF in WT AMCF, while in HET and KO AMCF, no further increase in CTGF was detected compared to the respective untreated control (Figure 5.32 B).

As several factors were unexpectedly found to be increased in p63RhoGEF KO AMCF, the impact of the genetic deletion regarding several myofibroblast genes was analyzed. Results of the qPCR revealed a significant augmentation in a dose-dependent manner, resulting in approximately a 2-fold up-regulation of TGF-β and Col1a1 in KO AMCF (Figure 5.33), validating the myofibroblast phenotype.
While no difference in sm-actin expression was detected on protein level (Figure 5.30 D), the mRNA level of sm-actin was significantly increased by 3- and 5-fold in HET and KO AMCF, respectively. This might argue for a higher mRNA degradation rate in HET and KO AMCF.

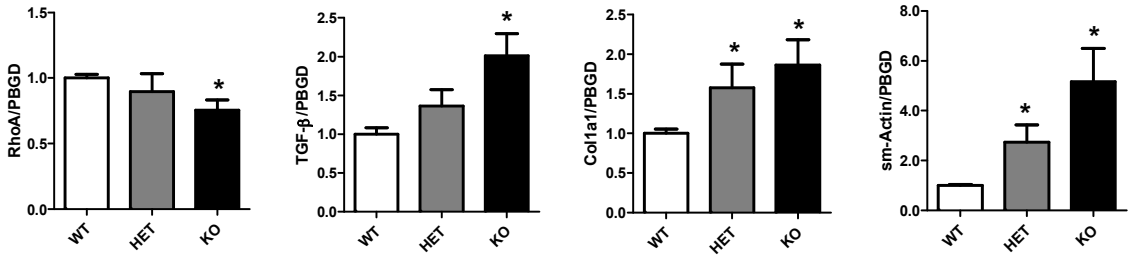

Figure 5.33: Basal characterization of gene transcription in AMCF
Cardiac fibroblasts isolated from adult mice were cultivated and serum-starved for 24 h. (A) Total RNA was isolated, cDNA was synthesized and qPCR was performed for RhoA, TGF-β (Transforming growth factor-β), Col1a1 (collagen type 1) and sm-Actin (smooth muscle-Actin). Values were normalized to the house-keeping gene PBGD and are given relative to WT group. Results are shown as means ± SEM, n = 4, *p < 0.05 vs. WT by ANOVA or two conditions by unpaired t-test.

5.5.3 Loss of p63RhoGEF expression improves cell survival/growth and proliferative capacity

In line with the paradox signaling in AMCF with a knockout of p63RhoGEF, immunoblot analysis for targets involved in survival and cell growth was performed. Detection of Akt, as a marker for cell survival, and ERK1/2 indicative of cell growth signaling, revealed a significant 60% higher phosphorylation for Akt and ERK1/2 (Figure 5.34 A). This points to a beneficial effect on survival and growth for KO AMCF in general.
In order to substantiate the results obtained by immunoblot analysis, a proliferation assay was carried out over a time period of 6 days. Cultivation with serum-containing medium led to a 4-fold rise in cell number in WT AMCF, whereas in KO AMCF an approximately 5-fold and in HET AMCF a significant 6-fold increase after 6 days of cultivation was observed (Figure 5.34 B).

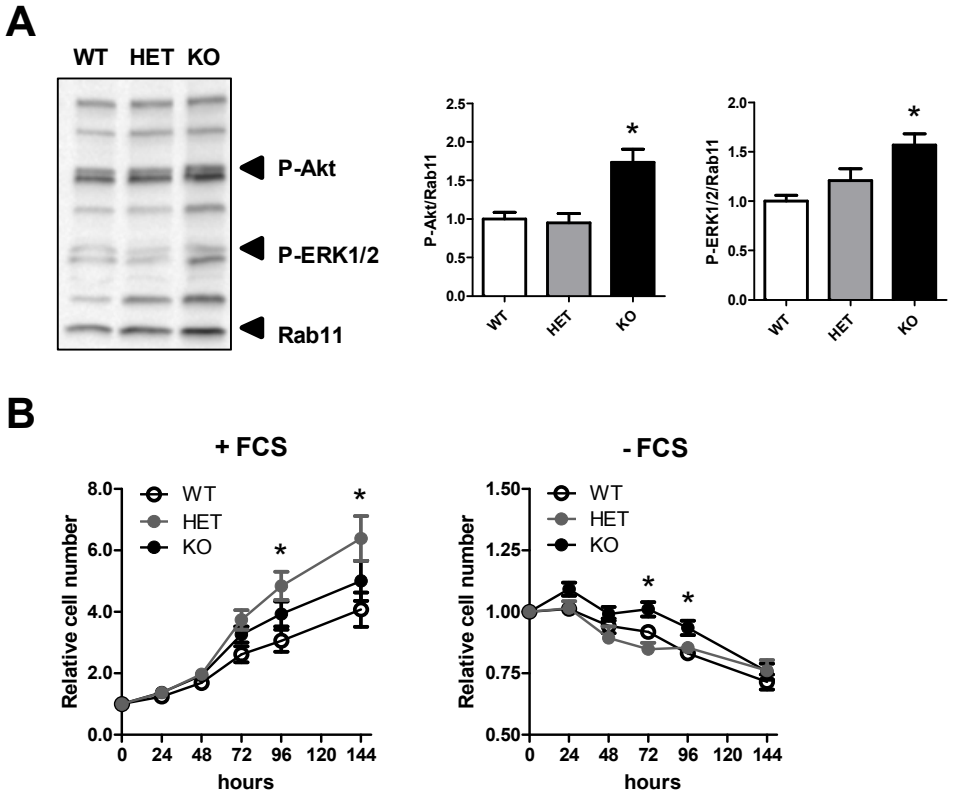

Figure 5.34: Influence of the genetic deletion of p63RhoGEF on cell survival/growth and proliferative capacity
(A) Cardiac fibroblasts isolated from adult mice were cultivated and serum-starved for 24 h. Protein lysates were prepared, and immunoblot analysis was performed. Representative immunoblots (left) and quantification of phosphorylated Akt and ERK1/2 (right) are shown. Values are given as means ± SEM normalized to the loading control Rab11 and relative to WT group, n = 5-6, *p < 0.05 vs. WT. (B) Cardiac fibroblasts isolated from adult mice were seeded on a 24-well plate (10.000 cells/well) and cultivated with or without serum-containing medium for up to 6 days. For each time point, cells were fixed and stained with DAPI and cell number was determined by cell nuclei counting. Values are presented as means ± SEM, WT n=11, HET n=6 and KO n=11, *p < 0.05 vs. 0 hours.

In contrast, cultivation under serum-free condition led to a 25% decrease in cell number of all 3 genotypes after 6 days. Interestingly, the KO AMCF showed almost no reduction or even a slight increase in cell number until day 4 of culture without serum compared to WT, suggesting a pro-survival effect for the KO AMCF in absence of serum, presumably due to activated survival pathways.

All together, the loss of p63RhoGEF in adult cardiac fibroblasts leads to a paradox signaling by up-regulation of downstream effectors demonstrated by CTGF and changes in the phosphorylation pattern of ROCK targets mostly in a dose-dependent manner. Moreover, in KO AMCF, survival pathways are up-regulated and the proliferation capacity is improved.

6 Discussion

The aim of this thesis was to investigate the role of the guanine nucleotide exchange factor p63RhoGEF, a specific activator of the RhoGTPase RhoA, in the heart and in cardiac fibroblasts in particular.
By gain-and-loss-of-function studies, the role of p63RhoGEF within the $G\alpha_{q/11}$-p63RhoGEF-RhoA signaling cascade in cardiac fibroblasts was further investigated. In the context of auto- and paracrine signaling, the impact of p63RhoGEF in cardiac fibroblasts on tissue properties as well as its influence on the contractile function of cardiomyocytes in 3D engineered tissue models was elucidated. A special focus was thereby laid on the regulation of the fibrosis marker CTGF. In the second part of the study, the relevance of p63RhoGEF expression and its genetic deletion in the healthy myocardium and under load-induced cardiac disease conditions was determined. Consequently, the role of p63RhoGEF expression and its deletion in isolated adult cardiac fibroblasts (AMCF) of the generated mouse line was examined.

6.1 Cellular function of p63RhoGEF in neonatal cardiac fibroblasts

In the scope of this project, the cellular function of p63RhoGEF in cardiac fibroblasts was further characterized. Previous research had demonstrated that p63RhoGEF regulates the $G\alpha_{q/11}$-dependent RhoA activation as well as CTGF expression and secretion induced by Ang II (as described in section 3). RhoA controls many different cellular functions including migration, proliferation and contraction mainly by regulating the actin cytoskeleton [183]. Activation of RhoA results in the formation of focal adhesion complexes [184] and induces the formation of actin stress fibers, which involves actin polymerization. In this process, actin filaments (F-actin) are assembled from monomeric globular actin (G-actin), which also binds the myocardin-related transcription factor MRTF, a co-factor of the SRF. High levels of cytoplasmatic G-actin retain the MRTF in the cytoplasm and negatively regulate MRTF function. Incorporation of G-actin into filamentous actin polymers during actin fiber assembly reduces the concentration of free G-actin in the cytosol and hence releases the bound MRTF enabling the translocation into the nucleus [185]. Within the nucleus MRTF interacts with the serum response factor (SRF) and activates the transcription of genes encoding for many contractile and cytoskeletal proteins as well as for fibrotic factors, e.g. sm-actin and CTGF [186-188]. In turn, nuclear MRTF can be complexed by nuclear G-actin, which prevents the MRTF-mediated activation of the SRF-dependent transcription and thereby promotes the MRTF nuclear export [189]. In this way, RhoA activation by p63RhoGEF could potentially influence actin dynamics and actin-dependent gene transcription.
With respect to cardiovascular cells, the influence of p63RhoGEF and RhoA on the actin cytoskeleton in smooth muscle cells of the rat aorta was investigated. The knockdown of p63RhoGEF in these cells reduced the formation of actin stress fibers along with

rearrangements of focal adhesions [169]. So far, for neonatal rat cardiac fibroblasts it has been possible to show that the knockdown of RhoA expression resulted in a less organized actin network with impaired actin structures [190] emphasizing the impact of p63RhoGEF and RhoA expression on the regulation and organization of the actin cytoskeleton. In addition, the actin-dependent regulation of the SRF by the co-factor MRTF in the underlying mechanisms of RhoA signaling was demonstrated in these cells [190]. Accordingly, the impact of p63RhoGEF expression on the SRF was implemented in the presented study.

The data revealed that p63RhoGEF regulates the Ang II-dependent activation of the SRF, as overexpression of p63RhoGEF increased SRF activity, while blocking the $G\alpha_{q/11}$-pathway using p63ΔN blunted its activity in the presence of Ang II. Consequently, inhibition of the MRTF by CCG1423 (CCG) blunted the Ang II-induced response of the SRF and reduced CTGF secretion. In this way, a direct link between SRF and CTGF in cardiac fibroblast could be established, which had previously been demonstrated in LPA-treated peritoneal fibroblasts [191]. Interestingly, CCG itself enhanced the basal SRF activity and increased the intracellular amount of CTGF. This could be explained by the involvement of other co-factors of the SRF. Inhibition of the MRTF translocation into the nucleus, where it activates the SRF and thereby regulates gene transcription, could result in a more effective interaction of the SRF with other co-factors like ETS-domain containing co-factors, e.g. Elk1 [192] leading to the observed higher SRF activity. Another plausible reason includes the contribution of other actin-dependent transcription factors, like of the YAP/TEAD complex, which was proven by Pobbati et al. to be important for CTGF regulation [193]. In this context, involvement of the Rho/ROCK signaling has already been reported [194]. As ROCK inhibition by H1152p was not effective in blocking the Ang II-dependent SRF activation, but reduced CTGF expression [195], a role of Rho/ROCK on CTGF expression via YAP/TEAD might be conceivable.

To date, no localization studies by immunostaining of p63RhoGEF in cardiac fibroblasts have been performed and results by confocal imaging demonstrated in both NRCF and AMCF that p63RhoGEF is localized at membrane structures which has been reported before [152]. A predominant localization at the trans-Golgi compartment and the base or pocket of primary cilia was found. These structures are highly involved in the secretion process suggesting that p63RhoGEF might be actively participating in the secretory mechanism. In addition, p63RhoGEF co-localizes with CTGF. As part of the pocket of primary cilia p63RhoGEF could be involved in controlling the secretion of specific proteins into the extracellular space [196]. Further studies will be needed to determine the localization and putative interaction partners involved in signaling within the basal body of primary cilia more specifically.

6.2 Influence of p63RhoGEF and its downstream effector CTGF on viscoelastic and contractile properties of 3D engineered tissue

A central part of this thesis covered the analysis of the role of p63RhoGEF in cardiac fibroblasts in the context of auto-and paracrine signaling. This involved the implementation of 3D engineered models to address the topic. In ECT (engineered connective tissue of collagen matrix and fibroblasts), it was demonstrated that p63RhoGEF regulates tissue stiffness. Overexpression of p63RhoGEF resulted in a greater rigidity, while blockade of the $G_{q/11}$-induced RhoA activation by p63ΔN resulted in a lower tissue rigidity. Moreover, p63RhoGEF seems to facilitate the secretion of CTGF, since after mechanical stress the CTGF content decreased dramatically when p63RhoGEF was overexpressed in these tissues. This result was not observed in ECT expressing p63ΔN suggesting that with the help of p63RhoGEF the release of secreted factors is more effective. This further substantiates the finding that in 2D culture p63RhoGEF led mainly to a change in the secreted proportion of CTGF. These findings strongly argue for a role of p63RhoGEF as a regulator of secretion per se.

In terms of cardiac fibrosis, the role of CTGF is not clear and is a subject of controversy in the literature. As CTGF was found to be upregulated in diverse fibrotic diseases, it has been widely accepted as a profibrotic factor [52]. However, recently published studies depicted conflicting data on the function of CTGF within the heart. While several studies support a cardioprotective function and thereby a beneficial effect of CTGF expression for cardiomyocyte survival [181, 182, 197, 198], other reports state that its expression has detrimental effects on cardiac fibrosis [69]. Still other studies postulate that CTGF has no influence in regard to cardiac diseases. Accornero et al. demonstrated that neither a heart-specific deletion nor overexpression of CTGF had any impact on cardiac remodeling and function with aging or after multiple acute stress stimuli [90]. This was further supported by another study showing that a conditional knockout of CTGF failed to prevent TAC-induced cardiac fibrosis and hypertrophy [86]. Therefore, in the present study, the direct contribution of CTGF in cardiac fibroblasts on tissue rigidity was investigated with the use of the defined ECT model. The data clearly showed that CTGF overexpression had no effect on the stiffness of the tissue suggesting that CTGF is not the determining factor causing the change of the biomechanical properties. In addition, the impact of the MRTF/SRF inhibition by CCG was analyzed in ECTs resulting in a decreased stiffness. As already seen in 2D the SRF/MRTF inhibition led to an increased expression of CTGF, which substantiates that CTGF is not relevant for tissue properties and, furthermore, that other transcriptional activities are regulating CTGF when MRTF is blocked. Therefore, the data of this thesis supports the latest studies that CTGF is likely not a mediator of cardiac fibrosis.

As a second 3D model, engineered heart muscle was generated to explore the impact of p63RhoGEF expression in fibroblasts and consequently the influence on cardiomyocyte function via paracrine signaling. Overexpression of p63RhoGEF in cardiac fibroblasts increased contractility and tissue rigidity in EHM accompanied by an enhanced CTGF level, whereas EHM with cardiac fibroblasts transduced with the p63ΔN construct showed a

decrease in contractility by trend and a reduction in CTGF level. Interestingly, when p63RhoGEF was mainly overexpressed in cardiomyocytes, no improved contractility was measured clearly pointing to a relevant contribution of p63RhoGEF expression in cardiac fibroblasts.

The improved contractility and the simultaneous higher resting tension, indicative of tissue stiffness seems to be contradictory at first, but might be explained by the different response of cardiac fibroblasts and cardiomyocytes in auto- and paracrine signaling. It is likely that cardiac fibroblasts not only secrete factors influencing the viscoelastic properties of the myocardium, but also factors that influence the contractile performance of cardiomyocytes. Factors like TGF-β1, FGF-2, LIF and CT-1 are just a few examples of bioactive molecules that are known to act in a bidirectional crosstalk [199]. Nonetheless, secretome analysis needs to be performed to identify responsible factors downstream of p63RhoGEF-RhoA signaling to explain the observed changes in tissue properties.

6.3 The relevance of p63RhoGEF expression in the pathophysiology of cardiovascular diseases

In 2002 p63RhoGEF was first characterized and shown to be predominantly expressed in heart and brain tissue [162]. However, since then no data has been added to its role in the heart *in vivo*. Therefore, the regulation of p63RhoGEF was analyzed in a pilot study that included tissue samples from two different heart disease mouse models: a pressure-induced afterload model obtained by transverse aortic constriction (TAC) and a volume-induced preload model generated by an aortocaval shunt (Shunt) surgery. Comparison of these two different hypertrophy models revealed that both p63RhoGEF and also CTGF were higher up-regulated after TAC, while only a slight up-regulation of both factors was detected in the shunt model. Interestingly, at the time points investigated, no cardiac fibrosis was detected in the shunt model but was apparent in the TAC model [175]. This demonstrates that p63RhoGEF plays a more relevant role in the underlying mechanisms of cardiac remodeling in pressure overload-associated heart disease. In this process, the TAC model mimics pressure-induced stress such as hypertension and valve dysfunction, causing a higher workload for the heart to be able to fulfill the body´s nutrient and oxygen demands, which initially induces a hypertrophic response as a compensatory mechanism. The results of this first pilot mouse study supports the findings in hypertensive patients, in whom p63RhoGEF expression correlates with the degree of blood pressure and deterioration of the cardiac function [171]. Moreover, this pilot study indicated that p63RhoGEF is also involved in mechanisms leading to cardiac fibrosis also *in vivo* as already suggested by the *in vitro* data.

To further address the function of p63RhoGEF *in vivo,* the genetic deletion of p63RhoGEF in mice was studied under basal and pathological conditions. This involved generation of a transgenic mouse line with a global knockout of p63RhoGEF from embryonic stage on. The

offspring of these mice were viable, fertile and showed no abnormal behavior. This first observation suggests that p63RhoGEF expression is not essential for embryonic development and its deletion is not lethal. In addition to mice with a total knockout (KO), animals with only a partial deletion and thus with only one p63RhoGEF allele (HET) were implemented in the study, reflecting a 50% knockdown of the protein.
One initial goal of this thesis was the establishment of a mouse line harboring a specific deletion of p63RhoGEF in cardiac fibroblasts. Towards this aim, the floxed p63RhoGEF mice were crossbred with a mouse line expressing the cre recombinase under control of an inducible collagen 1a2 promoter (Col1a2-Cre(ER)). This mouse model was first described in 2002 [200] and has been used several times for the knockout of a target gene in fibroblasts [201-203]. However, in our hands no knockout of p63RhoGEF in cardiac fibroblasts could be achieved with this model (data not shown). Recently, a study was published using a tamoxifen-inducible approach under a periostin promotor to ablate the population of activated fibroblast (myofibroblasts). This model is useful to induce a knockdown after induction of any stress (TAC, MI, Ang II infusion), as Periostin is up-regulated only in myofibroblasts and its expression in the healthy heart is restricted to valvular fibroblasts [204]. This approach could be implemented in the future to generate a mouse line, in which a knockdown of p63RhoGEF expression in myofibroblasts is achieved and its impact can be determined after TAC. However, this technique is not applicable to study any influence of a reduced p63RhoGEF expression in fibroblasts under healthy conditions.

6.3.1 Impact of the partial genetic deletion of p63RhoGEF in pressure overload-induced cardiac remodeling

On a basal level, the HET animals already manifested an impaired contractility as illustrated by a decrease in fractional area shortening (FAS) and ejection fraction (EF), accompanied by an enlargement of the left ventricular lumen measured by increase in volume. Upon induction of pressure overload by TAC surgery, these parameters were further aggravated, resulting in a phenotype with severe contractile dysfunction and a faster dilation within 5 weeks after intervention. Thus, it can be concluded that the partial deletion of p63RhoGEF seems to have a strong negative effect on the cardiac function. In the context of the underlying processes of cardiac remodeling, the reduced expression had no major effect on the development of cardiac hypertrophy. Left ventricular weight to body weight ratio, heart weight to tibia length ratio, and cardiomyocyte size after TAC were increased to the same extent as in the WT group. However, analysis of hypertrophy-associated marker expression showed that in the HET group, less of the cardioprotective ANP and BNP is expressed in the ventricle. In addition, the level of β-MHC to α-MHC was not increased after TAC, suggesting that the impaired contractile phenotype might be linked to reduced levels of protective marker expression as well as contractile proteins. Validation on protein level would substantiate these findings.

Moreover, partial deletion of p63RhoGEF led to a reduction of cardiac fibrosis by trend. In these hearts less interstitial and perivascular collagen deposition was detected. Surprisingly, on mRNA level the typical fibrosis marker like collagen type 1 and type 3 and CTGF were not largely different between the WT, HET and KO TAC groups. However, LGALS3 and TGF-beta were significantly less increased in the HET mice compared to the WT and KO animals.
LGALS3 (Gal-3) is a lectin that binds to β-galactosides, e.g. lactose and is thereby involved in cell-matrix interactions, cell-cell adhesion, apoptosis and inflammation. LGALS3 serves as a clinical biomarker for cardiac diseases and was shown to be markedly up-regulated in TAC mouse studies, where it was also associated with the severity of detrimental cardiac remodeling and inflammation [205]. In contrast, mice deficient in LGALS3 (Gal-3) were protected from fibrosis. For instance, Gonzales et al. showed that a Gal-3 deficiency in an angiotensin II-induced hypertension model prevents left ventricular dysfunction by reducing immune responses and myocardial fibrosis [206]. This is in good agreement with the results obtained, as a reduced level of LGALS3 seems to correlate with a decline in collagen deposition and thus fibrosis in the HET mice. Precisely, how LGALS3 interferes is still unclear.
The pro-fibrotic cytokine TGF-β is known to up-regulate collagen by Smad 3/4, to inhibit matrix metalloproteinase (MMP) expression and to enhance tissue inhibitor of metalloproteinase (TIMP) expression, leading to higher collagen synthesis and less degradation by MMPs [207]. In line with this, the level of MMP-2, a collagen-degrading MMP, was higher in the HET animals than in the WT animals, suggesting that an enhanced degradation of collagen could be one reason for the reduced fibrosis. However, the interplay between the numerous secreted proteins in the heart is complex and the analysis of single factors can only give a hint about the underlying processes. To gain deeper insight into the occurring changes, large screenings are necessary, which are still difficult to accomplish on protein level due to the low abundance of many bioactive molecules. Moreover, it is likely that also secreted non-protein components are involved in the overall regulation of cardiac function and fibrosis including, e.g. glycosaminoglycans and low molecular weight hormones [208-210].
The results observed in the HET group regarding contractile function and fibrosis are largely in line with the results obtained by the 3D cell culture models. As demonstrated in EHM, p63RhoGEF in cardiac fibroblasts not only influenced tissue stiffness but also the contractility of these tissues. Although this is a strong hint for a predominant function of p63RhoGEF in cardiac fibroblasts, especially as there was no effect when p63RhoGEF was expressed mainly in cardiomyocytes, this does not fully exclude a potential role of this activator of RhoA in cardiomyocytes. In that respect, it has to be considered that in the genetic HET mouse model p63RhoGEF expression is diminished during all developmental steps and so far it is not clear at which time point the impairment of the cardiac function occurs in these animals. Moreover, the cardiomyocytes in the EHM model display an immature neonatal state and do not reach full maturation or even resemble the diseased heart. Therefore, further studies are needed to clarify the role of p63RhoGEF in cardiomyocytes.

By comparing the phenotype of the HET mice with other genetic mouse models, targeting proteins residing in the same or similar signaling pathways, a potential role of p63RhoGEF in cardiomyocytes seems at least likely. In a recent mouse study, mice with a cardiomyocyte-specific knockout of RhoA were described to harbor a very similar phenotype upon chronic pressure overload as the partial genetic deletion of p63RhoGEF in this work. While the development of hypertrophy was not affected compared to the control group, the RhoA KO mice displayed an impaired contractile function associated with a greater dilation and less fibrosis accompanied by a reduced expression of fibrotic genes, e.g. TGF-β [144]. Furthermore, the authors were able to demonstrate that the cardiomyocyte-specific deletion of RhoA might affect the contractile properties by a modulated calcium signaling and myosin light chain (MLC) activation by a rapid decrease in phosphorylation of PLC-β, PKC and MLC shortly after TAC [144]. Although the analyses of the phosphorylation levels of these proteins were not analyzed within this work, it might be a reasonable point to explain the underlying molecular mechanisms leading to an impaired contractility in p63RhoGEF HET mice.

Apart from p63RhoGEF, LARG (RhoGEF12) represents another GEF, which can activate RhoA downstream of GPCRs. While the p63RhoGEF activation is $G\alpha_{q/11}$-dependent, LARG is activated by $G\alpha_{12/13}$-signaling. For the heart it was demonstrated that LARG mediates the integrin-β stretch-induced RhoA activation and hypertrophic gene transcription in cardiomyocytes. Mice with a cardiomyocyte specific deletion of LARG displayed no hypertrophy, less fibrosis and were protected from the development of cardiac decompensation. The beneficial effects of the deletion of LARG were further validated, when the ablation of LARG was initiated in preexisting hypertrophy and prevented further progression of cardiomyocyte growth, improved cardiac function and enhanced survival [131]. In comparison to the p63RhoGEF HET group, these mice not only developed less fibrosis due to reduced expression of fibrotic genes as the p63RhoGEF mice, but they were also protected from hypertrophic response. Even more relevant, these mice did not show any sign of decompensation by contractile dysfunction and dilation of chambers [131]. On a molecular level, hypertrophic markers, such as ANP, BNP and β-MHC were similarly less up-regulated in the p63RhoGEF HET mice compared to the mice with the cardiomyocyte-specific KO of LARG. Nevertheless, p63RhoGEF mice developed hypertrophy accompanied by a faster decompensation. Since both GEFs activate RhoA, the discrepancy between the completely different outcomes might be explained by the differential Gα signaling of these GEFs, which involves other RhoA-independent regulatory pathways.

Beside the activation of the p63RhoGEF-RhoA-ROCK pathway, $G\alpha_{q/11}$ can also activate the phospholipase C-β (PLC-β) pathway, which regulates calcium signaling by release of Ca^{2+}-ions from the ER [211]. Upon activation, PLC-β hydrolyzes phosphatidylinositol 4,5-bisphosphate (PIP_2) to diacyl glycerol (DAG) and inositol triphosphate (IP_3). Acting as second messengers, DAG activates protein kinase C (PKC), while IP_3 triggers the calcium release from the ER. The level of DAG is controlled by phosphorylation of the DAG kinase (DGK). In the heart, the isoform DGKε has been reported to act specifically on DAG produced by inositol cycling and

inactivates DAG by producing phosphatic acid (PA). In a transgenic mouse model, overexpression of DGKε was shown to restore the cardiac dysfunction upon chronic pressure overload, which is usually downregulated during a hypertrophy-associated response. Hearts of these mice exhibited reduced level of hypertrophy, fibrosis and apoptosis. Moreover, contractility was less impaired and the expression of TRPC 6 calcium channels, which regulate the entry of calcium into the cell, was decreased [212]. In summary, the interference with the PLC-β signaling pathway resembled the phenotype of the cardiomyocyte-specific LARG KO mouse model after TAC.

Interestingly, under normal condition mice with a cardiomyocyte-specific deletion of RhoA and LARG or with a reduction in DAG levels showed no functional or structural difference to the control mice. In contrast, under basal condition the p63RhoGEF HET mice displayed a contractile phenotype, which might be a consequence of the global genetic deletion, pointing to an influence of other cardiac cells on the contractile function of cardiomyocytes.

In addition, cardiomyocyte-specific deletion of LARG and RhoA and the global partial deletion of p63RhoGEF result in reduced fibrosis, emphasizing their roles in the regulation of fibrosis, most likely via RhoA/ROCK signaling, involving the MRTF/SRF-dependent activation, as shown by Lauriol and colleagues [144]. In mice with the overexpression of DGKε in cardiomyocytes as intervention within the PLC-β pathway, also less fibrosis occurred [212], arguing for an interaction with other pathways involved in fibrosis. Moreover, this points to an important contribution of cardiomyocytes for the development of fibrosis in paracrine signaling, as all comparing mouse studies except the p63RhoGEF mouse line included the modification of gene expression in cardiomyocytes only.

Regarding the development of cardiac fibrosis, the data obtained on the HET mice can be further confirmed by mouse studies investigating ROCK deletion. In a model of global haploinsufficient ROCK1$^{+/-}$ mice, the authors demonstrated in an Ang II infusion model as well as in the TAC model, that perivascular fibrosis and associated factors as TGF-beta, CTGF and collagen type 3 were less increased, while hypertrophy was established to the same extent after 4 weeks [142]. In the p63RhoGEF mouse study, concomitant with the reduced fibrosis only TGF-β was reduced out of the marker set compared to the study by Rikitake et al. The level of CTGF on mRNA was found to be similarly up-regulated in all 3 genotypes arguing that CTGF is not the causing factor for fibrosis. In this context, it was shown that CTGF and TGF-β on their own are considered to just weakly promote fibrosis and only in combination both were efficient in promoting fibrosis [74, 87, 213]. This fits very well with the data of the HET group, as the reduced level of TGF-β corresponds to less fibrotic tissue despite the highly up-regulated level of CTGF. Accordingly, when TGF-β and CTGF are both similarly up-regulated, more fibrosis occurs as seen in the WT and KO TAC groups.

6.3.2 Impact of the knockout of p63RhoGEF in pressure overload-induced cardiac remodeling

In contrast to the mice with the partial deletion of p63RhoGEF (HET), mice with a complete p63RhoGEF knockout (KO) displayed a similar phenotype as the WT group under basal condition and after TAC. The KO mice developed hypertrophy to the same extent as the WT group emphasizing that p63RhoGEF is not involved in the hypertrophic response. No major difference in contractile function and development of cardiac fibrosis compared to the WT TAC group was observed. Furthermore, analysis of hypertrophic and fibrotic marker expression revealed a similar up-regulation as detected in the WT. These data point to a compensatory processes that occur when p63RhoGEF is fully absent. Whether the loss of p63RhoGEF is compensated by other direct $G_{q/11}$-dependent RhoGEFs like Kalirin or Trio [164], by other Gα-signaling mediators ($G\alpha_{12/13}$), or by the $G\alpha_{q/11}$ competing PLC-β-dependent calcium signaling, which is RhoA independent, has to be further elucidated in these mice. The available data of other mouse studies examining the cardiomyocyte-specific deletion of RhoA, LARG and inhibition of the PLC-β pathway by DGKε overexpression discussed above might be possible candidates. As the RhoGEF LARG controls cardiac remodeling by the RhoA-dependent signaling and its cardiomyocyte-specific deletion protects mice from development of cardiac remodeling and heart failure [131], it could be a responsible factor for the compensation of the loss of p63RhoGEF expression by maintaining the function of RhoA. This would explain the development of hypertrophy, fibrosis and cardiac dysfunction to the same extent in the p63RhoGEF KO mice as in the WT mice. Interestingly, in the same study Takefuji showed that amongst the various RhoGEFs expressed in mouse cardiomyocytes and whole human heart, beside RhoGEF12 a high expression of Trio was found, whereas p63RhoGEF was only minimally expressed [131]. This might point to a relevant role for Trio in cardiomyocytes. Therefore, compensation for the loss of p63RhoGEF by maintaining the function of RhoA via Trio is conceivable. Although so far no data is available for Trio in animal studies with respect to cardiac diseases, its role in the regulation of the $G_{q/11}$-dependent RhoA activation for endothelial cells has recently been established *in vivo* proving for the first time the relevance of this pathway [214].

During the course of this study it became however obvious that the knockout of p63RhoGEF is not without effect. The loss of p63RhoGEF had a detrimental effect on the survival of these mice within the first 2 weeks after TAC intervention. Massive hypertrophy and fibrosis could be excluded, since LVW/BW, HW/TL and cardiomyocyte area as well as the collagen amount in the heart was only marginally increased at that time point. What other underlying mechanisms in the course of compensation might be activated and evoke the higher mortality rate is speculative at this point.

One possible compensatory effect includes the calcium signaling via the activation of PLC-β by $G\alpha_{q/11}$ leading to a release of Ca^{2+}-ions from the ER and regulating calcium signaling [211]. Due to loss of p63RhoGEF expression, the signaling downstream of $G\alpha_{q/11}$ might be shifted to the PLC-β pathway, which in turn can contribute to change in calcium signaling. As demonstrated, interfering with the PLC-β signaling pathway by cardiomyocyte-specific

overexpression of DGKε restored cardiac dysfunction and improved the survival rate [212]. It can be assumed that, in turn, an increased activation of this pathway would cause even more detrimental effects, such as dysregulation in calcium signaling and hence arrhythmias, which could explain the increased mortality rate seen in the KO male mice. In order to prove this hypothesis, further experiments, including ECG monitoring recordings by telemetry under basal and TAC conditions, could be implemented.

6.4 Influence of the genetic deletion of p63RhoGEF in adult mouse cardiac fibroblasts

In order to investigate the impact of the genetic deletion of p63RhoGEF in isolated cardiac fibroblasts, their marker profile was first assessed. In all isolated and cultivated AMCF, high levels of collagen type 1, FSP-1 and sm-actin were found on mRNA. Fibroblasts in culture tend to differentiate and adopt a more myofibroblast phenotype expressing high level of sm-actin. This also makes it challenging to study the function and behavior of a typical fibroblast residing in the tissue. Apart from sm-actin, only a slight amount of calponin was detected and no expression of other markers specific for smooth muscle cells and endothelial cells were detected on mRNA level. Consequently, it can be assumed that the isolated cell population contains hardly any other typical cardiovascular cells but mainly (myo)fibroblast-like cells. One obstacle in this approach is the lack of specific fibroblast and myofibroblast marker. As cardiac fibroblasts and myofibroblasts can be derived from very different cell sources, including amongst others resident cardiac fibroblasts, endothelial cells and bone marrow-derived circulating progenitor cells like monocytes and fibrocytes [32], they share many markers with other cell types. Therefore, their nature is normally identified by a combination of different markers and exclusion of other cell types harboring specific marker. Further possible fibroblast markers that could be included are the discoidin domain-containing receptor 2 (DDR2), platelet-derived growth factor receptor alpha (PDGFR-2) and Thy1/CD90 [8, 15, 215].

The morphology of the isolated AMCF was quite diverse in shape and degree of stress fiber formation amongst all cell populations. Stress fibers are a result of RhoA activation and are also another typical feature of myofibroblasts. However, the deletion of p63RhoGEF had no influence on the cell surface area, the level of cytoskeletal protein expression and actin fiber formation. In accordance with these contradictory results, expression and even more secretion of CTGF and further fibrotic marker such as sm-actin, TGF-β and collagen type 1 were likewise increased in HET and KO AMCF in a dose-dependent manner. Moreover, in these cells Ang II had no further effect on CTGF, while in WT fibroblasts a response to this stimulus was observed. This suggests that Ang II-dependent pathways are already active under basal condition and cannot be further induced by Ang II application. This is in sharp contrast to the 2D and 3D experiments with NCRF, where a p63RhoGEF-dependent regulation of CTGF expression, and especially secretion in response to Ang II, was validated

in multiple experiments and a knockdown in p63RhoGEF expression reduced the amount of CTGF on mRNA and protein level. The discrepancy might be explained by the different cell source and the approach used for the knockdown or knockout of p63RhoGEF. In NCRF cells, the knockdown or blocking was achieved by transient adenoviral infection, while AMCF are isolated from adult mice that carried the modification from embryonic stage on and initiate compensatory effects, even resulting in overcompensation in case of KO AMCF. The underlying mechanisms that are involved in the compensation for p63RhoGEF loss or reduction might include other Gα-signaling ($G\alpha_{12/13}$), $G\alpha_{q/11}$-dependent RhoGEFs (Trio/Kalirin), other transcription factors than MRTF/SRF for CTGF, or PLC-β-dependent calcium signaling, as discussed in detail in section 6.3.

Conclusion

Although a reduction in p63RhoGEF expression has a beneficial effect on the degree of cardiac fibrosis by decreasing the amount of collagen deposition, its expression is needed to maintain normal cardiac function under basal and stress condition. It thereby fulfills a role similar to RhoA, namely being both cardioprotective and cardiodeleterious, as it prevents the transition to dilation and failure, but initiates the fibrotic response in the heart under stress conditions.

7 Appendix

Table 7.1: Analysis of cardiac parameters by echocardiography in sham male mice

Abbrevations: 1 w = 1 week after surgery, 2 w = 2 weeks after surgery, 5 w = 5 weeks after surgery

Para-meter	WT M Sham				HET M Sham				KO M Sham			
	basal	1 w	2 w	5 w	basal	1 w	2 w	5 w	basal	1 w	2 w	5 w
n	6	6	4	4	9	9	7	5	8	8	8	7
HR (beats/ min)	423,8 ± 13,78	431,8 ± 26,24	452,5 ± 24,59	413,5 ± 18,76	450,1 ± 18,73	434,1 ± 6,06	448,3 ± 19,15	448,6 ± 15,41	431, 5 ± 14,8	461,5 ± 16,01	475, 3 ± 18,1	483,6 ± 16,75
BW (g)	25,3 ± 1,35	26,37 ± 1,11	28,0 ± 0,83	29,0 ± 0,74	25,83 ± 0,47	27,26 ± 0,49	27,63 ± 0,31	27,36 ± 0,37	27,7 5 ± 0,5	29,01 ± 0,43	29,1 9 ± 0,47	29,4 ± 0,42
LVW/BW (mg/g)	4,012 ± 0,34	3,87 ± 0,15	3,96 ± 0,15	3,84 ± 0,22	3,97 ± 0,13	4,29 ± 0,13	4,39 ± 0,18	4,52 ± 0,27	4,18 ± 0,3	3,99 ± 0,23	3,93 ± 0,21	4,47 ± 0,21
FAS (%)	34,04 ± 2,39	35,83 ± 4,21	30,43 ± 2,15	36,65 ± 1,32	32,74 ± 1,48	42,81 ± 2,38§	40,28 ± 1,81 §	34,69 ± 2,09	31,4 3 ± 1,37	36,66 ± 2,43	36,6 1 ± 3,14	36,89 ± 2,07
EF (%)	40,35 ± 1,89	43,10 ± 4,35	40,58 ± 3,51	42,49 ± 0,72	39,19 ± 1,75	48,82 ± 2,32§	47,09 ± 1,38 §	41,56 ± 2,68	38,5 6 ± 1,39	44,32 ± 2,5	44,2 5 ± 3,38	43,24 ± 2,160
Vol s (µL)	66,67 ± 8,39	61,12 ± 7,61	64,63 ± 4,49	67,43 ± 4,84	65,53 ± 3,4	58,50 ± 5,48	55,98 ± 3,98	64,42 ± 6,34	72,4 7 ± 5,6	63,88 ± 4,98	63,4 8 ± 5,48	66,52 ± 6,07
Vol d (µL)	110,5 ± 11,07	106,8 ± 8,35	108,8 ± 4,59	117,2 ± 8,32	107,9 ± 5,39	116,1 ± 9,59	105,7 ± 6,87	109,9 ± 8,64	117, 4 ± 7,7	114,5 ± 7,22	113, 4 ± 6,32	116,4 ± 7,41
LVID s (mm)	3,85 ± 0,2	3,73 ± 0,2	3,7 ± 0,16	3,87 ± 0,1	3,81 ± 0,08	3,51 ± 0,13	3,37 ± 0,18	3,68 ± 0,19	3,91 ± 0,11	3,6 ± 0,12	3,62 ± 0,15	3,52 ± 0,16
LVID d (mm)	4,74 ± 0,23	4,57 ± 0,14	4,56 ± 0,12	4,72 ± 0,17	4,65 ± 0,1	4,63 ± 0,12	4,36 ± 0,18	4,57 ± 0,27	4,65 ± 0,1	4,63 ± 0,12	4,64 ± 0,13	4,55 ± 0,14
CI (%)	742,5 ± 60,41	642,3 ± 51,63	718,0 ± 85,34	708,4 ± 50,21	749,9 ± 82,74	869,9 ± 49,67	796,3 ± 36,4	746,4 ± 74,1	705, 1 ± 56,2	804,8 ± 64,45	818, 3 ± 79,7	823,0 ± 62,86
CO (%)	18,52 ± 1,26	20,11 ± 3,2	20,01 ± 2,25	20,47 ± 1,13	19,3 ± 2,02	23,64 ± 1,25	22,0 ± 1,02	20,41 ± 1,97	20,5 2 ± 1,91	23,53 ± 2,18	23,7 1 ± 2,12	24,1 ± 1,68

Abbrevations: n = number; HR = heart rate; BW = body weight; LVW/BW = left ventricular weight/body weight; FAS = fractional area shortening; EF = ejection fraction; Vol s = systolic volume; Vol d = diastolic volume; LVID s = left ventricular inner diameter in systole; = LVID d = left ventricular inner diameter in diastole; CI = cardiac index; CO = cardiac output; $^{\S}p < 0.05$ vs. HET basal group.

Table 7.2: Analysis of cardiac parameters by echocardiography in sham female mice

Abbrevations: 1 w = 1 week after surgery, 2 w = 2 weeks after surgery, 5 w = 5 weeks after surgery

Para-meter	WT F Sham				HET F Sham				KO F Sham			
	basal	1 w	2 w	5 w	basal	1 w	2 w	5 w	basal	1 w	2 w	5 w
n	8	8	8	5	7	7	6	5	8	8	7	5
HR (beats/ min)	443,9 ± 22,51	463,1 ± 17,34	454,5 ± 15,21	451,4 ± 18,4	457,3 ± 16,36	463,9 ± 18,12	472,2 ± 29,6	452,8 ± 18,46	450, 3 ± 23,5	452,1 ± 19,28	451, 9 ± 12,4	455,0 ± 25,47
BW (g)	20,43 ± 0,7	21,43 ± 0,67	21,30 ± 0,91	21,52 ± 1,37	20,40 ± 0,66	21,47 ± 0,65	21,98 ± 0,86	23,64 ± 0,6 §	21,5 6 ± 1,19	22,95 ± 1,23	23,4 6 ± 1,16	23,23 ± 1,73
LVW/BW (mg/g)	4,08 ± 0,22	4,43 ± 0,18	3,92 ± 0,21	4,53 ± 0,31	4,09 ± 0,16	4,31 ± 0,19	4,08 ± 0,32	3,63 ± 0,53	4,23 ± 0,29	4,34 ± 0,24	4,12 ± 0,34	3,95 ± 0,36
FAS (%)	35,39 ± 2,18	36,13 ± 2,45	36,18 ± 1,64	35,85 ± 2,96	32,36 ± 1,92	37,85 ± 2,19	37,83 ± 4,1	42,29 ± 8,15	35,9 5 ± 2,95	42,96 ± 3,49	40,4 9 ± 3,22	33,88 ± 7,49
EF (%)	40,72 ± 2,2	42,76 ± 2,37	41,01 ± 1,75	40,62 ± 2,6	39,33 ± 1,81	44,08 ± 2.0	44,46 ± 3,82	48,15 ± 7,19	40,8 9 ± 2,58	48,99 ± 3,43	45,1 1 ± 3,17	39,50 ± 6,76
Vol s (µL)	53,71 ± 4,19	51,38 ± 4,32	55,2 ± 3,59	57,3 ± 6,47	53,86 ± 4,53	55,47 ± 4,79	49,96 ± 7,45	51,38 ± 8,8	57,0 3 ± 3,4	49,28 ± 5,42	54,4 7 ± 5,51	59,25 ± 12,11
Vol d (µL)	90,1 ± 5,09	89,05 ± 4,57	94,31 ± 7,36	97,01 ± 11,79	88,00 ± 4,92	98,24 ± 5,45	87,68 ± 9,34	97,53 ± 6,19	96,1 9 ± 3,08	95,67 ± 7,13	98,3 8 ± 7,32	90,96 ± 6,92
LVID s (mm)	3,512 ± 0,14	3,45 ± 0,15	3,39 ± 0,11	3,48 ± 0,18	3,53 ± 0,14	3,46 ± 0,17	3,25 ± 0,21	3,69 ± 0,26	3,47 ± 0,1	3,23 ± 0,17	3,41 ± 0,16	3,73 ± 0,39
LVID d (mm)	4,4 ± 0,15	4,38 ± 0,16	4,31 ± 0,17	4,42 ± 0,23	4,28 ± 0,13	4,37 ± 0,1	4,23 ± 0,2	4,53 ± 0,16	4,43 ± 0,08	4,37 ± 0,12	4,42 ± 0,13	4,45 ± 0,21
CI (%)	808,4 ± 87,66	840,2 ± 56,37	818,7 ± 60,91	814,5 ± 77,5	768,8 ± 39,09	891,7 ± 59,88	799,6 ± 55,76	622,9 ± 142,1	827, 4 ± 69,5	964,4 ± 80,32	853, 2 ± 77,3	652,5 ± 145,9
CO (%)	16,38 ± 1,73	17,55 ± 1,25	17,59 ± 1,78	17,75 ± 2,57	15,56 ± 0,49	19,8 ± 0,86§	17,65 ± 1,54	14,71 ± 3,3	17,8 7 ± 1,73	21,18 ± 2,02	19,8 6 ± 1,64	14,5 ± 2,7

Abbrevations: n = number; HR = heart rate; BW = body weight; LVW/BW = left ventricular weight/body weight; FAS = fractional area shortening; EF = ejection fraction; Vol s = systolic volume; Vol d = diastolic volume; LVID s = left ventricular inner diameter in systole; = LVID d = left ventricular inner diameter in diastole; CI = cardiac index; CO = cardiac output; $^{\S}p < 0.05$ vs. HET basal group.

8 Bibliography

1. Cohn, J.N. and W. Colucci, *Cardiovascular effects of aldosterone and post-acute myocardial infarction pathophysiology.* Am J Cardiol, 2006. **97**(10a): p. 4f-12f.
2. Chevalier, L., et al., *Athlete's heart patterns in elite rugby players: effects of training specificities.* Arch Cardiovasc Dis, 2013. **106**(2): p. 72-8.
3. Jessup, M. and S. Brozena, *Heart failure.* N Engl J Med, 2003. **348**(20): p. 2007-18.
4. Frey, N. and E.N. Olson, *Cardiac hypertrophy: the good, the bad, and the ugly.* Annu Rev Physiol, 2003. **65**: p. 45-79.
5. Guellich, A., H. Mehel, and R. Fischmeister, *Cyclic AMP synthesis and hydrolysis in the normal and failing heart.* Pflugers Arch, 2014. **466**(6): p. 1163-75.
6. Baudino, T.A., et al., *Cardiac fibroblasts: friend or foe?* Am J Physiol Heart Circ Physiol, 2006. **291**(3): p. H1015-26.
7. Manabe, I., T. Shindo, and R. Nagai, *Gene expression in fibroblasts and fibrosis: involvement in cardiac hypertrophy.* Circ Res, 2002. **91**(12): p. 1103-13.
8. Takeda, N., et al., *Cardiac fibroblasts are essential for the adaptive response of the murine heart to pressure overload.* J Clin Invest, 2010. **120**(1): p. 254-65.
9. Kuruvilla, S., et al., *Late gadolinium enhancement on cardiac magnetic resonance predicts adverse cardiovascular outcomes in nonischemic cardiomyopathy: a systematic review and meta-analysis.* Circ Cardiovasc Imaging, 2014. **7**(2): p. 250-8.
10. Swynghedauw, B., *Molecular mechanisms of myocardial remodeling.* Physiol Rev, 1999. **79**(1): p. 215-62.
11. Brown, R.D., et al., *The cardiac fibroblast: therapeutic target in myocardial remodeling and failure.* Annu Rev Pharmacol Toxicol, 2005. **45**: p. 657-87.
12. Martos, R., et al., *Diastolic heart failure: evidence of increased myocardial collagen turnover linked to diastolic dysfunction.* Circulation, 2007. **115**(7): p. 888-95.
13. de Jong, S., et al., *Biomarkers of myocardial fibrosis.* J Cardiovasc Pharmacol, 2011. **57**(5): p. 522-35.
14. Stein, M., et al., *Reduction of fibrosis-related arrhythmias by chronic renin-angiotensin-aldosterone system inhibitors in an aged mouse model.* Am J Physiol Heart Circ Physiol, 2010. **299**(2): p. H310-21.
15. Moore-Morris, T., et al., *Origins of cardiac fibroblasts.* J Mol Cell Cardiol, 2016. **91**: p. 1-5.
16. Souders, C.A., S.L. Bowers, and T.A. Baudino, *Cardiac fibroblast: the renaissance cell.* Circ Res, 2009. **105**(12): p. 1164-76.
17. Pinto, A.R., et al., *Revisiting Cardiac Cellular Composition.* Circ Res, 2016. **118**(3): p. 400-9.
18. Porter, K.E. and N.A. Turner, *Cardiac fibroblasts: at the heart of myocardial remodeling.* Pharmacol Ther, 2009. **123**(2): p. 255-78.
19. Camelliti, P., et al., *Fibroblast network in rabbit sinoatrial node: structural and functional identification of homogeneous and heterogeneous cell coupling.* Circ Res, 2004. **94**(6): p. 828-35.
20. Goldsmith, E.C., et al., *Organization of fibroblasts in the heart.* Dev Dyn, 2004. **230**(4): p. 787-94.
21. Acharya, A., et al., *The bHLH transcription factor Tcf21 is required for lineage-specific EMT of cardiac fibroblast progenitors.* Development, 2012. **139**(12): p. 2139-49.
22. Smith, C.L., et al., *Epicardial-derived cell epithelial-to-mesenchymal transition and fate specification require PDGF receptor signaling.* Circ Res, 2011. **108**(12): p. e15-26.
23. Ieda, M., et al., *Cardiac fibroblasts regulate myocardial proliferation through beta1 integrin signaling.* Dev Cell, 2009. **16**(2): p. 233-44.
24. Eghbali, M., et al., *Localization of types I, III and IV collagen mRNAs in rat heart cells by in situ hybridization.* J Mol Cell Cardiol, 1989. **21**(1): p. 103-13.

25. Kanekar, S., et al., *Cardiac fibroblasts form and function.* Cardiovasc Pathol, 1998. **7**(3): p. 127-33.
26. Spinale, F.G., *Myocardial matrix remodeling and the matrix metalloproteinases: influence on cardiac form and function.* Physiol Rev, 2007. **87**(4): p. 1285-342.
27. Reed, R.K., et al., *Blockade of beta 1-integrins in skin causes edema through lowering of interstitial fluid pressure.* Circ Res, 1992. **71**(4): p. 978-83.
28. Zhan, H. and L. Xia, *Excitation-contraction coupling between human atrial myocytes with fibroblasts and stretch activated channel current: a simulation study.* Comput Math Methods Med, 2013. **2013**: p. 238676.
29. Hinz, B., *The myofibroblast: paradigm for a mechanically active cell.* J Biomech, 2010. **43**(1): p. 146-55.
30. Petrov, V.V., R.H. Fagard, and P.J. Lijnen, *Stimulation of collagen production by transforming growth factor-beta1 during differentiation of cardiac fibroblasts to myofibroblasts.* Hypertension, 2002. **39**(2): p. 258-63.
31. Baum, J. and H.S. Duffy, *Fibroblasts and myofibroblasts: what are we talking about?* J Cardiovasc Pharmacol, 2011. **57**(4): p. 376-9.
32. Krenning, G., E.M. Zeisberg, and R. Kalluri, *The origin of fibroblasts and mechanism of cardiac fibrosis.* J Cell Physiol, 2010. **225**(3): p. 631-7.
33. Willems, I.E., et al., *The alpha-smooth muscle actin-positive cells in healing human myocardial scars.* Am J Pathol, 1994. **145**(4): p. 868-75.
34. Leslie, K.O., et al., *Cardiac myofibroblasts express alpha smooth muscle actin during right ventricular pressure overload in the rabbit.* Am J Pathol, 1991. **139**(1): p. 207-16.
35. Wang, D., et al., *Effects of pressure overload on extracellular matrix expression in the heart of the atrial natriuretic peptide-null mouse.* Hypertension, 2003. **42**(1): p. 88-95.
36. Szardien, S., et al., *Bone marrow-derived cells contribute to cell turnover in aging murine hearts.* Int J Mol Med, 2012. **30**(2): p. 283-7.
37. Kong, P., P. Christia, and N.G. Frangogiannis, *The pathogenesis of cardiac fibrosis.* Cell Mol Life Sci, 2014. **71**(4): p. 549-74.
38. Ali, S.R., et al., *Developmental heterogeneity of cardiac fibroblasts does not predict pathological proliferation and activation.* Circ Res, 2014. **115**(7): p. 625-35.
39. Bassett, E.G. and J.S. Wakefield, *Elastic fibers in myocardial scars in rats: development teraction with other components.* Connect Tissue Res, 2008. **49**(5): p. 321-7.
40. Bradham, D.M., et al., *Connective tissue growth factor: a cysteine-rich mitogen secreted by human vascular endothelial cells is related to the SRC-induced immediate early gene product CEF-10.* J Cell Biol, 1991. **114**(6): p. 1285-94.
41. Bork, P., *The modular architecture of a new family of growth regulators related to connective tissue growth factor.* FEBS Lett, 1993. **327**(2): p. 125-30.
42. Perbal, B., *CCN proteins: multifunctional signalling regulators.* Lancet, 2004. **363**(9402): p. 62-4.
43. Kim, H.S., et al., *Identification of a family of low-affinity insulin-like growth factor binding proteins (IGFBPs): characterization of connective tissue growth factor as a member of the IGFBP superfamily.* Proc Natl Acad Sci U S A, 1997. **94**(24): p. 12981-6.
44. Rodriguez, S., T.R. Gaunt, and I.N. Day, *Molecular genetics of human growth hormone, insulin-like growth factors and their pathways in common disease.* Hum Genet, 2007. **122**(1): p. 1-21.
45. Clayton, R.N., *Cardiovascular function in acromegaly.* Endocr Rev, 2003. **24**(3): p. 272-7.
46. Butt, R.P., G.J. Laurent, and J.E. Bishop, *Collagen production and replication by cardiac fibroblasts is enhanced in response to diverse classes of growth factors.* Eur J Cell Biol, 1995. **68**(3): p. 330-5.
47. van Eickels, M., H. Vetter, and C. Grohe, *Angiotensin-converting enzyme (ACE) inhibition attenuates insulin-like growth factor-I (IGF-I) induced cardiac fibroblast proliferation.* Br J Pharmacol, 2000. **131**(8): p. 1592-6.

48. Abreu, J.G., et al., *Connective-tissue growth factor (CTGF) modulates cell signalling by BMP and TGF-beta.* Nat Cell Biol, 2002. **4**(8): p. 599-604.
49. Nguyen, T.Q., et al., *CTGF inhibits BMP-7 signaling in diabetic nephropathy.* J Am Soc Nephrol, 2008. **19**(11): p. 2098-107.
50. Wang, S. and R. Hirschberg, *BMP7 antagonizes TGF-beta -dependent fibrogenesis in mesangial cells.* Am J Physiol Renal Physiol, 2003. **284**(5): p. F1006-13.
51. Inoki, I., et al., *Connective tissue growth factor binds vascular endothelial growth factor (VEGF) and inhibits VEGF-induced angiogenesis.* Faseb j, 2002. **16**(2): p. 219-21.
52. Shi-Wen, X., A. Leask, and D. Abraham, *Regulation and function of connective tissue growth factor/CCN2 in tissue repair, scarring and fibrosis.* Cytokine Growth Factor Rev, 2008. **19**(2): p. 133-44.
53. Gressner, O.A. and A.M. Gressner, *Connective tissue growth factor: a fibrogenic master switch in fibrotic liver diseases.* Liver Int, 2008. **28**(8): p. 1065-79.
54. Hashimoto, G., et al., *Matrix metalloproteinases cleave connective tissue growth factor and reactivate angiogenic activity of vascular endothelial growth factor 165.* J Biol Chem, 2002. **277**(39): p. 36288-95.
55. Dean, R.A., et al., *Identification of candidate angiogenic inhibitors processed by matrix metalloproteinase 2 (MMP-2) in cell-based proteomic screens: disruption of vascular endothelial growth factor (VEGF)/heparin affin regulatory peptide (pleiotrophin) and VEGF/Connective tissue growth factor angiogenic inhibitory complexes by MMP-2 proteolysis.* Mol Cell Biol, 2007. **27**(24): p. 8454-65.
56. Hishikawa, K., et al., *Overexpression of connective tissue growth factor gene induces apoptosis in human aortic smooth muscle cells.* Circulation, 1999. **100**(20): p. 2108-12.
57. Shimo, T., et al., *Connective tissue growth factor induces the proliferation, migration, and tube formation of vascular endothelial cells in vitro, and angiogenesis in vivo.* J Biochem, 1999. **126**(1): p. 137-45.
58. Oemar, B.S. and T.F. Luscher, *Connective tissue growth factor. Friend or foe?* Arterioscler Thromb Vasc Biol, 1997. **17**(8): p. 1483-9.
59. Daniels, A., et al., *Connective tissue growth factor and cardiac fibrosis.* Acta Physiol (Oxf), 2009. **195**(3): p. 321-38.
60. Brigstock, D.R., *The connective tissue growth factor/cysteine-rich 61/nephroblastoma overexpressed (CCN) family.* Endocr Rev, 1999. **20**(2): p. 189-206.
61. Chen, M.M., et al., *CTGF expression is induced by TGF- beta in cardiac fibroblasts and cardiac myocytes: a potential role in heart fibrosis.* J Mol Cell Cardiol, 2000. **32**(10): p. 1805-19.
62. Chuva de Sousa Lopes, S.M., et al., *Connective tissue growth factor expression and Smad signaling during mouse heart development and myocardial infarction.* Dev Dyn, 2004. **231**(3): p. 542-50.
63. Friedrichsen, S., et al., *Gene expression of connective tissue growth factor in adult mouse.* Growth Factors, 2005. **23**(1): p. 43-53.
64. Ivkovic, S., et al., *Connective tissue growth factor coordinates chondrogenesis and angiogenesis during skeletal development.* Development, 2003. **130**(12): p. 2779-91.
65. Blom, I.E., R. Goldschmeding, and A. Leask, *Gene regulation of connective tissue growth factor: new targets for antifibrotic therapy?* Matrix Biol, 2002. **21**(6): p. 473-82.
66. Igarashi, A., et al., *Regulation of connective tissue growth factor gene expression in human skin fibroblasts and during wound repair.* Mol Biol Cell, 1993. **4**(6): p. 637-45.
67. Leask, A., *TGFbeta, cardiac fibroblasts, and the fibrotic response.* Cardiovasc Res, 2007. **74**(2): p. 207-12.
68. Kemp, T.J., et al., *Phenylephrine and endothelin-1 upregulate connective tissue growth factor in neonatal rat cardiac myocytes.* J Mol Cell Cardiol, 2004. **37**(2): p. 603-6.
69. Ruperez, M., et al., *Connective tissue growth factor is a mediator of angiotensin II-induced fibrosis.* Circulation, 2003. **108**(12): p. 1499-505.

70. Recchia, A.G., et al., *Endothelin-1 induces connective tissue growth factor expression in cardiomyocytes.* J Mol Cell Cardiol, 2009. **46**(3): p. 352-9.
71. Ahmed, M.S., et al., *Connective tissue growth factor--a novel mediator of angiotensin II-stimulated cardiac fibroblast activation in heart failure in rats.* J Mol Cell Cardiol, 2004. **36**(3): p. 393-404.
72. Lavall, D., et al., *The mineralocorticoid receptor promotes fibrotic remodeling in atrial fibrillation.* J Biol Chem, 2014. **289**(10): p. 6656-68.
73. Touvron, M., et al., *Locally expressed IGF1 propeptide improves mouse heart function in induced dilated cardiomyopathy by blocking myocardial fibrosis and SRF-dependent CTGF induction.* Dis Model Mech, 2012. **5**(4): p. 481-91.
74. Frazier, K., et al., *Stimulation of fibroblast cell growth, matrix production, and granulation tissue formation by connective tissue growth factor.* J Invest Dermatol, 1996. **107**(3): p. 404-11.
75. Daniels, J.T., et al., *Mediation of transforming growth factor-beta(1)-stimulated matrix contraction by fibroblasts: a role for connective tissue growth factor in contractile scarring.* Am J Pathol, 2003. **163**(5): p. 2043-52.
76. Grotendorst, G.R., H. Rahmanie, and M.R. Duncan, *Combinatorial signaling pathways determine fibroblast proliferation and myofibroblast differentiation.* Faseb j, 2004. **18**(3): p. 469-79.
77. Zhang, C., et al., *Connective tissue growth factor regulates the key events in tubular epithelial to myofibroblast transition in vitro.* Cell Biol Int, 2004. **28**(12): p. 863-73.
78. Grotendorst, G.R., *Connective tissue growth factor: a mediator of TGF-beta action on fibroblasts.* Cytokine Growth Factor Rev, 1997. **8**(3): p. 171-9.
79. Goldschmeding, R., et al., *Connective tissue growth factor: just another factor in renal fibrosis?* Nephrol Dial Transplant, 2000. **15**(3): p. 296-9.
80. Moussad, E.E. and D.R. Brigstock, *Connective tissue growth factor: what's in a name?* Mol Genet Metab, 2000. **71**(1-2): p. 276-92.
81. Finckenberg, P., et al., *Angiotensin II induces connective tissue growth factor gene expression via calcineurin-dependent pathways.* Am J Pathol, 2003. **163**(1): p. 355-66.
82. Gabrielsen, A., et al., *Gene expression signals involved in ischemic injury, extracellular matrix composition and fibrosis defined by global mRNA profiling of the human left ventricular myocardium.* J Mol Cell Cardiol, 2007. **42**(4): p. 870-83.
83. Koitabashi, N., et al., *Increased connective tissue growth factor relative to brain natriuretic peptide as a determinant of myocardial fibrosis.* Hypertension, 2007. **49**(5): p. 1120-7.
84. Way, K.J., et al., *Expression of connective tissue growth factor is increased in injured myocardium associated with protein kinase C beta2 activation and diabetes.* Diabetes, 2002. **51**(9): p. 2709-18.
85. Ohnishi, H., et al., *Increased expression of connective tissue growth factor in the infarct zone of experimentally induced myocardial infarction in rats.* J Mol Cell Cardiol, 1998. **30**(11): p. 2411-22.
86. Fontes, M.S., et al., *Changes in Cx43 and NaV1.5 expression precede the occurrence of substantial fibrosis in calcineurin-induced murine cardiac hypertrophy.* PLoS One, 2014. **9**(1): p. e87226.
87. Mori, T., et al., *Role and interaction of connective tissue growth factor with transforming growth factor-beta in persistent fibrosis: A mouse fibrosis model.* J Cell Physiol, 1999. **181**(1): p. 153-9.
88. Brigstock, D.R., *Strategies for blocking the fibrogenic actions of connective tissue growth factor (CCN2): From pharmacological inhibition in vitro to targeted siRNA therapy in vivo.* J Cell Commun Signal, 2009. **3**(1): p. 5-18.
89. Gravning, J., et al., *CCN2/CTGF attenuates myocardial hypertrophy and cardiac dysfunction upon chronic pressure-overload.* Int J Cardiol, 2013. **168**(3): p. 2049-56.

90. Accornero, F., et al., *Genetic Analysis of Connective Tissue Growth Factor as an Effector of Transforming Growth Factor beta Signaling and Cardiac Remodeling.* Mol Cell Biol, 2015. **35**(12): p. 2154-64.
91. Wennerberg, K. and C.J. Der, *Rho-family GTPases: it's not only Rac and Rho (and I like it).* J Cell Sci, 2004. **117**(Pt 8): p. 1301-12.
92. Cherfils, J., *Structural mimicry of DH domains by Arfaptin suggests a model for the recognition of Rac-GDP by its guanine nucleotide exchange factors.* FEBS Lett, 2001. **507**(3): p. 280-4.
93. Vega, F.M. and A.J. Ridley, *Rho GTPases in cancer cell biology.* FEBS Lett, 2008. **582**(14): p. 2093-101.
94. Burridge, K. and K. Wennerberg, *Rho and Rac take center stage.* Cell, 2004. **116**(2): p. 167-79.
95. Heasman, S.J. and A.J. Ridley, *Mammalian Rho GTPases: new insights into their functions from in vivo studies.* Nat Rev Mol Cell Biol, 2008. **9**(9): p. 690-701.
96. Jaffe, A.B. and A. Hall, *Rho GTPases: biochemistry and biology.* Annu Rev Cell Dev Biol, 2005. **21**: p. 247-69.
97. Evers, E.E., et al., *Rho family proteins in cell adhesion and cell migration.* Eur J Cancer, 2000. **36**(10): p. 1269-74.
98. Etienne-Manneville, S. and A. Hall, *Rho GTPases in cell biology.* Nature, 2002. **420**(6916): p. 629-35.
99. Raftopoulou, M. and A. Hall, *Cell migration: Rho GTPases lead the way.* Dev Biol, 2004. **265**(1): p. 23-32.
100. Nobes, C.D. and A. Hall, *Rho, rac and cdc42 GTPases: regulators of actin structures, cell adhesion and motility.* Biochem Soc Trans, 1995. **23**(3): p. 456-9.
101. Ridley, A.J. and A. Hall, *Distinct patterns of actin organization regulated by the small GTP-binding proteins Rac and Rho.* Cold Spring Harb Symp Quant Biol, 1992. **57**: p. 661-71.
102. Jaffe, A.B. and A. Hall, *Rho GTPases in transformation and metastasis.* Adv Cancer Res, 2002. **84**: p. 57-80.
103. Ridley, A.J., *Rho GTPases and actin dynamics in membrane protrusions and vesicle trafficking.* Trends Cell Biol, 2006. **16**(10): p. 522-9.
104. Desrosiers, R.R., et al., *Modulation of Rho and cytoskeletal protein attachment to membranes by a prenylcysteine analog.* J Biol Chem, 2000. **275**(20): p. 14949-57.
105. Gohla, A., G. Schultz, and S. Offermanns, *Role for G(12)/G(13) in agonist-induced vascular smooth muscle cell contraction.* Circ Res, 2000. **87**(3): p. 221-7.
106. Shome, K., et al., *The activation of phospholipase D by endothelin-1, angiotensin II, and platelet-derived growth factor in vascular smooth muscle A10 cells is mediated by small G proteins of the ADP-ribosylation factor family.* Endocrinology, 2000. **141**(6): p. 2200-8.
107. Aoki, H., S. Izumo, and J. Sadoshima, *Angiotensin II activates RhoA in cardiac myocytes: a critical role of RhoA in angiotensin II-induced premyofibril formation.* Circ Res, 1998. **82**(6): p. 666-76.
108. Sah, V.P., et al., *Rho is required for Galphaq and alpha1-adrenergic receptor signaling in cardiomyocytes. Dissociation of Ras and Rho pathways.* J Biol Chem, 1996. **271**(49): p. 31185-90.
109. Blomquist, A., et al., *Identification and characterization of a novel Rho-specific guanine nucleotide exchange factor.* Biochem J, 2000. **352 Pt 2**: p. 319-25.
110. Rossman, K.L., C.J. Der, and J. Sondek, *GEF means go: turning on RHO GTPases with guanine nucleotide-exchange factors.* Nat Rev Mol Cell Biol, 2005. **6**(2): p. 167-80.
111. Kjoller, L. and A. Hall, *Signaling to Rho GTPases.* Exp Cell Res, 1999. **253**(1): p. 166-79.
112. Sah, V.P., et al., *The role of Rho in G protein-coupled receptor signal transduction.* Annu Rev Pharmacol Toxicol, 2000. **40**: p. 459-89.
113. Schmitz, A.A., et al., *Rho GTPases: signaling, migration, and invasion.* Exp Cell Res, 2000. **261**(1): p. 1-12.

114. Bishop, A.L. and A. Hall, *Rho GTPases and their effector proteins.* Biochem J, 2000. **348 Pt 2**: p. 241-55.
115. Hodge, R.G. and A.J. Ridley, *Regulating Rho GTPases and their regulators.* Nat Rev Mol Cell Biol, 2016. **17**(8): p. 496-510.
116. Boivin, D. and R. Beliveau, *Subcellular distribution and membrane association of Rho-related small GTP-binding proteins in kidney cortex.* Am J Physiol, 1995. **269**(2 Pt 2): p. F180-9.
117. Hirabayashi, T. and D. Saffen, *M1 muscarinic acetylcholine receptors activate zif268 gene expression via small G-protein Rho-dependent and lambda-independent pathways in PC12D cells.* Eur J Biochem, 2000. **267**(9): p. 2525-32.
118. Hall, A., *G proteins and small GTPases: distant relatives keep in touch.* Science, 1998. **280**(5372): p. 2074-5.
119. Clerk, A. and P.H. Sugden, *Signaling through the extracellular signal-regulated kinase 1/2 cascade in cardiac myocytes.* Biochem Cell Biol, 2004. **82**(6): p. 603-9.
120. Wheeler, A.P. and A.J. Ridley, *Why three Rho proteins? RhoA, RhoB, RhoC, and cell motility.* Exp Cell Res, 2004. **301**(1): p. 43-9.
121. Mackay, D.J. and A. Hall, *Rho GTPases.* J Biol Chem, 1998. **273**(33): p. 20685-8.
122. Xiang, S.Y., S.S. Dusaban, and J.H. Brown, *Lysophospholipid receptor activation of RhoA and lipid signaling pathways.* Biochim Biophys Acta, 2013. **1831**(1): p. 213-22.
123. Boureux, A., et al., *Evolution of the Rho family of ras-like GTPases in eukaryotes.* Mol Biol Evol, 2007. **24**(1): p. 203-16.
124. Wettschureck, N. and S. Offermanns, *Mammalian G proteins and their cell type specific functions.* Physiol Rev, 2005. **85**(4): p. 1159-204.
125. Vogt, S., et al., *Receptor-dependent RhoA activation in G12/G13-deficient cells: genetic evidence for an involvement of Gq/G11.* J Biol Chem, 2003. **278**(31): p. 28743-9.
126. Hunter, J.C., et al., *Nitric oxide inhibits endothelin-1-induced neonatal cardiomyocyte hypertrophy via a RhoA-ROCK-dependent pathway.* J Mol Cell Cardiol, 2009. **47**(6): p. 810-8.
127. Hoshijima, M., et al., *The low molecular weight GTPase Rho regulates myofibril formation and organization in neonatal rat ventricular myocytes. Involvement of Rho kinase.* J Biol Chem, 1998. **273**(13): p. 7725-30.
128. Kuwahara, K., et al., *The effects of the selective ROCK inhibitor, Y27632, on ET-1-induced hypertrophic response in neonatal rat cardiac myocytes--possible involvement of Rho/ROCK pathway in cardiac muscle cell hypertrophy.* FEBS Lett, 1999. **452**(3): p. 314-8.
129. Sah, V.P., et al., *Cardiac-specific overexpression of RhoA results in sinus and atrioventricular nodal dysfunction and contractile failure.* J Clin Invest, 1999. **103**(12): p. 1627-34.
130. Kuwahara, K., et al., *Myocardin-related transcription factor A is a common mediator of mechanical stress- and neurohumoral stimulation-induced cardiac hypertrophic signaling leading to activation of brain natriuretic peptide gene expression.* Mol Cell Biol, 2010. **30**(17): p. 4134-48.
131. Takefuji, M., et al., *RhoGEF12 controls cardiac remodeling by integrating G protein- and integrin-dependent signaling cascades.* J Exp Med, 2013. **210**(4): p. 665-73.
132. Lin, G., et al., *Acute inhibition of Rho-kinase improves cardiac contractile function in streptozotocin-diabetic rats.* Cardiovasc Res, 2007. **75**(1): p. 51-8.
133. Torsoni, A.S., et al., *Early activation of p160ROCK by pressure overload in rat heart.* Am J Physiol Cell Physiol, 2003. **284**(6): p. C1411-9.
134. Xiao, H., et al., *Inhibition of Rho and Rac geranylgeranylation by atorvastatin is critical for preservation of endothelial junction integrity.* PLoS One, 2013. **8**(3): p. e59233.
135. Li, Y., et al., *Fasudil protects the heart against ischemia-reperfusion injury by attenuating endoplasmic reticulum stress and modulating SERCA activity: the differential role for PI3K/Akt and JAK2/STAT3 signaling pathways.* PLoS One, 2012. **7**(10): p. e48115.
136. Balakumar, P. and M. Singh, *Differential role of rho-kinase in pathological and physiological cardiac hypertrophy in rats.* Pharmacology, 2006. **78**(2): p. 91-7.

137. Higashi, M., et al., *Long-term inhibition of Rho-kinase suppresses angiotensin II-induced cardiovascular hypertrophy in rats in vivo: effect on endothelial NAD(P)H oxidase system.* Circ Res, 2003. **93**(8): p. 767-75.
138. Xiao, J.W., et al., *Acute effects of Rho-kinase inhibitor fasudil on pulmonary arterial hypertension in patients with congenital heart defects.* Circ J, 2015. **79**(6): p. 1342-8.
139. D'Angelo, D.D., et al., *Transgenic Galphaq overexpression induces cardiac contractile failure in mice.* Proc Natl Acad Sci U S A, 1997. **94**(15): p. 8121-6.
140. Mende, U., et al., *Transient cardiac expression of constitutively active Galphaq leads to hypertrophy and dilated cardiomyopathy by calcineurin-dependent and independent pathways.* Proc Natl Acad Sci U S A, 1998. **95**(23): p. 13893-8.
141. Yang, X., et al., *Mechanism of fibrotic cardiomyopathy in mice expressing truncated Rho-associated coiled-coil protein kinase 1.* Faseb j, 2012. **26**(5): p. 2105-16.
142. Rikitake, Y., et al., *Decreased perivascular fibrosis but not cardiac hypertrophy in ROCK1+/- haploinsufficient mice.* Circulation, 2005. **112**(19): p. 2959-65.
143. Zhang, Y.M., et al., *Targeted deletion of ROCK1 protects the heart against pressure overload by inhibiting reactive fibrosis.* Faseb j, 2006. **20**(7): p. 916-25.
144. Lauriol, J., et al., *RhoA signaling in cardiomyocytes protects against stress-induced heart failure but facilitates cardiac fibrosis.* Sci Signal, 2014. **7**(348): p. ra100.
145. Okamoto, R., et al., *FHL2 prevents cardiac hypertrophy in mice with cardiac-specific deletion of ROCK2.* Faseb j, 2013. **27**(4): p. 1439-49.
146. Momotani, K. and A.V. Somlyo, *p63RhoGEF: A New Switch for Gq-Mediated Activation of Smooth Muscle.* Trends in Cardiovascular Medicine, 2012. **22**(5): p. 122-127.
147. Xiang, S.Y., et al., *RhoA protects the mouse heart against ischemia/reperfusion injury.* J Clin Invest, 2011. **121**(8): p. 3269-76.
148. Eva, A., et al., *The predicted DBL oncogene product defines a distinct class of transforming proteins.* Proc Natl Acad Sci U S A, 1988. **85**(7): p. 2061-5.
149. Hart, M.J., et al., *Cellular transformation and guanine nucleotide exchange activity are catalyzed by a common domain on the dbl oncogene product.* J Biol Chem, 1994. **269**(1): p. 62-5.
150. Schmidt, A. and A. Hall, *Guanine nucleotide exchange factors for Rho GTPases: turning on the switch.* Genes Dev, 2002. **16**(13): p. 1587-609.
151. Lemmon, M.A. and K.M. Ferguson, *Signal-dependent membrane targeting by pleckstrin homology (PH) domains.* Biochem J, 2000. **350 Pt 1**: p. 1-18.
152. Aittaleb, M., et al., *Plasma membrane association of p63 Rho guanine nucleotide exchange factor (p63RhoGEF) is mediated by palmitoylation and is required for basal activity in cells.* J Biol Chem, 2011. **286**(39): p. 34448-56.
153. Shankaranarayanan, A., et al., *Galpha q allosterically activates and relieves autoinhibition of p63RhoGEF.* Cell Signal, 2010. **22**(7): p. 1114-23.
154. Welch, H.C., et al., *P-Rex1, a PtdIns(3,4,5)P3- and Gbetagamma-regulated guanine-nucleotide exchange factor for Rac.* Cell, 2002. **108**(6): p. 809-21.
155. Das, B., et al., *Control of intramolecular interactions between the pleckstrin homology and Dbl homology domains of Vav and Sos1 regulates Rac binding.* J Biol Chem, 2000. **275**(20): p. 15074-81.
156. Bellanger, J.M., et al., *Different regulation of the Trio Dbl-Homology domains by their associated PH domains.* Biol Cell, 2003. **95**(9): p. 625-34.
157. Zheng, Y., *Dbl family guanine nucleotide exchange factors.* Trends Biochem Sci, 2001. **26**(12): p. 724-32.
158. Stam, J.C. and J.G. Collard, *The DH protein family, exchange factors for Rho-like GTPases.* Prog Mol Subcell Biol, 1999. **22**: p. 51-83.
159. Seasholtz, T.M., M. Majumdar, and J.H. Brown, *Rho as a mediator of G protein-coupled receptor signaling.* Mol Pharmacol, 1999. **55**(6): p. 949-56.

160. Lutz, S., et al., *The guanine nucleotide exchange factor p63RhoGEF, a specific link between Gq/11-coupled receptor signaling and RhoA.* J Biol Chem, 2005. **280**(12): p. 11134-9.
161. Mao, J., et al., *Guanine nucleotide exchange factor GEF115 specifically mediates activation of Rho and serum response factor by the G protein alpha subunit Galpha13.* Proc Natl Acad Sci U S A, 1998. **95**(22): p. 12973-6.
162. Souchet, M., et al., *Human p63RhoGEF, a novel RhoA-specific guanine nucleotide exchange factor, is localized in cardiac sarcomere.* J Cell Sci, 2002. **115**(Pt 3): p. 629-40.
163. Rojas, R.J., et al., *Galphaq directly activates p63RhoGEF and Trio via a conserved extension of the Dbl homology-associated pleckstrin homology domain.* J Biol Chem, 2007. **282**(40): p. 29201-10.
164. Lutz, S., et al., *Structure of Galphaq-p63RhoGEF-RhoA complex reveals a pathway for the activation of RhoA by GPCRs.* Science, 2007. **318**(5858): p. 1923-7.
165. Lutz, S., et al., *p63RhoGEF and GEFT are Rho-specific guanine nucleotide exchange factors encoded by the same gene.* Naunyn Schmiedebergs Arch Pharmacol, 2004. **369**(5): p. 540-6.
166. Guo, X., et al., *A Rac/Cdc42-specific exchange factor, GEFT, induces cell proliferation, transformation, and migration.* J Biol Chem, 2003. **278**(15): p. 13207-15.
167. Goedhart, J., et al., *Signaling efficiency of Galphaq through its effectors p63RhoGEF and GEFT depends on their subcellular location.* Sci Rep, 2013. **3**: p. 2284.
168. van Unen, J., et al., *Plasma membrane restricted RhoGEF activity is sufficient for RhoA-mediated actin polymerization.* Sci Rep, 2015. **5**: p. 14693.
169. Wuertz, C.M., et al., *p63RhoGEF--a key mediator of angiotensin II-dependent signaling and processes in vascular smooth muscle cells.* FASEB J, 2010. **24**(12): p. 4865-76.
170. Momotani, K., et al., *p63RhoGEF couples Galpha(q/11)-mediated signaling to Ca2+ sensitization of vascular smooth muscle contractility.* Circ Res, 2011. **109**(9): p. 993-1002.
171. Calo, L.A., et al., *Increased level of p63RhoGEF and RhoA/Rho kinase activity in hypertensive patients.* J Hypertens, 2014. **32**(2): p. 331-8.
172. Truett, G.E., et al., *Preparation of PCR-quality mouse genomic DNA with hot sodium hydroxide and tris (HotSHOT).* Biotechniques, 2000. **29**(1): p. 52, 54.
173. Louch, W.E., K.A. Sheehan, and B.M. Wolska, *Methods in cardiomyocyte isolation, culture, and gene transfer.* J Mol Cell Cardiol, 2011. **51**(3): p. 288-98.
174. Laemmli, U.K., *Cleavage of structural proteins during the assembly of the head of bacteriophage T4.* Nature, 1970. **227**(5259): p. 680-5.
175. Toischer, K., et al., *Differential cardiac remodeling in preload versus afterload.* Circulation, 2010. **122**(10): p. 993-1003.
176. Coletti, D., et al., *Serum Response Factor in Muscle Tissues: From Development to Ageing.* Eur J Transl Myol, 2016. **26**(2): p. 6008.
177. Selvaraj, A. and R. Prywes, *Expression profiling of serum inducible genes identifies a subset of SRF target genes that are MKL dependent.* BMC Mol Biol, 2004. **5**: p. 13.
178. Cen, B., A. Selvaraj, and R. Prywes, *Myocardin/MKL family of SRF coactivators: key regulators of immediate early and muscle specific gene expression.* J Cell Biochem, 2004. **93**(1): p. 74-82.
179. Pedersen, L.B., J.B. Mogensen, and S.T. Christensen, *Endocytic Control of Cellular Signaling at the Primary Cilium.* Trends Biochem Sci, 2016. **41**(9): p. 784-97.
180. Avasthi, P. and W. Marshall, *Ciliary secretion: switching the cellular antenna to 'transmit'.* Curr Biol, 2013. **23**(11): p. R471-3.
181. Zhao, X., et al., *Induction of the matricellular protein CCN1 through RhoA and MRTF-A contributes to ischemic cardioprotection.* Journal of Molecular and Cellular Cardiology. **75**: p. 152-161.
182. Panek, A.N., et al., *Connective tissue growth factor overexpression in cardiomyocytes promotes cardiac hypertrophy and protection against pressure overload.* PLoS One, 2009. **4**(8): p. e6743.
183. Ridley, A.J., *The GTP-binding protein Rho.* Int J Biochem Cell Biol, 1997. **29**(11): p. 1225-9.

184. Spiering, D. and L. Hodgson, *Dynamics of the Rho-family small GTPases in actin regulation and motility.* Cell Adh Migr, 2011. **5**(2): p. 170-80.
185. Posern, G. and R. Treisman, *Actin' together: serum response factor, its cofactors and the link to signal transduction.* Trends Cell Biol, 2006. **16**(11): p. 588-96.
186. Parmacek, M.S., *Myocardin-related transcription factors: critical coactivators regulating cardiovascular development and adaptation.* Circ Res, 2007. **100**(5): p. 633-44.
187. Nakerakanti, S.S., et al., *Fli1 and Ets1 have distinct roles in connective tissue growth factor/CCN2 gene regulation and induction of the profibrotic gene program.* J Biol Chem, 2006. **281**(35): p. 25259-69.
188. Halayko, A.J. and J. Solway, *Molecular mechanisms of phenotypic plasticity in smooth muscle cells.* J Appl Physiol (1985), 2001. **90**(1): p. 358-68.
189. Posern, G., et al., *Mutant actins that stabilise F-actin use distinct mechanisms to activate the SRF coactivator MAL.* Embo j, 2004. **23**(20): p. 3973-83.
190. Jatho, A., et al., *RhoA Ambivalently Controls Prominent Myofibroblast Characteritics by Involving Distinct Signaling Routes.* PLoS One, 2015. **10**(10): p. e0137519.
191. Sakai, N., et al., *LPA1-induced cytoskeleton reorganization drives fibrosis through CTGF-dependent fibroblast proliferation.* Faseb j, 2013. **27**(5): p. 1830-46.
192. Esnault, C., et al., *Rho-actin signaling to the MRTF coactivators dominates the immediate transcriptional response to serum in fibroblasts.* Genes Dev, 2014. **28**(9): p. 943-58.
193. Pobbati, A.V., et al., *Structural and functional similarity between the Vgll1-TEAD and the YAP-TEAD complexes.* Structure, 2012. **20**(7): p. 1135-40.
194. Cai, H. and Y. Xu, *The role of LPA and YAP signaling in long-term migration of human ovarian cancer cells.* Cell Commun Signal, 2013. **11**(1): p. 31.
195. Ongherth, A., et al., *p63RhoGEF regulates auto- and paracrine signaling in cardiac fibroblasts.* J Mol Cell Cardiol, 2015. **88**: p. 39-54.
196. Ghossoub, R., et al., *The ciliary pocket: a once-forgotten membrane domain at the base of cilia.* Biol Cell, 2011. **103**(3): p. 131-44.
197. Moe, I.T., et al., *CCN2 exerts direct cytoprotective actions in adult cardiac myocytes by activation of the PI3-kinase/Akt/GSK-3beta signaling pathway.* J Cell Commun Signal, 2013. **7**(1): p. 31-47.
198. Ahmed, M.S., et al., *Mechanisms of novel cardioprotective functions of CCN2/CTGF in myocardial ischemia-reperfusion injury.* Am J Physiol Heart Circ Physiol, 2011. **300**(4): p. H1291-302.
199. Kakkar, R. and R.T. Lee, *Intramyocardial fibroblast myocyte communication.* Circ Res, 2010. **106**(1): p. 47-57.
200. Zheng, B., et al., *Ligand-dependent genetic recombination in fibroblasts : a potentially powerful technique for investigating gene function in fibrosis.* Am J Pathol, 2002. **160**(5): p. 1609-17.
201. Zimmermann, A.S., et al., *Epidermal or dermal specific knockout of PHD-2 enhances wound healing and minimizes ischemic injury.* PLoS One, 2014. **9**(4): p. e93373.
202. Neelisetty, S., et al., *Renal fibrosis is not reduced by blocking transforming growth factor-beta signaling in matrix-producing interstitial cells.* Kidney Int, 2015. **88**(3): p. 503-14.
203. Parapuram, S.K., et al., *Loss of PTEN expression by mouse fibroblasts results in lung fibrosis through a CCN2-dependent mechanism.* Matrix Biol, 2015. **43**: p. 35-41.
204. Kaur, H., et al., *Targeted Ablation of Periostin-Expressing Activated Fibroblasts Prevents Adverse Cardiac Remodeling in Mice.* Circ Res, 2016. **118**(12): p. 1906-17.
205. Filipe, M.D., et al., *Galectin-3 and heart failure: prognosis, prediction & clinical utility.* Clin Chim Acta, 2015. **443**: p. 48-56.
206. Gonzalez, G.E., et al., *Cardiac-deleterious role of Galectin-3 in Angiotension II-induced Hypertension.* American Journal of Physiology - Heart and Circulatory Physiology, 2016.
207. Verrecchia, F. and A. Mauviel, *Transforming growth factor-beta and fibrosis.* World J Gastroenterol, 2007. **13**(22): p. 3056-62.

208. Ghatak, S., et al., *Roles of Proteoglycans and Glycosaminoglycans in Wound Healing and Fibrosis.* Int J Cell Biol, 2015. **2015**.
209. Chowdhury, B., et al., *Murine hyaluronidase 2 deficiency results in extracellular hyaluronan accumulation and severe cardiopulmonary dysfunction.* J Biol Chem, 2013. **288**(1): p. 520-8.
210. Klingberg, F., B. Hinz, and E.S. White, *The myofibroblast matrix: implications for tissue repair and fibrosis.* J Pathol, 2013. **229**(2): p. 298-309.
211. Rhee, S.G., *Regulation of phosphoinositide-specific phospholipase C.* Annu Rev Biochem, 2001. **70**: p. 281-312.
212. Niizeki, T., et al., *Diacylglycerol kinase-epsilon restores cardiac dysfunction under chronic pressure overload: a new specific regulator of Galpha(q) signaling cascade.* Am J Physiol Heart Circ Physiol, 2008. **295**(1): p. H245-55.
213. Leask, A., *Potential therapeutic targets for cardiac fibrosis: TGFbeta, angiotensin, endothelin, CCN2, and PDGF, partners in fibroblast activation.* Circ Res, 2010. **106**(11): p. 1675-80.
214. Mikelis, C.M., et al., *RhoA and ROCK mediate histamine-induced vascular leakage and anaphylactic shock.* Nat Commun, 2015. **6**: p. 6725.
215. Banerjee, I., et al., *Determination of cell types and numbers during cardiac development in the neonatal and adult rat and mouse.* Am J Physiol Heart Circ Physiol, 2007. **293**(3): p. H1883-91.

9 Own publications

Ongherth, A., S. Pasch, C. M. Wuertz, K. Nowak, N. Kittana, C. A. Weis, A. Jatho, C. Vettel, M. Tiburcy, K. Toischer, G. Hasenfuss, W. H. Zimmermann, T. Wieland and S. Lutz (2015). "p63RhoGEF regulates auto- and paracrine signaling in cardiac fibroblasts." J Mol Cell Cardiol **88**: 39-54.

Vettel, C., S. Lammle, S. Ewens, C. Cervirgen, J. Emons, **A. Ongherth**, M. Dewenter, D. Lindner, D. Westermann, V. O. Nikolaev, S. Lutz, W. H. Zimmermann and A. El-Armouche (2014). "PDE2-mediated cAMP hydrolysis accelerates cardiac fibroblast to myofibroblast conversion and is antagonized by exogenous activation of cGMP signaling pathways." Am J Physiol Heart Circ Physiol **306**(8): H1246-1252.